金属表面上に化学吸着した分子の価電子励起に起因する紫外レーザー刺激脱離の研究

間瀬　一彦

STUDY OF ULTRAVIOLET-LASER STIMULATED DESORPTION OF MOLECULES CHEMISORBED ON A METAL SURFACE INDUCED BY VALENCE-ELECTRON EXCITATION

by

KAZUHIKO MASE

Thesis submitted to the University of Tokyo
for the Degree of Ph. Doctor

December 1990

Acknowledgements

I sincerely wish to thank Prof. Y. Murata for his heartful encouragement and fruitful discussion throughout the work. I am deeply grateful to Prof. Y. Achiba, Mr. M. Kubota, and Dr. K. Fukutani for the valuable supports and discussion. I also wish to acknowledge Dr. M. Yamada, Prof. S. Watanabe, Dr. A. Endoh, Dr. M. Watanabe, Dr. H. Shiromaru, and Prof. N. Nishida for the useful advices and supports. Finally, I express my gratitude to Mr. S. Mizuno and Mr. M.-B. Song for the helpful experimental assistants.

Sincerely, Kazuhiko Mase

CONTENTS

CHAPTER 1

Introduction

Two kinds of investigations are presented in the thesis. One is the study of nitric oxide (NO) adsorption-induced structural transformation of a platinum (001) surface (Pt(001)) at temperatures of 80-410 K using low-energy electron diffraction (LEED). The other is the study of ultraviolet-laser stimulated desorption of NO chemisorbed on Pt(001) induced by valence-electron excitation. The significance and the historical background of each investigation are described. The studies related to the present work are reviewed.

1.1 Significance of the present work

I have carried out two kinds of investigations. One is the study of nitric oxide (NO) adsorption-induced structural transformation of a platinum (001) surface (Pt(001)) at temperatures of 80-410 K using low-energy electron diffraction (LEED) and a single-domain Pt(001) reconstructed surface. The other is the photostimulated desorption study of NO chemisorbed on Pt(001) induced by valence-electron excitation using an ArF excimer laser (λ = 193 nm, 6.41 eV). In this chapter, I briefly describe the significance and the historical background of each investigation.

Surfaces often exhibit characteristic structural transformation, which has been one of the most important subjects in the history of surface science [1]. Recently, adsorption-induced structural transformations of metal surfaces have offered exciting topics in this field [2]. A Pt(001) surface exhibits the following remarkable features: (1) The topmost Pt layer of a clean Pt(001) surface has a hexagonal structure instead of the bulk-like (1x1) structure [3, 4]. (2) The reconstructed surface is relaxed to the (1x1) structure with adsorption of molecules such as NO [5] and CO [6]. In Chapter 2 of the thesis, I report a LEED study of the structural transformation of a single-domain Pt(001) reconstructed surface induced by NO adsorption at temperatures of 80-410 K. The structural transformation of the topmost Pt layer and the NO layer growth process are observed to be remarkably dependent on the surface temperature. At 330-390 K, a double-domain NO-c(2x4) layer grows while relaxing the topmost

hexagonal Pt layer into the (1x1) structure. On the other hand, a single-domain NO-c(2x4) layer grows anisotropically at 230-270 K. The (20x5)→(1x1) structural transformation of the topmost Pt layer was found to occur abruptly in relatively narrow NO exposure range of 0.8-1.0 L at 80 K. The mechanism of the single-domain reconstructed surface formation is discussed. A detailed model is proposed for the microscopic mechanism of the (20x5)→(1x1) structural transformation accompanied by the anisotropic single-domain NO-c(2x4) layer growth observed at 230-270 K. The present study will contribute to further understanding of the microscopic mechanisms for adsorption-induced structural transformations of metal surfaces.

Recently, study of laser-induced surface processes has developed as a new important field in surface science owing to rapid progresses in laser and vacuum technology [7]. Especially, photostimulated desorption has attracted interest of many surface scientists, because it is one of the most fundamental photo-chemical surface processes [8, 9]. There has been, however, only few studies on ultraviolet-laser stimulated desorption induced by electronic excitations for molecules chemisorbed on metal [10-12]. In the latter part of the thesis, I report a study of desorption of NO chemisorbed on Pt(001) induced by ArF excimer laser irradiation (λ = 193 nm, 6.41 eV) using a positive ion detection system (Chapter 3), the (2+2) resonance-enhanced multiphoton ionization ((2+2)REMPI) technique (Chapter 4), and the (1+1)REMPI technique (Chapter 5 and 6). The laser fluence dependences of desorption yield, translational and internal energy distributions,

and desorption cross sections were measured. All of the results support that desorption of chemisorbed NO is induced by valence-electron excitation. The present results are compared in detail with those reported in the other state-selective studies of electron-stimulated and photostimulated desorption, and the mechanism of the observed photostimulated desorption is discussed. The present study will open a way for elucidation of the mechanism of photochemical processes of molecules chemisorbed on metal.

Before describing the present investigations, I briefly review the related studies in the following sections. First, I introduce the structure and the properties of NO chemisorbed on Pt(001) in Section 1.2, then survey the history of study on desorption induced by valence-electron excitations in Section 1.3, and review the other state-selective studies of desorption induced by valence-electron excitations for NO chemisorbed on metal or modified metal in Section 1.4.

1.2 Structure and properties of NO chemisorbed on Pt(001)

The most stable structure of a clean Pt(001) surface exhibits a (20x5)-like LEED pattern, for which a model is proposed that the topmost Pt layer is reconstructed hexagonally with a rotation angle of 0.7° [3, 4] (fig. 1-1). Four possible domains are usually present in a reconstructed surface. In the thesis, I use the customary indication of (20x5) to represent the stable rotated hexagonal structure. An almost clean Pt(001)-(1x1) surface can also be prepared by NO and H_2 treatments [13]. The metastable

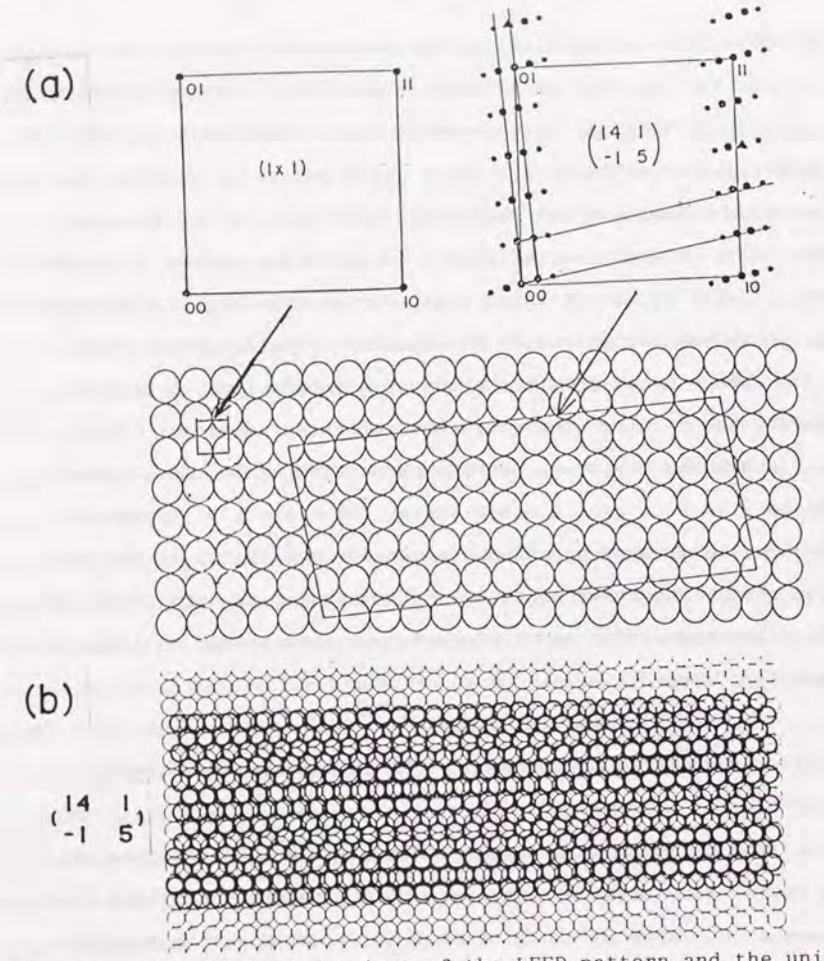

Fig. 1-1. (a) Schematic drawings of the LEED pattern and the unit cell for the unreconstructed and reconsrtructed Pt(001) surfaces. The dot size is roughly proportional to average spot intensity. Triangular dots represent "hexagonal spots" due to a hexagonal layer. (b) Rotated hexagonal model for a Pt(001)-(20x5) surface. The top-layer atoms are shown as thick circles, while the next layer atoms are shown as thin circles. (From ref. [4].)

Pt(001)-(1x1) surface is reported to be stabilized by a residual H-coverage of ~0.08 monolayers (ML) (~1x10^{14} atoms/cm^2) [6]. The metastable (1x1) structure transforms irreversively to the metastable (1x5) structure at ~420 K, to the metastable non-rotated hexagonal structure above 600 K, then finally to the stable rotated hexagonal structure above 1100 K [14].

Bonzel et al. have studied NO adsorbed on a Pt(001)-(20x5) surface at 300-670 K using LEED, Auger electron spectroscopy (AES), and ultraviolet and X-ray photoemission spectroscopies (UPS and XPS), and reported the following results: (1) With NO adsorption at temperatures lower than 340 K, the LEED pattern changes into a double-domain c(2x4)-like pattern, i. e. a (1x1) pattern accompanied by four fuzzy spots located at (1/2 1/4), (1/2 3/4), (1/4 1/2), and (3/4 1/2) in the reciprocal unit cell. This pattern is not a simple c(2x4) pattern, because (0 1/2), (1 1/2), (1/2 0), and (1/2 1) spots are missing [5]. (2) NO is chemisorbed on the Pt(001) surface molecularly with a bent configuration [5]. (3) UPS spectra for a nearly-NO-saturated Pt(001) surface exhibit three peaks at 2.7, 9.6, and 14.8 eV below the Fermi level, which are assigned to the 2π, $1\pi+5\sigma$, and 4σ orbital of molecular NO, respectively (fig. 1-2) [5]. (4) The NO-saturation coverage at 320 K is ~0.38 ML (~5x10^{14} molecules/cm^2) [15]. (5) A Pt(001)-(20x5) surface is able to adsorb NO at temperatures up to 410 K [13]. (6) The initial sticking coefficient of NO on a Pt(001)-(20x5) surface is ~0.6 at 300 K [13]. (7) The dissociation of adsorbed NO starts above ~400 K [13].

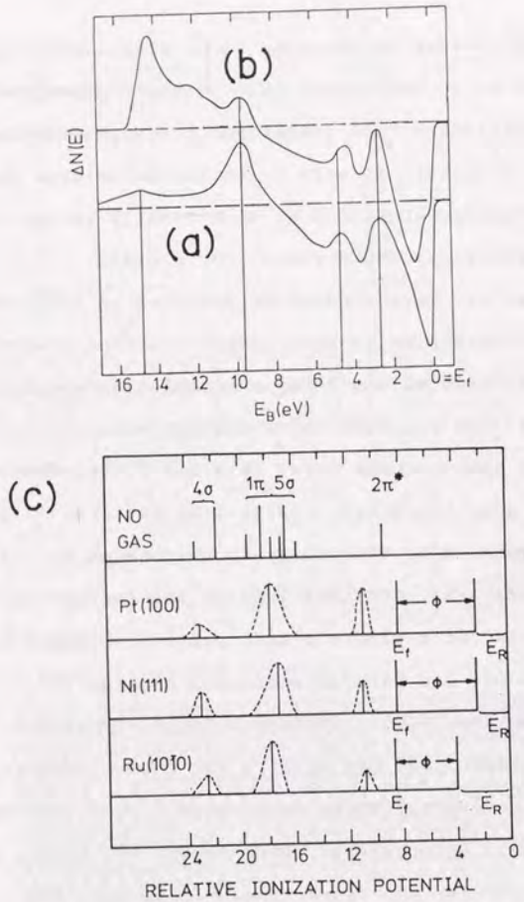

Fig. 1-2. (a) Difference UPS spectrum for a nearly-NO-saturated Pt(001) surface at temperatures lower than 340 K with respect to a clean Pt(001)-(20x5) surface, $h\nu$ = 40.8 eV. (b) Same as (a) but for $h\nu$ = 21.2 eV. (c) Comparison of UPS spectra of gaseous and adsorbed NO. The spectra of adsorbed NO were shifted relative to the gas phase spectrum until maximum overlap occurs between the $1\pi+5\sigma$ group and the measured peak at 9.5 eV below the Fermi level. (From ref. [5].)

The same group has investigated NO adsorbed on Pt(001)-(20x5) at 300 and 140 K using high-resolution electron energy loss spectroscopy (HREELS), LEED, and AES [16]. The HREELS spectra are shown in fig. 1-3. The configuration of chemisorbed NO was discussed on the basis of symmetry arguments. For NO adsorbed on Pt(001)-(20x5) at 300 K, two N-O stretching peaks were observed at 1630 and 1805 cm^{-1}. The former peak is greater than the latter. They concluded that 1630 cm^{-1} energy loss represents NO chemisorbed on an on-top site in the Pt-(1x1) surface with N-side down with a bent configuration, while 1805 cm^{-1} energy loss corresponds to NO chemisorbed on an on-top site at defects probably with a straight configuration. With NO adsorption at 140 K, the LEED pattern changes into a diffuse (1x5) pattern. With NO exposure of 0.2 L (1 L = $1x10^{-6}$ Torr·s) at 140 K, only a single N-O stretching energy loss appears at 1690 cm^{-1}, which is assigned to a bent NO molecule. With larger NO exposure of 5 L at 140 K, an additional N-O stretching peak appears at 1790 cm^{-1}, which is assigned to a NO chemisorbed on an on-top site in the Pt-(20x5) surface probably with a straight configuration.

In a study of NO adsorbed on Pt(001)-(20x5) at 300 K using reflection-absorption infrared spectroscopy (RAIRS), Banholzer and Masel observed a shift of the N-O stretching energy loss from 1634 to 1641 cm^{-1} with increasing NO exposure from 1.5 to 9 L [17]. They attributed the shift to the dipole coupling of adjacent NO molecules. The N-O stretching was observed to shift to 1629 cm^{-1}, when the NO-saturated surface was heated from 300 to 408 K. On the basis of these results, they concluded that the adsorbed NO

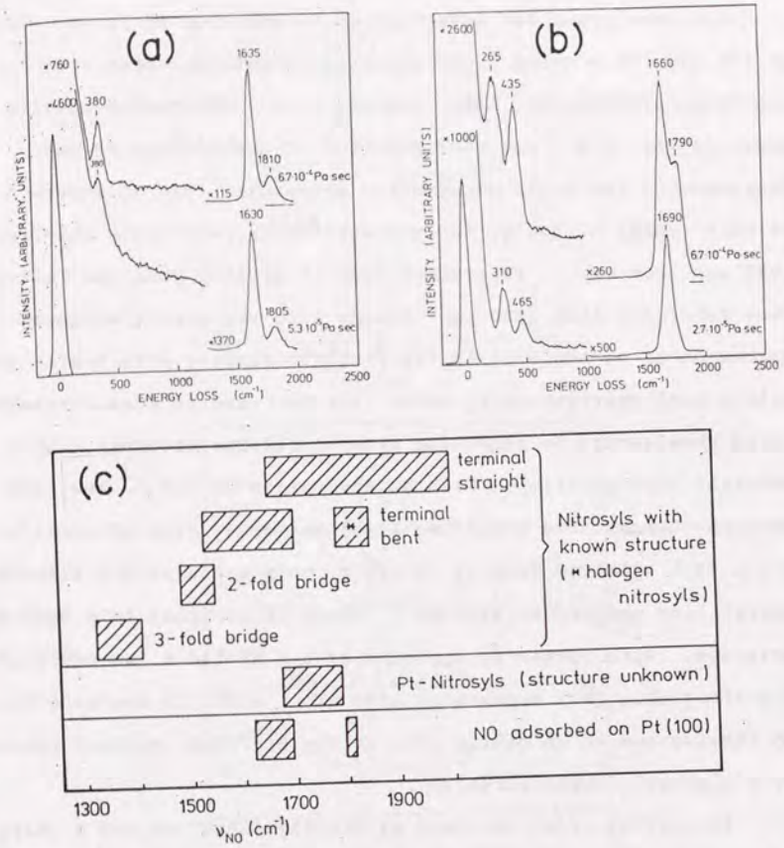

Fig. 1-3. (a) HREELS spectra of NO adsorbed on a Pt(001)-(20x5) surface at 300 K. The peak at 380 cm^{-1} probably represents the Pt-N-O bending. ($1x10^{-4}$ Pa·s = 0.76 L.) (b) HREELS spectra of NO adsorbed at 140 K on a Pt(001)-(20x5) surface. The peak at 310-265 cm^{-1} probably represents the Pt-NO stretching. (c) Summary plot of the experimentally observed ranges of the N-O stretching frequency for nitrosyl complexes and NO adsorbed on a Pt(001) surface. The notations "terminal (on-top) straight, etc." indicate the structure of the metal-NO system. (From ref. [16].)

islands are formed at 300 K, but the islands break up with heating to 408 K.

Recently, Gardner et al. measured RAIRS spectra of NO adsorbed on Pt(001)-(20x5) at 90 K as a function of NO exposure [18] (fig. 1-4(a)). With NO exposure at 90 K, the N-O stretching peak first appears at 1678 cm^{-1}, then shifts to 1697 cm^{-1}. With further NO exposure, however, the peak at 1697 cm^{-1} rapidly diminishes while a new peak appears at ~1630 cm^{-1} accompanied by a broader peak at ~1800 cm^{-1}. This drastic change occurred in a relatively narrow exposure range of 0.5-0.7 L. They assigned the initial peak at 1678-1697 cm^{-1} and the new peak at ~1630 cm^{-1} to NO chemisorbed on the Pt-(20x5) surface and NO on the Pt-(1x1) surface, respectively, and concluded that the (20x5)→(1x1) structural transformation of the top-most Pt layer occurs at the critical amount of NO exposure. The critical amount was found to depend on the surface temperature (fig. 1-4(b)).

Schmidt et al. measured temperature programed desorption spectra (TPDS) of NO adsorbed on Pt(001)-(20x5) at 120 K [19, 20] (fig. 1-5(a) and (b)). Four prominent NO desorption peaks were observed at 550, 500, 340, and 150 K. The low temperature peaks at 340 and 150 K were observed to develop only after larger NO exposure. The high temperature shoulder at 550 K is suggested to be induced by the (1x1)→(20x5) structural transformation of the Pt(001) surface. The NO-NO interaction in binding state at 340 K is suggested to be repulsive, because the desorption peak shifts to the lower temperature region with increasing NO exposure. The activation energy of desorption for the binding states at 500 and

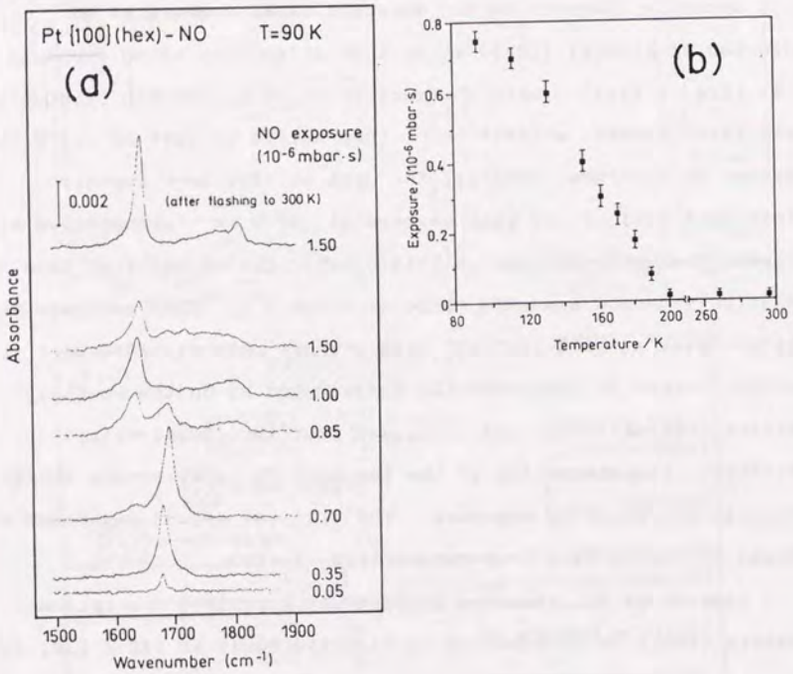

Fig. 1-4. (a) RAIRS spectra of NO adsorbed on Pt(001)-(20x5) at 90 K, shown as a function of exposure. Top curve is the spectrum of an NO-saturated Pt(001) surface after flashing to 300 K followed by recooling to 90 K. (1×10^{-6} mbar·s = 0.76 L.) (b) Surface temperature dependence of the critical amount of NO exposure required to induce the (20x5)→(1x1) structural transformation. The critical amount was taken as the point where the ~1680 cm^{-1} peak reaches its maximum frequency. (From ref. [18].)

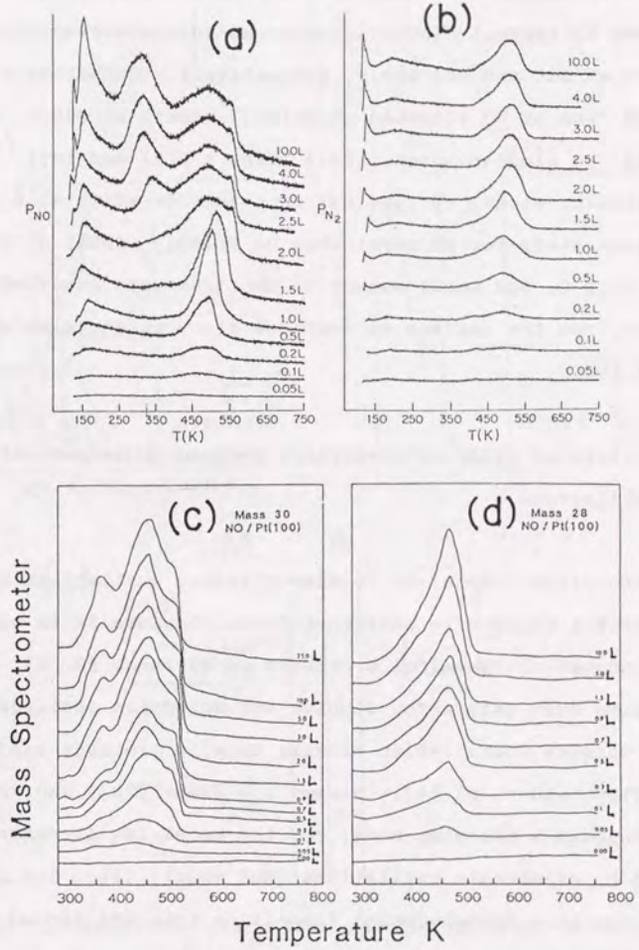

Fig. 1-5. (a) Mass 30 (NO) and (b) mass 28 (N_2) TPDS spectra for NO adsorbed on Pt(001)-(20x5) at 120 K for a heating rate of 17 K/s. (From ref. [20].) (c) Mass 30 (NO) and (d) mass 28 (N_2) TPDS spectra for NO adsorbed on Pt(001)-(20x5) at 300 K for a heating rate of 14 K/s. (From ref. [21].)

340 K is estimated as 36 and 25 kcal/mole, respectively. N_2 and O_2 formed by thermal dissociation of NO were observed to be desorbed at 500 and 700-900 K, respectively. Gohndrone and Masel measured TPDS of NO adsorbed on Pt(001)-(20x5) at 300 K, and obtained the similar spectra [21] (fig. 1-5(c) and (d)).

Schwalke et al. carried out an electron-stimulated ion desorption study for NO chemisobed on Pt(001)-(20x5) at 300 K [22]. Only O^+ and small amount of O_2^+ ions were observed to be desorbed from the surface at incident electron energies above 565 ± 5 eV.

1.3 History of study on desorption induced by valence-electron excitations

Desorption induced by valence-electron excitations has been an important subject in surface science, because it is one of the most fundamental dynamical processes on surfaces [8, 9]. However, there have been only a few studies for molecules chemisorbed on metal, because deexcitation process usually proceeds rapidly on metal (10^{-14}~10^{-15} s) [9]. Menzel and Gomer [23], and Redhead [24] proposed a two-step model for the mechanism of desorption induced by electronic excitations (MGR model) (fig. 1-6(a)). The first step is a Franck-Condon transition from the ground state of an adsorbate to an antibonding state of the system. Then, the excited adsorbate moves away from the surface along the repulsive potential surface. If the lifetime of the excited adsorbate is long enough, the adsorbate acquire enough energy, and is desorbed

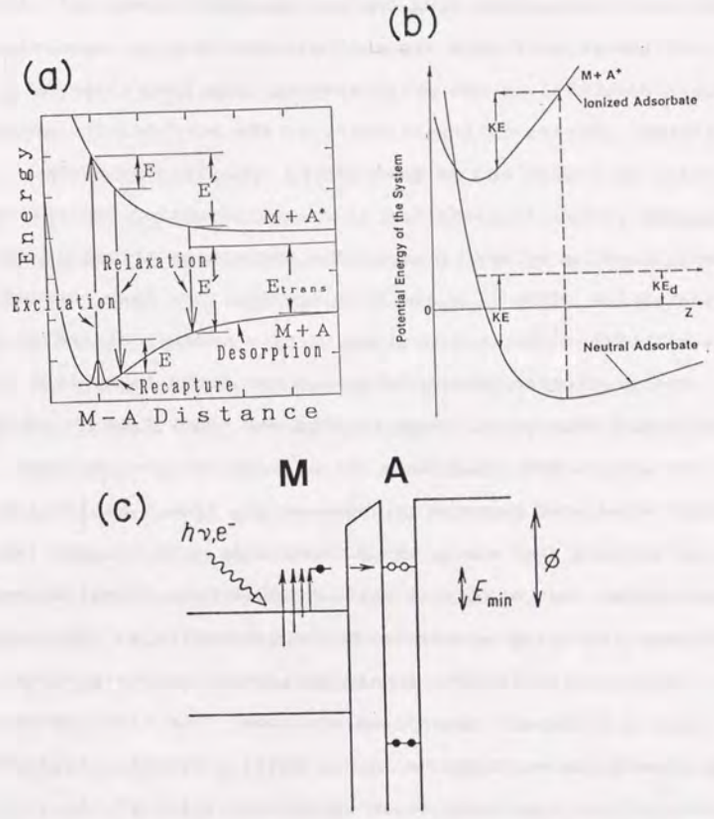

Fig. 1-6. (a) Model for desorption induced by electronic excitation (MGR model). M and A represent the metal surface and the adsorbate, respectively. (b) Model for desorption induced by electronic excitation proposed by Antoniewicz (from ref. [25]). (c) Model for the intermediate excited state formation from which the non-thermal desorption proceeds proposed by Menzel et al. (from ref. [27]).

as a neutral molecule after deexcitation. Antoniewicz proposed a modified two-step model [25] (fig. 1-6(b)). The first step is a Franck-Condon transition from the ground state to an ionic state. The ionic adsorbate starts its motion toward the surface owing to the image potential of the metal surface. In the following deexcitation process in the vicinity of the surface, the adsorbate aquire enough energy and is desorbed as a neutral molecule.

Menzel et al. investigated electron-stimulated desorption of CO chemisorbed on W, and observed the desorption threshold energy of 2.5-5 eV [26, 27]. For the W-CO system, they also carried out a photostimulated desorption study using a mercury discharge lamp [28]. The desorption threshold energy was found to be less than 2.75 eV. The desorption cross section was about 5×10^{-21} cm^2 at ~5 eV. A simple MGR model does not account for the observed electron-stimulated desorption, because the lowest excitation state of CO lies 6 eV above the ground state. To account for the low threshold, they suggested that the CO-W bond formation may lead to new low-lying unoccupied molecular orbitals. Two possible models are proposed for the intermediate excited state formation from which non-thermal desorption proceeds. The first mechanism is the electronic excitations in the metal substrate, followed by elastic electron tunneling to an unoccupied state of the adsorbate-metal complex through the surface barrier (fig. 1-6(c)). The second mechanism is similar to the initial process of a MGR model, i. e. the Franck-Condon transition from the ground state to a neutral repulsive state of the adsorbate-metal complex.

Since the pioneering works described above, desorption

induced by valence-electron excitations have been investigated using an electron gun, a discharge lamp, or a laser for a wide range of the metal-adsorbate and modified metal-adsorbate systems such as Ni-NO [29], Pt(111)-NO [10, 12, 30], Pd(111)-NO [11], Pt(111)-O_2+NO [31], Ru(001)-CO [32], Ru(001)-N_2 [32], W-H_2 [27], Pd(111)-O_2 [33-35], Pt(111)-O_2 [36], Ag(110)-O_2 [37], Pd(111)-O [34], Ni(001)-NiO-NO [38], Ni(111)-NiO-NO [39], Ni(111)-O-NO [39], Ni(111)-S-NO [39], and so on. In the thesis, however, I confine the survey to the state selective electron-stimulated or photo-stimulated desorption studies of NO chemisorbed on metal or modified metal surfaces, which are most related to the present work. In these studies, desorbed NO molecules in the ground electronic states ($X^2\Pi_\Omega$,(v",J"), where Ω", v", and J" represent the z-principal axis component of the total electron angular momentum, vibrational quantum number, and rotational quantum number, respectively) are detected using a (1+1) resonance-enhanced multiphoton ionization ((1+1)REMPI) or a laser-induced fluorescence (LIF) technique, which has proved to be a powerful tool in elucidation of desorption mechanisms [40].

1.4 State-selective studies of desorption induced by valence-electron excitations for NO chemisorbed on metal or modified metal surfaces

Burns investigated electron-stimulated desorption of NO chemisorbed on a Ni film at 80 K using (1+1)REMPI [29]. The translational energy distribution peaks at 0.1 eV, corresponding

to a translational temperature of 1200 K, if a Maxwell distribution is assumed. The $X^2\Pi(v"=1)/X^2\Pi(v"=0)$ population ratio corresponds to a vibrational temperature of 700 K. The rotational energy was characterized by a nearly-Boltzmann distribution with a rotational temperature of ~400 K. On the basis of these results, they concluded that the desorption is induced by valence-electron excitations.

Using (1+1)REMPI, Burns et al. carried out a rather thorough electron-stimulated study for NO chemisorbed on Pt(111) at 80 K [30]. The translational energy distributions of desorbed NO indicated that two desorption channels are present, i. e. a dominant low-energy channel (peaks at 0.05 eV, corresponding to ~580 K, if a Maxwell distribution is assumed)) with a threshold of ~6 eV, and a high-energy channel (peaks at 0.35 eV) with a threshold of ~20 eV. The high-energy channel was attributed to multiple-hole states created by complex electronic excitations. Desorbed NO in the two spin orbit states (the $X^2\Pi_{1/2}(v"=0)$ and $X^2\Pi_{3/2}(v"=0)$ states) exhibited similar rotational distributions characterized by nearly-Boltzmann distributions with rotational temperatures of 500~640 K. On the basis of these results, they concluded that NO is desorbed via a long-lived relatively-free-rotor excited state created by the $2\pi_a \leftarrow 5\sigma$ transition of chemisorbed NO. A calculation based on a single-atom approximation indicated that the lifetime of a 5σ hole is relatively long ($\sim 1\times10^{-14}$ s). This model was supported by calculations using a two-dimensional wavepacket propagation method, where the NO-Pt distance and the NO-Pt polar angle are considered. A simple model

potential surface was used in the calculations on the basis of the assumption that the intermediate excited state resembles an O_2 molecule adsorbed on Pt(111).

Buntin et al. have investigated laser-stimulated desorption of NO chemisorbed on Pt(111) at 120 K for 1064, 532, and 355 nm (1.2, 2.3, and 3.5 eV, respectively) using an LIF technique [10]. Two desorption channels were observed to be present. One was assigned to a laser-induced thermal desorption associated with weakly bound NO. The other was assigned to a non-thermal desorption associated with chemisorbed NO on on-top site. The latter channel exhibited the following characteristics: (1) The desorption yield is proportional to laser fluence. The quantum yields for desorption are 5×10^{-9}, 4×10^{-8}, 5×10^{-8} for 1064, 532, and 355 nm, respectively. (2) The translational energy is independent of laser fluence. (Non-Maxwell distributions, ~1200 K for 532 and 355 nm, if a Maxwell distribution is assumed). (3) The internal energy exhibits a non-Boltzmann distribution with markedly inverted spin-orbit population. (4) The $X^2\Pi(v"=1)/X^2\Pi(v"=0)$ population ratios for 355, 532, 1064 nm are 0.04, 0.04, and <0.004, respectively. (NO in thermal equibilium at 840 K gives a v"=1/v"=0 ratio of 0.04.) (5) The desorption flux exhibits a $\cos^{11}\theta$ distribution for NO in the $X^2\Pi_{3/2}(v"=0,J"=17.5)$ state. On the basis of these results, Buntin et al. proposed a model that NO is desorbed by an Antoniewicz-type mechanism (See Section 1.3 and fig. 1-6(b)) via a temporal negative ion state created by an elastic electron tunneling from photogenerated hot carriers in the metal substrate to an unoccupied state of chemisorbed NO (See

fig. 1-6(c)). Comparison of the pump laser polarization dependence of the desorption yield between the incident angles of 0° and 70° supported the conclusion that excitations not in the chemisorbed NO but in metal substrate is responsible for the non-thermal desorption.

Budde et al. have investigated laser-stimulated desorption of NO adsorbed on a non-metallic Ni(001)-NiO surface at 140 K for 193 and 248 nm (6.41 and 5.0 eV, respectively) using LIF, and observed two desorption channels [38]. One channel was tentatively assigned to a laser-induced thermal desorption. The following results are reported for the other desorption channel: (1) The quantum yield for desorption is of the order of 10^{-2} for 193 nm, corresponding to a cross section of ~2×10^{-17} cm^2. (2) The translational temperature increases from ~1000 to ~3000 K with increasing internal energy, if a Maxwell distribution is assumed. (3) The rotational energy of desorbed NO in the $X^2\Pi_{1/2}(v"=0)$ state exhibits a nearly-Boltzmann distribution with a rotational temperature of ~360 K for 193 nm. However, the rotational energy in the $X^2\Pi_{3/2}(v"=0)$ state is markedly non-Boltzmann for low J" levels, and the $X^2\Pi_{1/2}(v"=0)/X^2\Pi_{3/2}(v"=0)$ population ratio reaches values of ~40 in the low J" region. (4) The $X^2\Pi(v"=1)/X^2\Pi(v"=0)$ population ratio is 0.01, corresponding to a vibrational temperature of ~600 K. On the basis of these results, they concluded that desorption is induced by electronic excitations. However, the detailed mechanism was not proposed.

Prybyla et al. have carried out a photostimulated desorption study for NO chemisorbed on Pd(111) at 300 K using 200-fs laser

pulse of 2.0-eV photon energy and (1+1)REMPI [11]. They reported the following results: (1) The laser fluence dependence of the desorption yield is represented by a power-law relation with an exponent of n = 3.3. The quantum yield for desorption is 3×10^{-4} for an absorbed fluence of 3 mJ/cm^2, corresponding to a cross section of 4×10^{-19} cm^2. (2) The translational temperature is ~1200 K for an absorbed fluence of 3 mJ/cm^2, if a Maxwell distribution is assumed. (3) The rotational energy is represented by two Boltzmann distributions with rotational temperatures of 400 and 2600 K. The two spin-orbit states exhibit similar populations for most J" levels, corresponding to a very high spin-orbit temperature. (4) The $X^2\Pi(v"=1)/X^2\Pi(v"=0)$ population ratio is ~0.3 corresponding to a vibrational temperature of 2200 K. They concluded that high density of electronic excitation in the metal substrate induced by the 200-fs laser pulse leads to novel desorption channels involving both the ground and excited electronic states of the chemisorbed NO.

Recently, Schwarzwald et al. have carried out a preliminary study of photostimulated desorption for NO chemisorbed on Pt(111) at 90 K for 193 nm using a (1+1)REMPI two-dimensional imaging technique [12]. The following results are reported: (1) The desorption yield is proportional to laser fluence. The quantum yield for desorption is in the range of 10^{-4}~10^{-5}. (2) The translational energy is independent of laser fluence. (A non-Maxwell distribution, ~1620 K, if a Maxwell distribution is assumed). (3) The rotational energy distribution appears non-Boltzmann in general with the high rotational levels much more

populated than those in equibilium with the substrate temperature. (4) The desorption flux exhibits a $\cos^4\theta$ distribution. These results indicate that photostimulated desorption is induced by electronic excitations. However, difinitive conclusion was not drawn for the mechanism.

Most of the electron-stimulated and the photostimulated desorption studies described in the present section were carried out contemporaneously with the present work. Recently, these phenomena have begun to attract interest of more and more researchers in the field of not only surface science, but also molecular science, photochemistry, and applied physics concerned with the technological processes such as photoetching and sputtering. Nevertheless, the elementary processes of the non-thermal desorption are far from being understand. This field will be developed the more in future.

References

[1] The Structure of Surfaces, eds. M.A. Van Hove and S.Y. Tong (Springer-Verlag, Berlin, 1985); The Structure of Surface-2, eds. J.F. van der Veen and M.A. Van Hove (Springer-Verlag, Berlin, 1988).

[2] T. Gritsch, D. Coulman, R.J. Behm, and G. Ertl, Phys. Rev. Lett. 63, 1086 (1989); S. Rousset, S. Gauthier, O. Siboulet, W. Sacks, M. Belin, and J. Klein, Phys. Rev. Lett. 63, 1265 (1989); D.J. Coulman, J. Wintterlin, R.J. Behm, and G. Ertl, Phys. Rev. Lett. 64, 1761 (1990).

[3] P. Heilmann, K. Heinz, and K. Müller, Surf. Sci. 83, 487 (1979).

[4] M.A. Van Hove, R.J. Koestner, P.C. Stair, J.P. Bibérian, L.L. Kesmodel, I. Bartoš, and G.A. Somorjai, Surf. Sci. 103, 189 (1981).

[5] H.P. Bonzel and G. Pirug, Surf. Sci. 62, 45 (1977).

[6] P.R. Norton, J.A. Davies, D.K. Creber, C.W. Sitter, and T.E. Jackman, Surf. Sci. 108, 205 (1981).

[7] T.J. Chuang, Surf. Sci. Rep. 3, 1 (1983).

[8] Desorption Induced by Electronic Transitions, DIET-1, eds. N.H. Tolk, M.M. Traum, J.C. Tully, and T.E. Madey (Springer-Verlag, Berlin, 1983); Desorption Induced by Electronic Transitions, DIET-2, eds. W. Brenig and D. Menzel (Springer-Verlag, Berlin, 1985); Desorption Induced by Electronic Transitions, DIET-3, eds. R.H. Stulen and M.L. Knotek (Springer-Verlag, Berlin, 1987).

[9] Ph. Avouris and R.E. Walkup, Ann. Rev. Phys. Chem. 40, 173 (1989), and references therein.

[10] S.A. Buntin, L.J. Richter, R.R. Cavanagh, and D.S. King, Phys. Rev. Lett. 61, 1321 (1988); S.A. Buntin, L.J. Richter, D.S. King, and R.R. Cavanagh, J. Chem. Phys. 91, 6429 (1989).

[11] J.A. Prybyla, T.F. Heinz, J.A. Misewich, M.M.T. Loy, and J.H. Glownia, Phys. Rev. Lett. 64, 1537 (1990).

[12] R. Schwartzwald, A. Mödl, and T.J. Chuang, Surf. Sci., in press.

[13] H.P. Bonzel, G. Brodén, and G. Pirug, J. Catal. 53, 96 (1978).

[14] K. Heinz, E. Lang, K. Strauss, and K. Müller, Surf. Sci. 120, L401 (1982).

[15] G. Brodén, G. Pirug, and H.P. Bonzel, Surf. Sci. 72, 45 (1978).

[16] G. Pirug, H.P. Bonzel, H. Hopster, and H. Ibach, J. Chem. Phys. 71, 593 (1979).

[17] W.F. Banholzer and R.I. Masel, Surf. Sci. 137, 339 (1984).

[18] P. Gardner, M. Tüshaus, R. Martin, and A.M. Bradshaw, Vacuum 41, 304 (1990).

[19] R.J. Gorte, L.D. Schmidt, and J.L. Gland, Surf. Sci. 109, 367 (1981).

[20] M.W. Lesley and L.D. Schmidt, Surf. Sci. 155, 215 (1985).

[21] J.M. Gohndrone and R.I. Masel, Surf. Sci. 209, 44 (1989).

[22]. Schwalke, H. Niehus, and G. Comsa, Surf. Sci. 137, 23 (1984).

[23] D. Menzel and R. Gomer, J. Chem. Phys. 41, 3311 (1964).

[24] P.A. Redhead, Can. J. Phys. 42, 886 (1964).

[25] P.R. Antoniewicz, Phys. Rev. B 21, 3811 (1980).

[26] D. Menzel, Ber. Bunsenges. Phys. Chem. 72, 591 (1968).

[27] D. Menzel, P. Kronauer, and E. Jelend, Ber. Bunsenges. Phys. Chem. 75, 1074 (1971).

[28] P. Kronauer and D. Menzel, in: Adsorption-Desorption Phenomena, ed. F. Ricca (Academic Press, New York, 1972) p.313.

[29] A.R. Burns, Phys. Rev. Lett. 55, 525 (1985); A.R. Burns, J. Vac. Sci. Technol. A 4, 1499 (1986).

[30] A.R. Burns, E.B. Stechel, and D.R. Jennison, Phys. Rev. Lett.58, 250 (1987); A.R. Burns, D.R. Jennison, and E.B. Stechel,

J. Vac. Sci. Technol. A 5, 671 (1987); A.R. Burns, E.B. Stechel, and D.R. Jennison, J. Vac. Sci. Technol. A 6, 895 (1988).

[31] W.D. Mieher and W. Ho, J. Chem. Phys. 92, 5162 (1990).

[32] P. Feulner, R. Treichler, and D. Menzel, Phys. Rev. B 24, 7427 (1981).

[33] X. Guo, L. Hanley, and J.T. Yates, Jr., J. Chem. Phys. 90, 5200 (1989); L. Hanley, X. Guo, and J.T. Yates, Jr., J. Chem. Phys. 91, 7220 (1989); J. Yoshinobu, X. Guo, and J.T. Yates, Jr., Chem. Phys. Lett. 169, 209 (1990).

[34] A. Hoffman, X. Guo, and J.T. Yates, Jr., J. Chem. Phys. 90, 5793 (1989).

[35] M. Wolf, E. Hasselbrink, J.M. White, and G. Ertl, J. Chem. Phys. 93, 5327 (1989).

[36] X.-Y. Zhu, S.R. Hatch, A. Campion, and J.M. White, J. Chem. Phys. 91, 5011 (1989); J.M. White, S.R. Hatch, X.-Y. Zhu, and A. Campion, Vacuum 41, 282 (1990).

[37] S.R. Hatch, X.-Y. Zhu, J.M. White, and A. Campion, J. Chem. Phys. 92, 2681 (1990).

[38] F. Budde, A.V. Hamza, P.M. Ferm, G. Ertl, D. Weide, P. Andresen, and H.-J. Freund, Phys. Rev. Lett. 60, 1518 (1988); P.M. Ferm, F. Budde, A.V. Hamza, S. Jakubith, G. Ertl, D. Weide, P. Andresen, and H.J. Freund, Surf. Sci. 218, 467 (1989).

[39] J. Yoshinobu, X. Guo, and J.T. Yates, Jr., J. Chem. Phys. 92, 7700 (1990).

[40] D.S. King and R.R. Cavanagh, in: Advances in Chemical Physics Vol. 75, ed. K.P. Lawley (John Wiley & Sons, New York, 1989) p.45.

CHAPTER 2

LEED Observation of NO Adsorption-Induced Structural Transformation on Single-Domain Pt(001)-(20x5) Surface

NO adsorption-induced structural transformation of Pt(001) surface at temperatures of 80-140 K is studied using LEED and a single-domain Pt(001)-(20x5) surface. The structural transformation and the NO layer growth process are observed to depend on the surface temperature remarkably. At 330-390 K, a double-domain NO-c(2x4) layer grows while relaxing the topmost hexagonal Pt layer into the (1x1) structure. On the other hand, a single-domain NO-c(2x4) layer grows anisotropically at 230-270 K. At 80 K, the (20x5)→(1x1) structural transformation of the topmost Pt layer occurs abruptly in an NO exposure range of 0.8-1.0 L. The mechanism of the single-domain Pt(001)-(20x5) surface formation is discussed. A detailed model for the microscopic mechanism of the anisotropic growth of the single-domain NO-c(2x4) layer at 230-270 K is proposed.

2.1 Introduction

As is stated in Section 1.2, a clean Pt(001) surface is known to exhibit a (20x5)-like LEED pattern, for which a model is proposed that the topmost Pt layer is reconstructed hexagonally with a rotation angle of 0.7° [1, 2] (see fig. 1-1). In detailed investigations using LEED, Behm et al. have proposed a "nucleation and growth" mechanism for the structural transformation of a Pt(001)-(20x5) surface into the bulk-like (1x1) structure induced by CO adsorption, i. e. the (20x5)→(1x1) transformation starts at some parts of the surface owing to the nucleation of adsorbed CO, and proceeds from there over the rest area of the surface [3, 4]. This model was supported by scanning tunneling microscopy (STM) studies [5, 6] and a Rutherford backscattering (RBS) study [7].

The (20x5)→(1x1) transformation of a Pt(001) surface is also induced by adsorption of NO [8, 9]. Bonzel et al. investigated NO adsorbed on Pt(001)-(20x5) at 300 K, and reported that NO is chemisorbed molecularly [8] with N-end down on an on-top site [9] (see Section 1.2). In an STM study of a Pt(001)-(20x5) surface, Ritter et al. observed striped hillocks after submonolayer NO adsorption at 295 K, and assigned them to the Pt-(1x1) islands with mono-atomic height (fig. 2-1) [6]. Ritter et al. have also reported the following results [6]: (1) The step does not act as an especially active center for the striped Pt-(1x1) island formation. (2) The Pt-(1x1) islands grow preferentially in the direction coincident with the corrugations of the reconstructed Pt-(20x5) area. (3) Then, the islands begin to grow laterally,

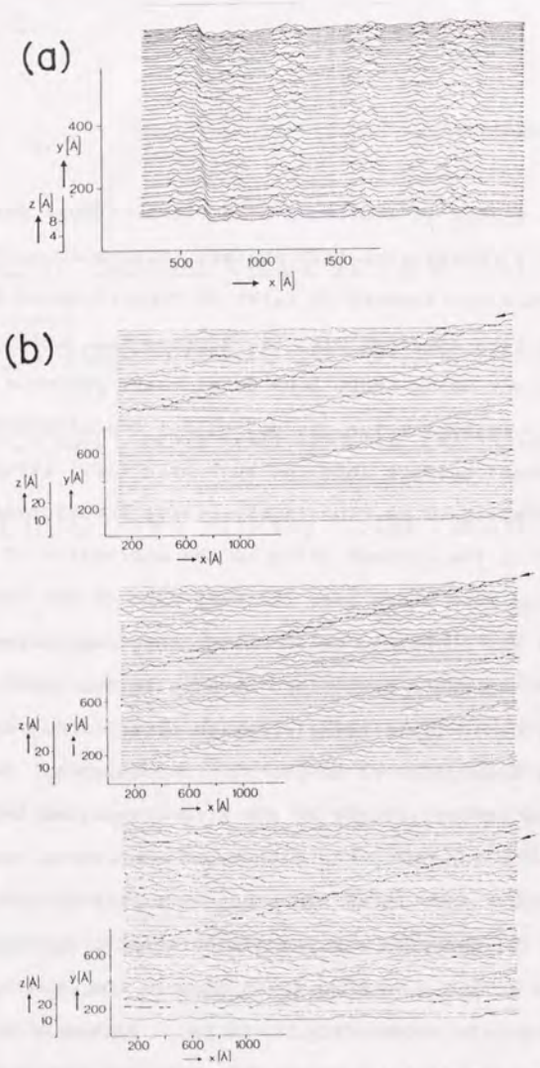

Fig. 2-1. (a) STM image of a Pt(001)-(20x5) surface after submonolayer adsorption of NO at 295 K. A monoatomic step separates two flat terraces in the left-hand side of the image. (b) Sequence of STM images of a Pt(001)-(20x5) surface during NO exposure at 295 K (NO pressure = 4×10^{-8} Torr). Arrows mark a monoatomic step passing through the area. (From ref. [6].)

normal to the preferential growth direction.

To elucidate the detailed microscopic mechanism for the anisotropic (20x5)→(1x1) structural transformation of topmost Pt layer and the NO layer growth process, I have carried out a LEED study of NO adsorption on a single-domain Pt(001)-(20x5) surface at 80-410 K. The structural transformation and the NO layer growth process were observed to depend on the surface temperature remarkably. At 330-390 K, a double-domain NO-c(2x4) layer was observed to grow while relaxing the topmost hexagonal Pt layer into the (1x1) structure. On the other hand, a single-domain NO-c(2x4) layer grows anisotropically at 230-270 K. At 80 K, the (20x5)→(1x1) structural transformation of the topmost Pt layer was found to occur abruptly in a relatively narrow NO exposure range of 0.8-1.0 L. The mechanism of the single-domain Pt(001)-(20x5) surface formation was discussed. A detailed model for the microscopic mechanism of the anisotropic growth of the single-domain NO-c(2x4) layer observed at 230-270 K is proposed.

2.2 Experiment

Measurments were carried out in an ultra-high-vacuum (UHV) chamber (base pressure < 7×10^{-11} Torr) equiped with four-grid LEED/Auger electron spectroscopy (AES) optics (ULVAC-PHI 15-120). A Pt single crystal (purity = 99.999%, Aremco Products) was oriented with an X-ray diffraction technique, and cut with a multi-wire saw within 2° of the (001) plane. A Pt crystal disk of 6-mm-diameter with 0.7-mm-thick was polished mechanically to

1/4 μm with diamond paste, and was mounted on a sample holder attached to the end of a low-temperature manipulator [10]. An electron bombardment gun was placed just behind the Pt crystal, so that surface cleaning could be carried out without changing the sample position. The Pt(001) surface was cleaned through a standard procedure [2]. The surface temperature was monitored with a Pt-Pt·Rh13% thermocouple spot-welded on the side of the crystal. The cleanliness of the surface was checked by LEED and AES. Before every LEED observation, the Pt(001) surface was cleaned with a combination of O_2 treatment (3×10^{-7} Torr, 1190 K, 10 min) and flashing in UHV (1400 K, 30 s). Then, the clean Pt(001)-(20x5) surface was exposed to NO (purity = 99.9%) at various surface temperatures, and quickly cooled down to 80±3 K with liquid nitrogen. The surface temperature during NO exposure was kept at a constant value by controlling the filament current of the electron bombardment gun behind the Pt crystal. The NO pressure measured with a B-A ionization gauge (typically 1×10^{-7} Torr, unless otherwise stated) and the exposure time were recorded with a transient recorder. NO exposure was corrected by a facter of 1.16 for the gauge sensitivity against NO gas. Every LEED observation was carried out under a pressure of lower than 1×10^{-9} Torr at the surface temperature of 80±3K.

2.3 Results

2.3.1 Single-domain clean Pt(001)-(20x5) surface

The clean Pt(001) surface exhibits a sharp (20x5)-like LEED pattern. In some area of the surface, only a single-domain out of the four possible domains is present, as is shown in fig. 2-2(a). I have prepared an almost clean Pt(001)-(1x1) surface through NO and H_2 treatments [11] (fig. 2-2(b)) (see Section 1.2), and observed how the atomic and domain structure changes after annealing at various temperatures (fig. 2-2(c)-(f)). The results are consistent with those reported in a LEED study by Heinz et al. [12], i. e. the (1x1) structure transforms to a (1x5) structure, and to a non-rotated hexagonal structure, then finally to a rotated hexagonal structure above ~1100 K (see Section 1.2). The single-domain pattern is observed to be enhanced after annealing at 950 K, and becomes predominant after annealing above 1100 K.

2.3.2 NO adsorption at 330-410 K

Figure 2-3 shows the LEED patterns of the single-domain Pt(001)-(20x5) surface after various NO exposures at various surface temperatures. The LEED pattern remained almost unchanged after NO exposure above 410 K (fig. 2-3(a)), which is in agreement with a study by Bozel et al. [11] (see Section 1.2). With NO exposure of ~2.0 L (1 L = 1×10^{-6} Torr·s) at 330-390 K, a c(2x4)- and c(4x2)-like pattern appears (fig. 2-3(b)-(e)), which is known to characterize the double-domain NO layer on a Pt(001)-(1x1) surface [8, 9, 11]. The contrast of the c(2x4)-like pattern to the (20x5) pattern shows that the sticking coefficient of NO on a Pt(001)-(20x5) surface increases as the surface temperature

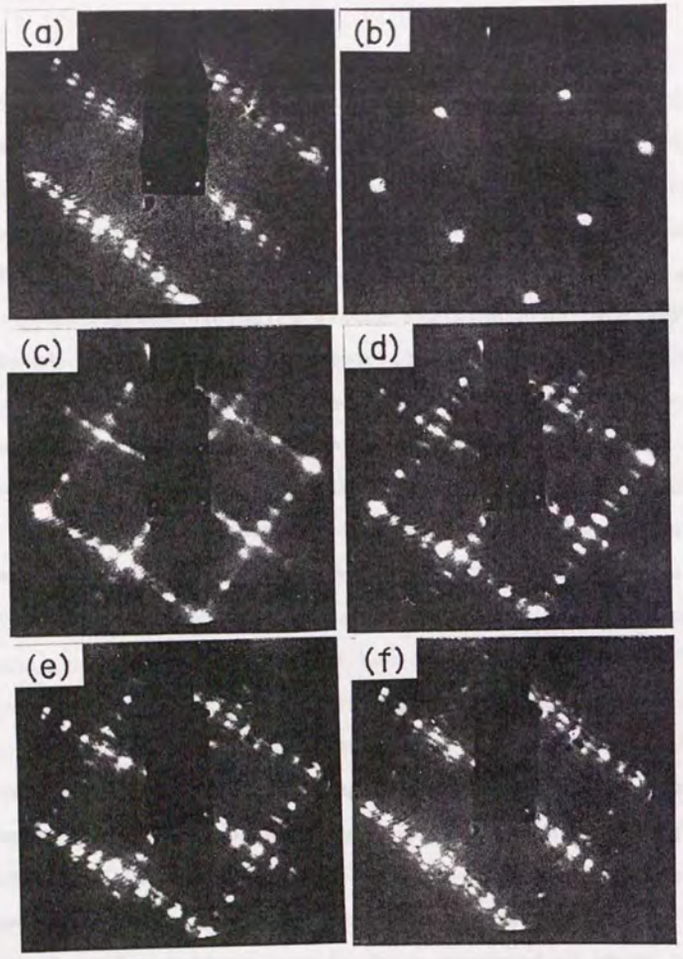

Fig. 2-2. (a) LEED pattern of a clean single-domain Pt(001)-(20x5) surface. (b) LEED pattern of an almost clean Pt(001)-(1x1) surface. (c)-(f) LEED patterns of an almost clean Pt(001)-(1x1) surface after annealing at (c) 500 K, (d) 650, (e) 950, and (f) 1100 K. The primary electron energy (E_p) was 85 eV for every pattern. The LEED patterns are slightly distorted by the voltage applied to the lens system of the electron gun in the LEED optics.

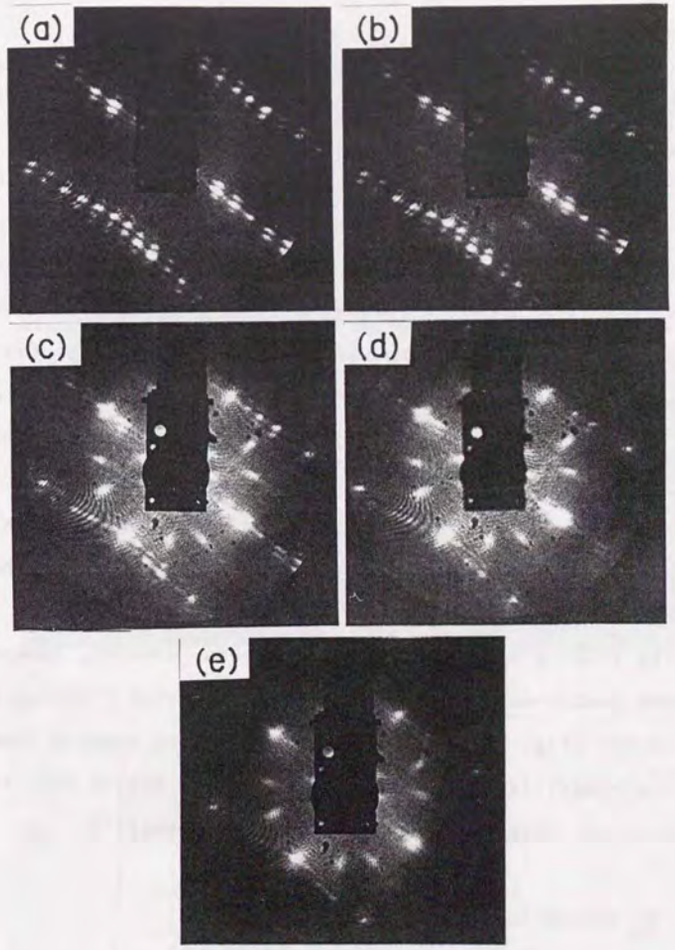

Fig. 2-3. LEED patterns of a single-domain Pt(001)-(20x5) surface after NO exposure of ~2 L at various surface temperatures: (a) 2.1 L at 412±5 K, (b) 2.3 L at 387±3 K, (c) 1.8 L at 359±3 K, (d) 2.0 L at 346±3 K, (e) 2.1 L at 332±5 K. E_p = 75 eV for every pattern.

decreases. The c(2x4)-like pattern was observable for a wide primary electron energy range of 30-120 eV (fig. 2-4(a)-(e)).

With increasing NO exposure at 359 K, the double-domain c(2x4)-like pattern becomes bright, while the (20x5) pattern gradually disappear (fig. 2-5(a)-(c)). These observations are consistent with a study using reflection-absorption infrared spectroscopy (RAIRS) by Banholzer and Masel, which reported that adsorbed NO form islands at 300 K [13] (see Section 1.2). A trace of the (1x5) spots were observable even after NO exposure of 8.5 L at $1x10^{-7}$ Torr, (fig. 2-5(c)). The c(2x4)-like pattern, however, becomes streaky and fuzzy with prolonged annealing at 358 K in UHV (fig. 2-5(d)). With NO exposure of 70 L at $2x10^{-6}$ Torr, the LEED pattern changed into a (1x1) pattern with high background intensity (fig. 2-5(e)). The (1x1) pattern, however, changes into a streaky double-domain c(2x4)-like pattern after flashing at 359 K in UHV (fig. 2-5(f)). These observations suggest that the (1x1) and c(2x4)-like structures at 359 K are stable only in an NO atmosphere of $\sim 2x10^{-6}$ and $\sim 1x10^{-7}$ Torr, respectively.

2.3.3 NO adsorption at 230-300 K

Figure 2-6 shows the LEED patterns of the single-domain Pt(001)-(20x5) surface after NO exposure of ~2 L at surface temperatures of 220-300 K. The (1/2 1/4) and (1/2 3/4) spots were found to be brighter than the (1/4 1/2) and (3/4 1/2) spots at 280-300 K (fig. 2-6(a) and (b)). Only the (1/2 1/4) and (1/2 3/4) spots were observable at 230-270 K (fig. 2-6(c)-(e)). Fuzzy

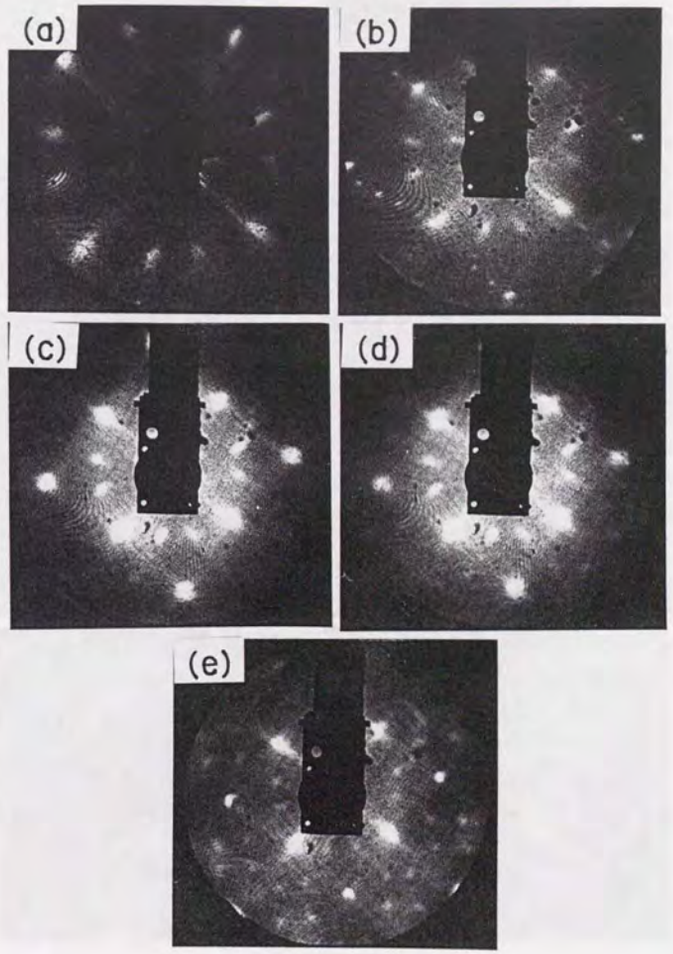

Fig. 2-4. LEED patterns of a single-domain Pt(001)-(20x5) surface after NO exposure of 6.7 L at 358±6 K. E_p = (a) 39 eV, (b) 65 eV, (c) 85 eV, (d) 92 eV, (e) 115 eV, respectively.

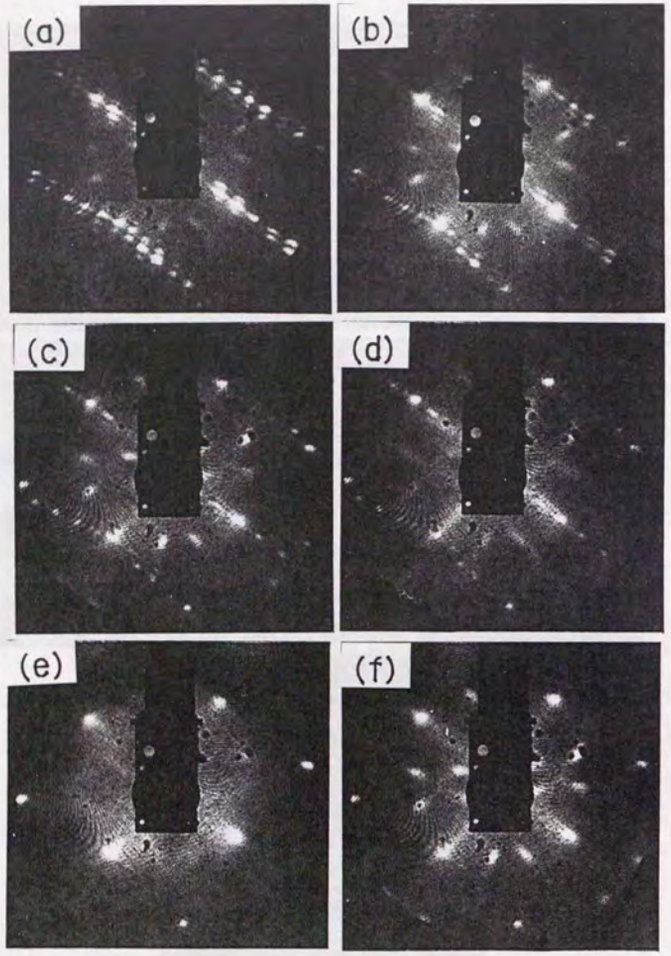

Fig. 2-5. LEED patterns of a single-domain Pt(001)-(20x5) surface after various NO exposures at 359±5 K: (a) 0.68 L, (b) 3.4 L, (c) 8.5 L, (d) 8.5 L followed by annealing at 359±5 K for 30 s in UHV, (e) 70 L, (f) 70 L followed by flashing at 359±5 K for 2 s in UHV. E_p = 75 eV for (a) and (b), and 65 eV for (c)-(f), respectively. NO pressure was 1×10^{-7} Torr for (a)-(d), and 2×10^{-6} Torr for (e) and (f), respectively.

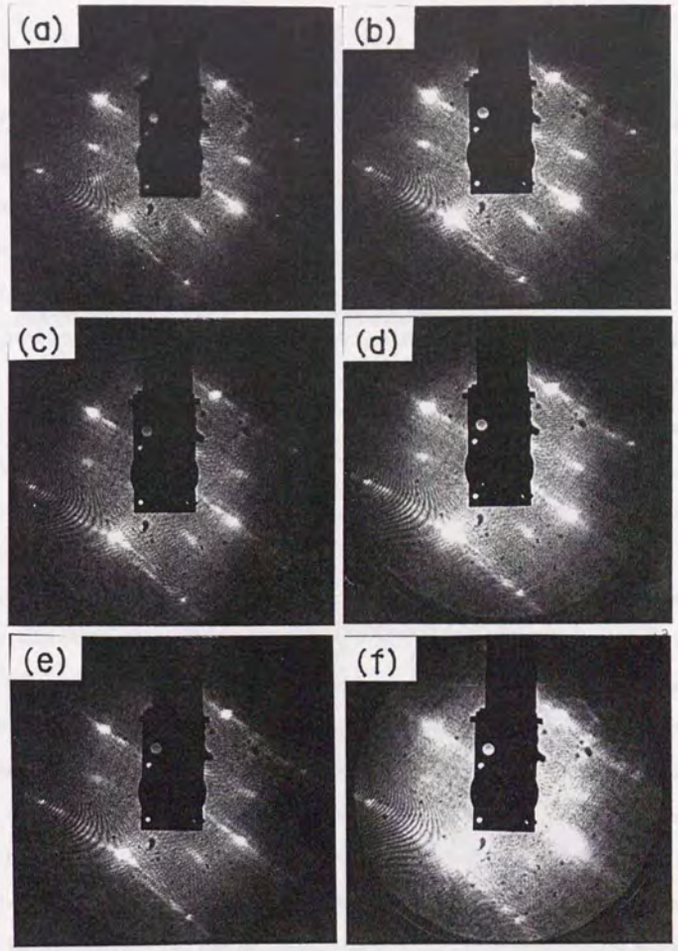

Fig. 2-6. LEED patterns of a single-domain Pt(001)-(20x5) surface after NO exposure of ~2 L at various surface temperatures: (a) 2.0 L at 300±3 K, (b) 1.8 L at 283±4 K, (c) 1.9 L at 272±4 K, (d) 2.1 L at 243±4 K, (e) 1.7 L at 231±5 K, (f) 2.2 L at 216±6 K. E_p = 75 eV for every pattern.

(1/2 1/4) and (1/2 3/4) spots with high background intensity were observed at 216 K (fig. 2-6(f)). Streaky spots at (1/2 1/4) and (1/2 3/4) are observable even after NO exposure of 0.26 L at 260 K (fig. 2-7(a)). The NO coverage is supposed to be less than 0.08 monolayers (ML) in this stage, even though the sticking coefficient is unity. This observation indicates that NO is aligned with twofold periodicity along the [110] derection. The most area of the Pt(001) surface is supposed to remain reconstructed, because the (1x1) spots are hardly enhanced. With increasing NO exposure, the (1x1) spots are enhanced, and the (1/2 1/4) and (1/2 3/4) spots become brighter and less streaky (fig. 2-7(b)-(e)). These observations indicate that (1) single-domain NO-c(2x4) islands are formed, that (2) the (20x5)→(1x1) transformation of the topmost Pt layer occurs only in the vicinity of adsorbed NO molecules, and that (3) the order of the NO-c(2x4) structure is higher in the [110] direction than in the [1$\bar{1}$0] direction during the island growth. The (20x5) pattern was scarcely observable after NO exposure of 2.2 L (fig. 2-7(e)), i. e. the (20x5)→(1x1) transformation is almost completed. With further NO exposure, the streaky (1/2 1/4) and (1/2 3/4) spots become spotty and gradually disappear (fig. 2-7(e) and (f)). The (1x1) pattern changes into a double-domain c(2x4)-like pattern with prolonged annealing at 260 K in UHV (fig. 2-7(g)). These observations suggest that the NO-(1x1) structure is compressed as compared with the NO-c(2x4) structure, and that the (1x1) structure is metastable in UHV at 260 K.

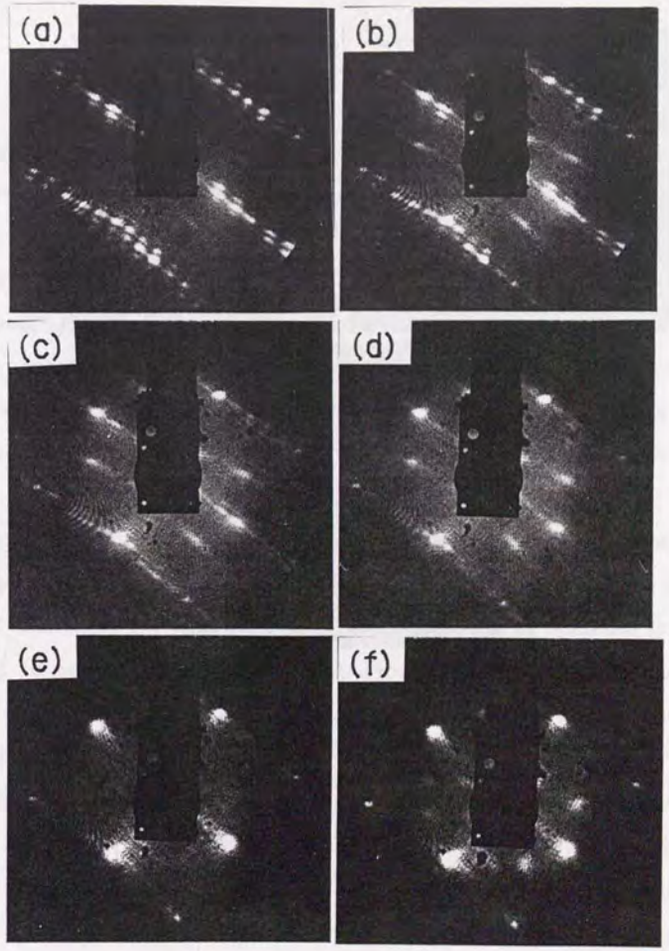

Fig. 2-7. LEED patterns of a single-domain Pt(001)-(20x5) surface after various NO exposures at 260±5 K: (a) 0.26 L, (b) 0.73 L, (c) 1.43 L, (d) 2.2 L, (e) 6.4 L, (f) 6.4 L followed by annealing at 260±5 K for 90 s in UHV. E_p = 75 eV for every pattern.

2.3.4 NO adsorption at 80-190 K

With NO exposure of ~2 L at 80-190 K, the LEED pattern changed into a diffuse (20x5) (or (1x5)) pattern with enhanced (1x1) spots and high background intensity (fig. 2-8(a)-(c)). The c(2x4)-like pattern was not observed in this temperature region. The enhancement of the (1x1) pattern, however, was not observed for NO exposures up to 0.7 L at 80 K (fig. 2-9(a) and (b)). The (1x1) spots is enhanced in a relatively narrow NO exposure range of 0.8-1.0 L (fig. 2-9(c) and (d)). In a recent study using RAIRS, Gardner et al. have reported that the (20x5)→(1x1) structural transformation of the topmost Pt layer occurs in a narrow NO exposure range of 0.5-0.7 L at 90 K [14] (see fig. 1-4). The discrepancy in the amount of the critical NO exposure is probably because of the uncertainty in the calibration of the pressure gauge. The abrupt change of the LEED pattern was not observed when the LEED filament was turned on during NO exposure, probably because of disturbing influence of electron impact. The LEED pattern remains unchanged for increasing NO exposure, except for the increase of background intensity (fig. 2-9(e) and (f)). These results indicate that some portion of the NO-saturated Pt(001) surface is relaxed to the (1x1) structure, while the rest remains reconstructed. Figure 2-10 shows LEED patterns of a single-domain Pt(001)-(20x5) surface after NO exposure of 5.2±0.2 L at 80 K followed by brief annealing at various temperatures. The diffuse (20x5) pattern is hardly observable after annealing at 260 K (fig. 2-10(a)). The double-domain

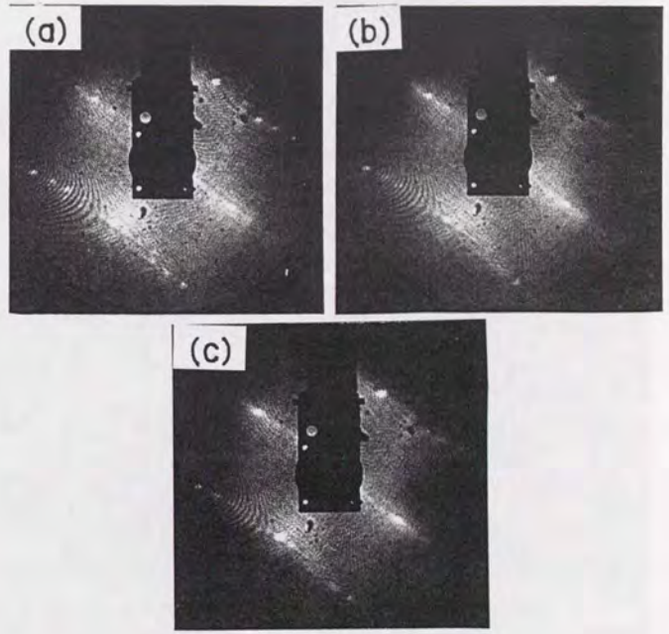

Fig. 2-8. LEED patterns of a single-domain Pt(001)-(20x5) surface after NO exposure of ~2 L at various surface temperatures: (a) 2.4 L at 80±3 K, (b) 1.9 L at 145±27 K, (c) 2.2 L at 192±5 K. E_p = 75 eV for every pattern.

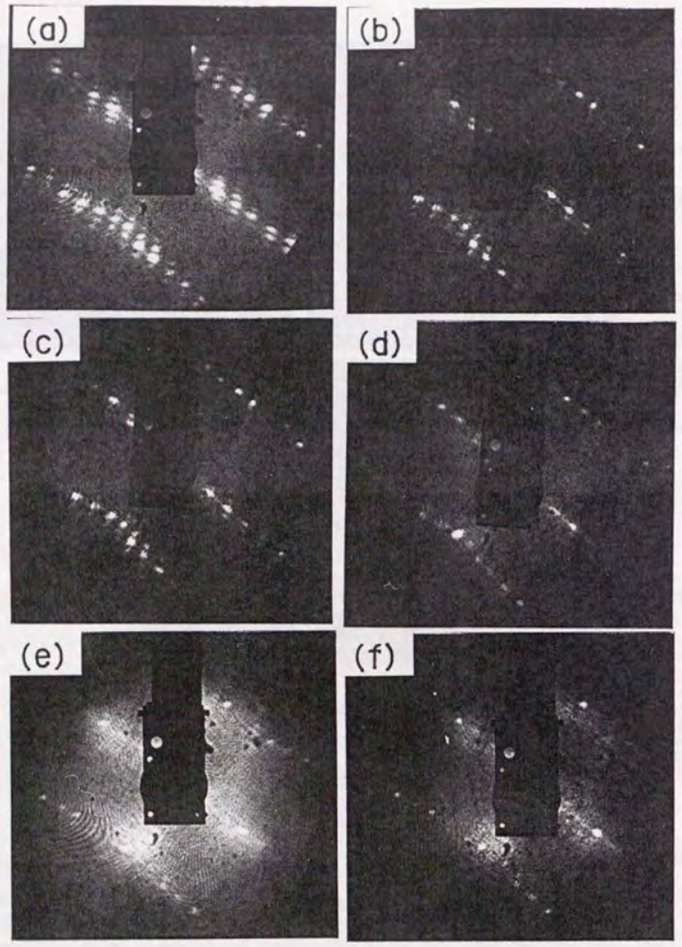

Fig. 2-9. LEED patterns of a single-domain Pt(001)-(20x5) surface after various NO exposures at 80±3 K: (a) 0.44 L, (b) 0.71 L, (c) 0.84 L, (d) 1.04 L, (e) 14.7 L, (f) 55 L. E_p = 75 eV for every pattern. NO pressure was 1×10^{-7} Torr for (a)-(d), 1×10^{-6} Torr for (e) and (f), respectively.

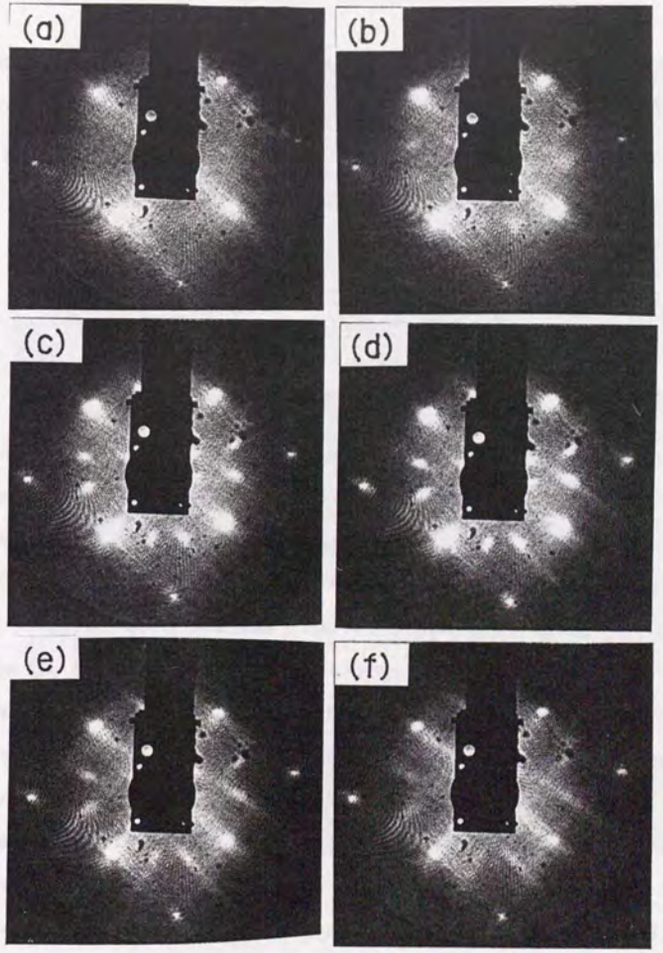

Fig. 2-10. LEED patterns of a single-domain Pt(001)-(20x5) surface after NO exposure of 5.2±0.2 L at 80 K followed by brief annealing at (a) 260±4 K, (b) 280±4 K, (c) 300±3 K, (d) 329±3 K, (e) 358±4 K, (f) 385±4 K. E_p = 75 eV for every pattern.

c(2x4)-like pattern becomes brighter with increasing annealing temperature from 280 to 330 K (fig. 2-10(b)-(d)), and becomes streaky and fuzzy from 360 to 390 K (fig. 2-10(e) and (f)).

2.4 Discussion

2.4.1 Mechanism of single-domain clean Pt(001)-(20x5) surface formation

As is stated in Section 2.3.1, only a single-domain out of the four possible domains was observed in the present clean Pt(001)-(20x5) surface. The single-domain formation has been also reported in LEED studies of Pt[4(001)x(111)] and Pt[9(001)x(111)] stepped surfaces [11] and a Pt(001) surface misorented by 3.8° [15]. Sequences of monoatomic steps parallel to the directions of the reconstruction (±4.4° against the [110] direction) are observed in a recent study using reflection electron microscopy (REM) [16] (fig. 2-11). STM images also exhibit preferential presence of a monoatomic step along the [110] direction separating the Pt-(20x5) terraces with the corrugation almost parallel to the step [6, 17] (see fig. 2-1). Therefore, the most probable model for the single-domain Pt(001)-(20x5) surface formation is a heterogeneous nucleation and growth mechanism, i. e. the single-domain Pt-(20x5) layer begins to grow at the steps parallel to the direction of the reconstruction, and develops from there over the rest area of the surface. The single-domain formation, however, is not likely to require a high step density, because the almost

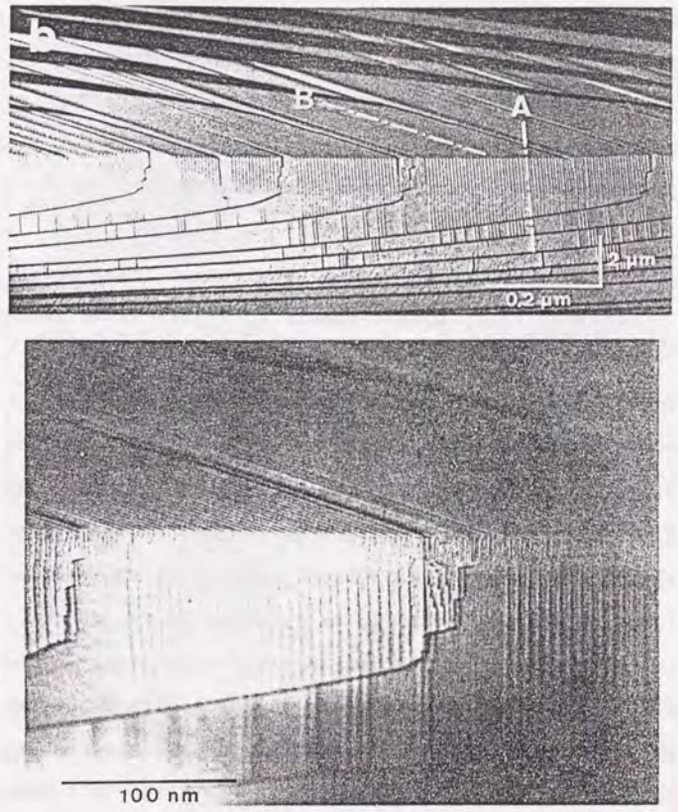

Fig. 2-11. REM images of the (001) facets of a Pt single crystal sphere recorded with the 10.00 reflection near the [110] azimuth. The specimen was transfered through air into the microscope after cleaning in UHV. Straight steps are developed in two different directions marked by A and B. The distance between the neighboring steps is approximately 6.1 nm. These steps are parallel to the unit cell of the rotated hexagonal reconstruction (±4.4° against the [110] direction, see fig. 1-1). This small angle is enormously enlarged in the images because of the foreshortening. (From ref. [16].)

clean Pt(001)-(1x1) surface exhibited a sharp (1x1) LEED pattern without splitting (see fig. 2-2(b)). The single-domain formation process becomes predominant above 1100 K (see fig. 2-2(e)), probably because the surface diffusion of the topmost Pt atoms is highly activated in this temperature region.

2.4.2 Mechanism of (20x5)→(1x1) structural transformation accompanied by single-domain NO-c(2x4) layer growth at 230-270 K

On the basis of the LEED observations stated in Section 2.3.3, I propose a model for the microscopic mechanism of the (20x5)→(1x1) structural transformation of the topmost hexagonal Pt layer accompanied by anisotropic growth of the single-domain NO-c(2x4) layer at 230-270 K, as is shown in fig. 2-12. The initial stage is NO adsorption on (1x1)-type sites in the Pt(001)-(20x5) surface with twofold periodicity along the [110] direction (fig. 2-12(a)). The (1x1)-type site represents the on-top site of the Pt atom located in the hollow site of the second Pt layer. This type of NO adsorption is expected to occur most preferentially, because the (20x5)→(1x1) transformation of the topmost Pt layer is not required. The full coverage in this initial stage is 0.1 ML, which is consistent with the LEED observation that the (1x1) spots are hardly enhanced after NO exposure of 0.26 L at 260 K (see fig. 2-7(a)). Studies of CO adsorption on Pt(001) using LEED [4], STM [5] and RBS [7] have also reported that the (20x5)→(1x1) transformation does not occur

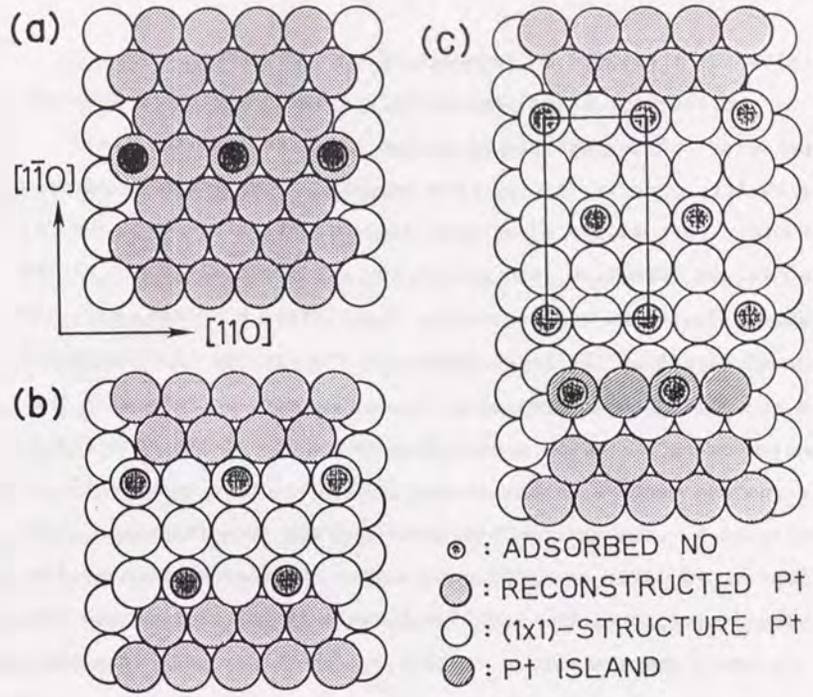

Fig. 2-12. Schematic drawings for the microscopic mechanism of the (20x5)→(1x1) transformation of the topmost Pt layer accompanied by anisotropic growth of the single-domain NO-c(2x4) layer at 230-270 K. The hexagonally reconstructed Pt layer is represented as the simplified (1x5) structure with the top/hollow registry. (a) Initial stage: NO is adsorbed at (1x1)-type sites on the reconstructed topmost Pt layer with twofold periodicity along the [110] direction. (b) Next stage: The single-domain NO-c(2x4) layer begins to grow while relaxing the reconstructed topmost Pt layer into the (1x1) structure. (c) Anisotropic (20x5)→(1x1) transformation of the topmost Pt layer squeezes out striped Pt-(1x1) islands. NO is adsorbed also on the Pt island. The unit cell of the NO-c(2x4) structure is shown with a solid line.

below the threshold CO covarage of 0.05-0.08 ML.

In the next stage, the NO-c(2x4) layer begins to grow while relaxing the topmost reconstructed Pt layer into the (1x1) structure (fig. 2-12(b)). The adsorbed NO molecules aligned with twofold periodicity along the [110] direction act as a nuclear for NO island formation, and causes the preferential growth of the single-domain NO-c(2x4) layer. The Pt(1x1)-NO-c(2x4) structure grows faster in the [110] direction than in the [1$\bar{1}$0] direction, because the boundary along [110] can be commensurate with the neighboring Pt-(20x5) area. Thus the order of the NO-c(2x4) structure becomes higher in the [110] direction than in the [1$\bar{1}$0] direction. The anisotropic (20x5)→(1x1) transformation of the topmost Pt layer squeezes out striped Pt islands, because the atomic density of the (20x5) structure is 20% higher than that of the (1x1) structure (fig. 2-12(c)). The Pt islands take the (1x1) structure so that the boundary along the [110] direction can be commensurate with the neighboring Pt-(20x5) or Pt-(1x1)-NO-c(2x4) area. NO is adsorbed also on the striped Pt-(1x1) islands. The striped Pt islands with the (1x1) structure of monolayer-height are observed in an STM study of NO adsorption on Pt(001)-(20x5) at 295 K [6] (see fig 2-1 and Section 1.2). The NO-c(2x4) layer continues to grow until the entire area is transformed into the (1x1) structure.

The proposed mechanism of the (20x5)→(1x1) transformation of the topmost Pt layer accompanied by anisotropic growth of the single-domain NO-c(2x4) layer is formulated as follows:

$$Pt(001)\text{-}(20x5)+NO_{ads} \rightarrow [Pt(001)\text{-}(20x5)+NO_{ad}] \quad (2\text{-}1)$$

$$[Pt(001)\text{-}(20x5)+NO_{ad}] \rightarrow Pt(001)\text{-}(20x5)_{(1x1)}+NO_{ad} \quad (2\text{-}2a)$$

$$[Pt(001)\text{-}(20x5)+NO_{ad}] \rightarrow [Pt(001)\text{-}(20x5)_{[110]}+NO_{ad}] \rightarrow Pt(001)\text{-}(1x1)_{[110]}+NO_{ad} \quad (2\text{-}2b)$$

$$[Pt(001)\text{-}(20x5)+NO_{ad}] \rightarrow [Pt(001)\text{-}(20x5)_{[1\bar{1}0]}+NO_{ad}] \rightarrow Pt(001)\text{-}(1x1)_{[1\bar{1}0]}+NO_{ad} \quad (2\text{-}2c)$$

$$[Pt(001)\text{-}(20x5)+NO_{ad}] \rightarrow [Pt(001)\text{-}(20x5)_{[1\bar{1}0]}+NO_{ad}] \rightarrow Pt(001)\text{-}(1x1)_{[1\bar{1}0]}+NO_{ad}+Pt(001)\text{-}(1x1)_{island} \quad (2\text{-}3)$$

$$Pt(001)\text{-}(1x1)_{island}+NO_{gas} \rightarrow Pt(001)\text{-}(1x1)_{island}+NO_{ad} \quad (2\text{-}4)$$

The brackets indicate the metastable intermediate state. The subscript of (1x1) in eq. (2-2a) indicates the (1x1)-type sites on the reconstructed Pt-(20x5) area, as is shown in fig. 2-12(a). The subscripts of [110] and [1$\bar{1}$0] in eqs. (2-2b), (2-2c), and (2-3) indicate the adsorption site at the boundary of the Pt-(1x1)-NO-c(2x4) structure in the [110] and the [1$\bar{1}$0] direction, respectively, as is shown in fig. 2-12(b). The subscript of "island" in eqs. (2-3) and (2-4) indicates the sites on the Pt island, as is shown in fig. 2-12(c). The single-domain NO layer is formed when the priority order of the adsorption process is (2-2a) > (2-2b) > (2-2c). The priority order, however, changes to (2-2a) ≃ (2-2b) ≃ (2-2c) at higher temperatures, because the mobility of the surface Pt atoms increases. Thus the double-domain NO-c(2x4) layer is formed at temperatures of 330-390 K.

2.4.3 (20x5)→(1x1) structural transformation at 80 K

As is stated in Section 2.3.4, the (20x5)→(1x1) structural transformation of the topmost Pt layer was found to occur abruptly

in the NO exposure range of 0.8-1.0 L at 80K. Furthermore, the Pt-(20x5) area remains locally even after prolonged NO exposure of 55 L. These results suggest that the mobility of the Pt surface atoms is decreased, and that the diffusion of the adsorbed NO is frozen. The structural transformation of the remained Pt-(20x5) area is probably blocked by the surrounding Pt-(1x1) area.

Lesley and Schmidt observed four NO desorption peaks at 550, 500, 325, and 150 K in temperature programed desorption spectra for a Pt(001)-(20x5) surface after NO exposure of 10 L at 120 K [18] (see fig. 1-5(a) and (b), and Section 1.2). The desorption peak at 150 K is probably derived from NO chemisorbed on the remained Pt-(20x5) area, because the (20x5) pattern is not observable after anealing at 260 K (see fig. 2-10(a)). The NO-(1x1) layer on the Pt-(1x1) structure is probably resposible for the desorption peak at 325 K, because the (1x1) pattern have changed into a bright double-domain c(2x4)-like pattern after annealing at 330 K (see fig. 2-10(d)).

References

[1] P. Heilmann, K. Heinz, and K. Müller, Surf. Sci. 83, 487 (1979).

[2] M.A. van Hove, R.J. Koestner, P.C. Stair, J.P. Bibérian, L.L. Kesmodel, I. Bartoš, and G.A. Somorjai, Surf. Sci. 103, 189 (1981).

[3] P.A. Thiel, R.J. Behm, P.R. Norton, and G. Ertl, Surf. Sci. 121, L553 (1982).

[4] R.J. Behm, P.A. Thiel, P.R. Norton, and G. Ertl, J. Chem. Phys. 78, 7437 (1983); P.A. Thiel, R.J. Behm, P.R. Norton, and G. Ertl, J. Chem. Phys. 78, 7448 (1983).

[5] W. Hosler, E. Ritter, and R.J. Behm, Ber. Bunsenges. Phys. Chem. 90, 205 (1986).

[6] E. Ritter, R.J. Behm, G. Potschke, and J. Wintterlin, Surf. Sci. 181, 403 (1987).

[7] T.E. Jackman, K. Griffiths, J.A. Davies, and P.R. Norton, J. Chem. Phys. 79, 3529 (1983).

[8] H.P. Bonzel and G. Pirug, Surf. Sci. 62, 45 (1977).

[9] G. Pirug, H.P. Bonzel, H. Hopster, and H. Ibach, J. Chem. Phys. 71, 593 (1979).

[10] Y. Murata, H. Tochihara, and M. Kubota, in: Metallization and Metal-Semiconductor Interfaces, ed. I.P. Batra (Plenum Press, New York, 1989) p.367.

[11] H.P. Bonzel, G. Brodén, and G. Pirug, J. Catal. 53, 96 (1978).

[12] K. Heinz, E. Lang, K. Strauss, and K. Müller, Surf. Sci. 120, L401 (1982).

[13] W.F. Banholzer and R.I. Masel, Surf. Sci. 137, 339 (1984).

[14] P. Gardner, M. Tüshaus, R. Martin, and A.M. Bradshaw, Vacuum 41, 304 (1990).

[15] H. Gutleben and E. Bechtold, Surf. Sci. 236, 313 (1990).

[16] G. Lehmpfuhl and Y. Uchida, Surf. Sci. 235, 295 (1990).

[17] R.J. Behm, W. Hösler, E. Ritter, and G. Binnig, Phys. Rev. Lett. 56, 228 (1986).

[18] M.W. Lesley and L.D. Schmidt, Surf. Sci. 155, 215 (1985).

CHAPTER 3

Ultraviolet-Laser Stimulated Desorption of NO Chemisorbed on Pt(001) Studied Using Positive Ion Detection System

Photostimulated desorption of NO chemisorbed on a Pt(001) surface at 80 and 300 K has been studied using a positive ion detection system. An ArF excimer laser (λ = 193 nm, 6.41 eV) is used as the pump laser. NO^+ is the only ion species detected when an NO-saturated Pt(001) surface is irradiated by the pump laser. The NO^+ yield is proportional to the third power of laser fluence. The translational energy distribution of the NO^+ ions is independent of laser fluence. A two-step model is proposed as the most probable NO^+ formation mechanism. The first step is desorption of neutral NO induced by valence-electron excitation from chemisorbed NO with one-photon absorption. Then, the desorbed NO is ionized in the vicinity of the surface by the two-photon ionization process. Relatively large desorption cross sections estimated from the decay of the NO^+ yield support the above NO^+ formation mechanism.

3.1 Introduction

Desorption induced by valence-electron excitations has been an important subject in surface science, because it is one of the most fundamental dynamical processes on surfaces [1] (see Sections 1.1 and 1.3). For molecules chemisorbed on metal, however, there have been only a few studies on ultraviolet-laser stimulated desorption induced by electronic excitations [2-4], partly because thermal processes often dominate over photochemical processes, and partly because deexcitation of molecules proceeds rapidly on metal (see Section 1.3). Buntin et al. found that thermal as well as photochemical channel is operative for laser-induced desorption of NO on Pt(111) at 1064, 532, and 355 nm [2]. In a photostimulated desorption study of NO [5] and CO [6] adsorbed on a clean Ni and Ni-NiO surface, only the non-metallic Ni-NiO surface exhibited measurable photostimulated desorption.

In this chapter, I report an ultraviolet-laser stimulated desorption study of molecules chemisorbed on metal induced by valence-electron excitation. An ArF excimer laser (λ = 193 nm, 6.41 eV) is used as the pump laser. I detected positive ions generated on an NO-saturated Pt(001) surface at 80 and 300 K irradiated by the pump laser. NO^+ was the only ion species detected. The yield and the translational energy distribution of the NO^+ ions were measured as a function of laser fluence. The NO^+ yield is proportional to the third power of laser fluence over a wide laser fluence range. The translational energy distribution of the NO^+ ions is independent of laser fluence, and is peaked at

~0.25 eV. On the basis of these observations, I proposed a two-step model as the most probable NO^+ formation mechanism. The first step is desorption of neutral NO induced by valence-electron excitation from the chemisorbed NO with one-photon absorption. Then the desorbed NO molecule is ionized in the vicinity of the surface by a two-photon ionization process. The cross section for photostimulated desorption was estimated from the decay of the NO^+ yield. The relatively large values of the cross section supports the above NO^+ formation mechanism. The desorption cross section was found to depend on the adsorption state of NO.

3.2 Experiment

The apparatus used is composed of two ultra-high-vacuum (UHV) chambers (fig. 3-1), a pump laser, and a positive ion detection system. The Pt(001) surface is cleaned in a UHV chamber for sample preparation (base pressure = 5×10^{-10} Torr) through a conventional method [7]. The cleanliness of the surface is verified by LEED and Auger electron spectroscopy (AES). The surface temperature during the sample preparation is monitored with an optical pyrometer. After surface cleaning, the Pt crystal is transferred to the manipulator in the other UHV chamber for the desorption measurements (base pressure = 2×10^{-10} Torr) and placed on the pump laser path. The sample temperature is monitored by a chromel-alumel thermocouple attached to the sample holder.

Figure 3-2 shows a schematic drawing of the experimental arrangement for the ultraviolet-laser stimulated desorption study.

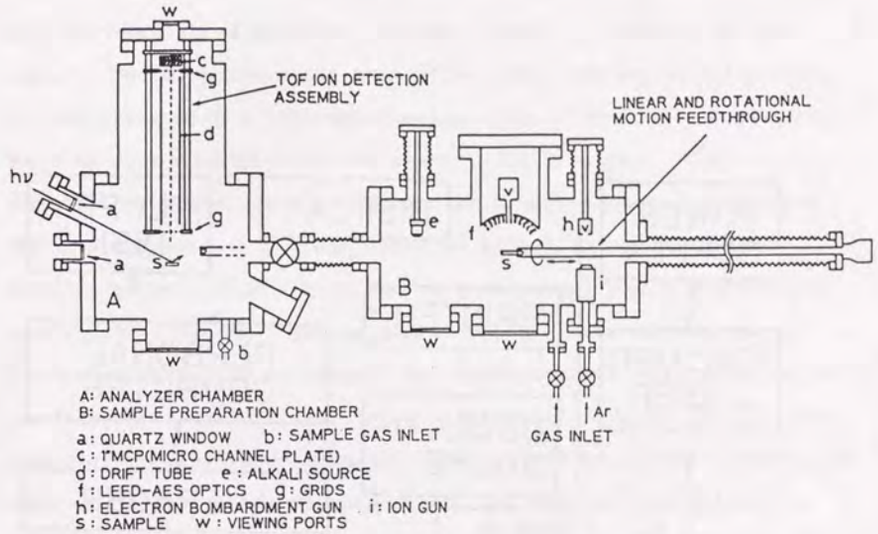

Fig. 3-1. Schematic drawing of the UHV chambers. Pumps, some valves, B-A ion gauges, and the manipulator are omitted.

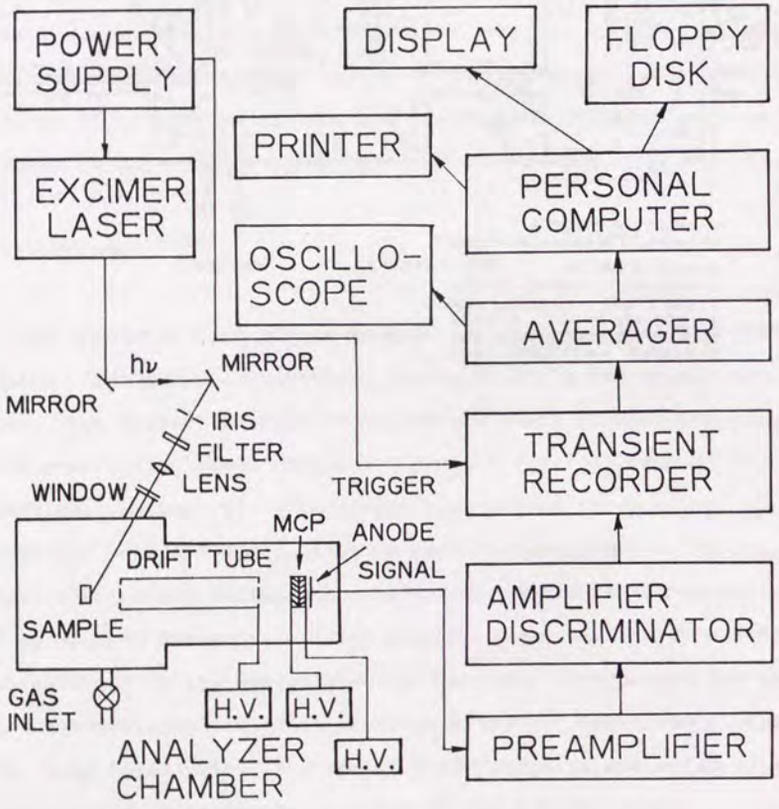

Fig. 3-2. Schematic drawing of the ultraviolet-laser optics and block diagram for the ultraviolet-laser stimulated desorption measurement.

An ArF excimer laser (Lambda Physik EMG 150 MSC, λ = 193 nm, full width at half maximum (FWHM) of the laser pulse = 11 ns, the standard deviation of laser fluence = ±6%) is used as the pump laser. The original laser beam with (5x25)-mm^2 rectangular size is apertured with a 1.28-mm-diameter iris to produce a laser beam with an approximately uniform spacial distribution. The uniformity of the laser is checked by a burn-pattern measurement using a Poraloid film. The laser is gently focused onto the Pt(001) surface at 65° from the surface normal via a quartz lens and a quartz window. The alignment of the laser optics was performed with a He-Ne laser. The typical laser spot area on the surface was 1.73×10^{-3} cm^2. A set of neutral density (ND) filters was used to vary laser fluence. The typical laser shot repetition rate was 3 Hz. Laser fluence on the surface was restricted to below 60 mJ/cm^2 to avoid damage and plasma formation on the surface. I calculated the surface temperature rise induced by laser irradiation using an equation for laser-induced surface heating [8], optical constants of Pt for 193 nm [9], and thermal properties of Pt at 80 and 300 K [10]. In the calculation I have employed a laser intensity which is uniform in space and Gaussian in time with FWHM of 11 ns. A laser shot with laser fluence of 60 mJ/cm^2 was found to induce surface temperature rise with maximum temperature of 350 and 530 K for a Pt surface at 80 and 300 K, respectively. The FWHM of the surface temperature rise was 22 ns for the both cases. No significant ion desorption was observed from a clean Pt(001)-(20x5) surface for a laser shot with laser fluence below

60 mJ/cm^2. Unless otherwise stated, measurements in this chapter were carried out under the above typical conditions.

The clean Pt(001)-(20x5) surface was exposed to NO to the saturation coverage at 80 or 300 K. NO gas with 99.9% purity was used without further purification. When NO gas was introduced to the UHV chamber, it was pumped only with a turbo-molecular pump. A titanium sublimation pump and an ion sputtering pump were separated from the chamber by a gate valve so that NO molecules would not be decomposed on the active titanium surface. A B-A ion gauge filament was turned off during measurements to reduce the noise. Positive ions generated on the NO-saturated surface under laser irradiation were accelerated in the surface normal direction to the front mesh of a drift tube biased at a negative voltage. After flying through the electric-field-free region of 320-mm length in the drift tube, the ions were again accelerated and detected by a 20-mm-diameter dual microchannel plate (MCP) assembly. The distance between the Pt surface and the front mesh of the drift tube was typically 30 mm. The drift tube voltage was adjusted to attract all the ions into the detector. The ion signals were amplified with a preamplifier and an amplifier, and stored as a time-of-flight (TOF) spectrum in a transient recorder with a signal averager (Electronica ELK-5120AVE, memory volume = 16 kwords, minimum sampling clock = 20 ns/word, resolving power = 10 bits). The transient recorder was remote-controlled with a personal computer (EPSON PC-286) via a GP-IB interface. After averaging signal over several laser shots, the TOF spectrum was transferred to the computer for storage, display, printout, and

analysis. The TOF spectrum during signal averaging can be monitored by an oscilloscope. A typical TOF spectrum is shown in fig. 3-3. An intense peak at 0 μs accompanied by a large undershoot is the incident photon signal. The mass number of the ion species was deduced from the TOF. The integrated ion signal was calculated numerically with the computer.

In order to ascertain that the integrated ion signal gives the accurate relative ion yield, the photo-ionization yield of gaseous NO for 193 nm was measured as a function of laser fluence with the present system. The result is shown in fig. 3-4. The ambient NO pressure was 2.0×10^{-6} Torr. The laser shot repetition rate was 10 Hz. The diameter of the iris was about 5 mm. The volume of laser irradiation region in front of the positive-ion detection assembly was about 1.6×10^{-2} cm^3, which contains about 1.0×10^{9} NO molecules. Laser fluence at each datum was calculated with transmissivity of the ND filter and laser fluence averaged over 30 laser shots before and after the measurement. Laser fluence was measured with a pyroelectric joulemeter (Molectron J3). The horizontal error bar was estimated from the standard deviation of laser fluence and the error in transmissivity of the ND filter. Laser fluence for the following photostimulated desorption measurements was also calculated in this manner. The NO^+ yield was estimated from the integrated NO^+ signal in the TOF spectrum averaged over 32 laser shots. The vertical error bar for the NO^+ yield of fig. 3-4 was estimated from the standard deviation of five data. The NO^+ yield was proportional to the square of laser fluence, which is consistent with the fact that

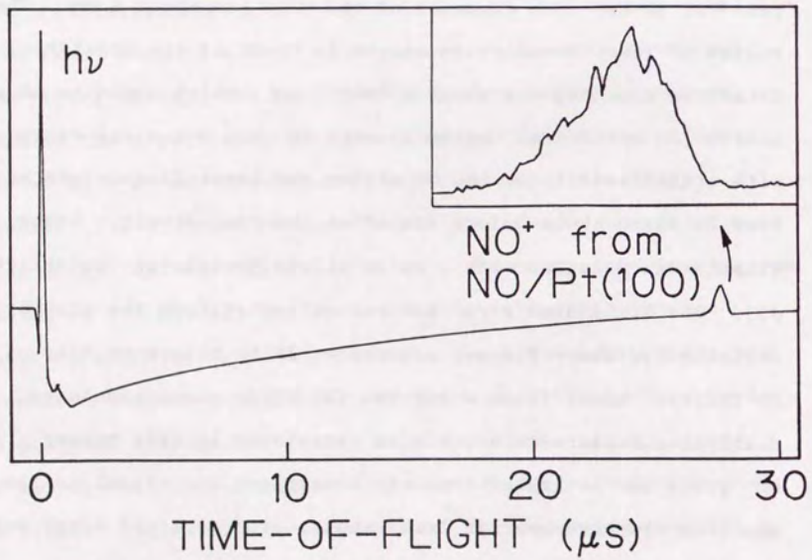

Fig. 3-3. Typical TOF spectrum of NO^+ ions generated on an NO-saturated Pt(001) surface irradiated by the pump laser. The inset is the enlarged figure of the NO^+ signal.

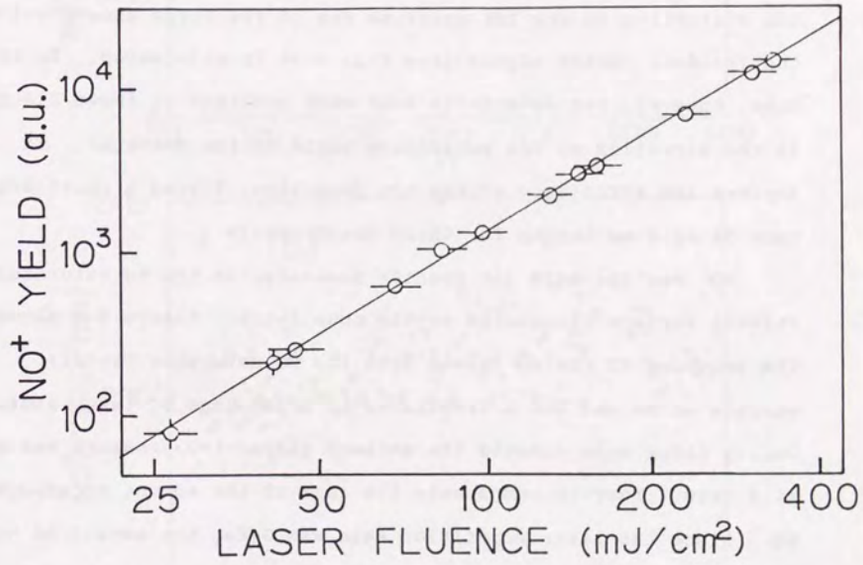

Fig. 3-4. Laser fluence dependence of the integrated NO^+ signal for the photo-ionizaton of NO in gas phase. The abscissa is laser fluence at the center of the ionization region. The solid straight line is the regression line fitted by the least-squares method. The slope of the regression line is 2.021 with a correlation coefficient of 0.9996.

gaseous NO is ionized by a two-photon process for 193 nm [11]. This result demonstrates that the ion yield obtained in this manner is linearly proportional to the true ion yield.

When the generated ions comprise only one species, its translational energy distribution can be measured by grounding the drift tube. In this case a discriminator was connected between the amplifier and the transient recorder. Since the discriminator converts every signal to a pulse signal without any undershoot, the distortion in the TOF spectrum due to the large undershoot of the incident photon signal (see fig. 3-3) is eliminated. In this case, however, the detectable ions were confined to those ejected in the direction of the acceptance angle of the detector. To improve the efficiency of the ion detection, I used a short drift tube of 29.9-mm length for these measurements.

NO^+ was the only ion species generated on the NO-saturated Pt(001) surface irradiated by the pump laser. Figure 3-5 shows the sequence of the NO^+ yield from the NO-saturated Pt(001) surface at 80 and 300 K irradiated by a sequence of laser shots. During these measurements the ambient gaseous-NO pressure was kept at 2.0×10^{-7} Torr to compensate the loss of the amount of adsorbed NO. Since the laser repetition rate was 3 Hz, the amount of NO exposure during the laser shot interval was 0.07 L (1 L = 1×10^{-6} Torr·s). The NO^+ signal from ambient NO molecules, which can be easily measured by removing the Pt sample from the laser path, was found to be three or two orders of magnitude smaller than that from adsorbed NO. At 80 K the NO^+ yield remained unchanged from the first to 600th laser shot. This result

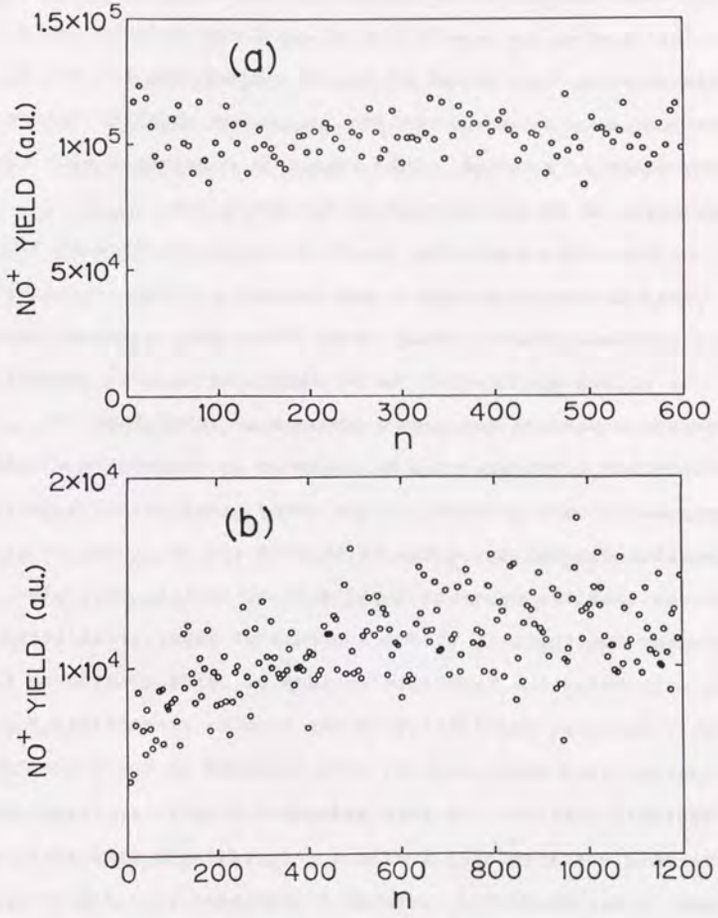

Fig. 3-5. Plots of the NO^+ yield averaged over every 6 laser shots against the number of the pump laser shot (n), when the ambient gaseous NO pressure is kept at 2.0×10^{-7} Torr. (a) At 80 K. Laser fluence on the surface is 55±3 mJ/cm². (b) At 300 K. Laser fluence on the surface is 54±3 mJ/cm².

suggests that the state of the adsorbed NO under laser irradiation is the same as that before laser irradiation, i. e. laser irradiation does not modify the NO-saturated Pt(001) surface. NO physisorbed on chemisorbed NO is not responsible for the $NO^{\cdot}$ formation, because no incubation period was observed before a steady state is reached. This result is consistent with the LEED observation at 80 K mentioned in Section 2.3.4.

On the other hand, for the NO-saturated surface at 300 K, the $NO^{\cdot}$ yield increased gradually and reached a steady state after about 800 laser shots. This result shows that a laser-induced process gradually modifies the NO-saturated Pt(001) surface. A favorable candidate for such a process is laser-induced dissociation of chemisorbed NO followed by adsorption of atomic oxygen and atomic nitrogen. In a study of ultraviolet-laser stimulated desorption of the Ni(001)-NO system, Budde et al. also observed that the desorption yield of NO neutral molecules increases continuously with a sequence of laser irradiation [5]. They attributed the result to buildup of surface oxide on the Ni(001) surface, and identified the species responsible for the photostimulated desorption with NO adsorbed on the non-metallic Ni(001)-NiO surface. In this respect a Pt(001) surface is much different from a Ni(001) surface. According to studies by several groups, homogeneous NiO layer with thickness of a few monolayers is formed on a Ni(001) surface with oxygen adsorption [12], while platinum oxide is not formed on a Pt(001) surface [13]. Platinum nitride is also not formed on a Pt surface. Bonzel and Pirug measured the difference curve in ultraviolet photoelectron

spectroscopy (UPS) for a Pt(001)-(1x1) surface contaminated with adsorbed atomic oxygen (and possibly atomic nitrogen) with respect to a clean Pt(001)-(20x5) surface [14]. They found that the difference UPS curve is nearly identical with that for a clean Pt(001)-(1x1) surface with respect to a clean Pt(001)-(20x5) surface. Their observation seems to indicate that adsorbed atomic oxygen and atomic nitrogen do not change the metallic property of a Pt(001) surface. Furthermore, in a study of NO adsorbed on a Pt(001) surface at 120 K, Gorte et al. found that the temperature programmed desorption spectrum of NO is essentially unchanged by preadsorption of atomic oxygen at room temperature [15]. Therefore, I tentatively assign the species responsible for the $NO^{\cdot}$ formation at 300 K to NO chemisorbed on the metallic Pt surface, which is modified probably with adsorbed atomic oxygen and atomic nitrogen. All of the following measurements at 300 K in this chapter were carried out after the steady state was reached.

3.3 Results

The $NO^{\cdot}$ yield from NO adsorbed on a Pt(001)-(20x5) surface at 80 and 300 K is shown in fig. 3-6 as a function of the pump laser fluence. The ambient gaseous NO was kept at 2.0×10^{-7} Torr during the measurements. The $NO^{\cdot}$ yield was obtained from the TOF spectrum averaged over 32 laser shots. The vertical error bar was estimated from the standard deviation of three data. The $NO^{\cdot}$ yield is proportional to the third power of laser fluence over the

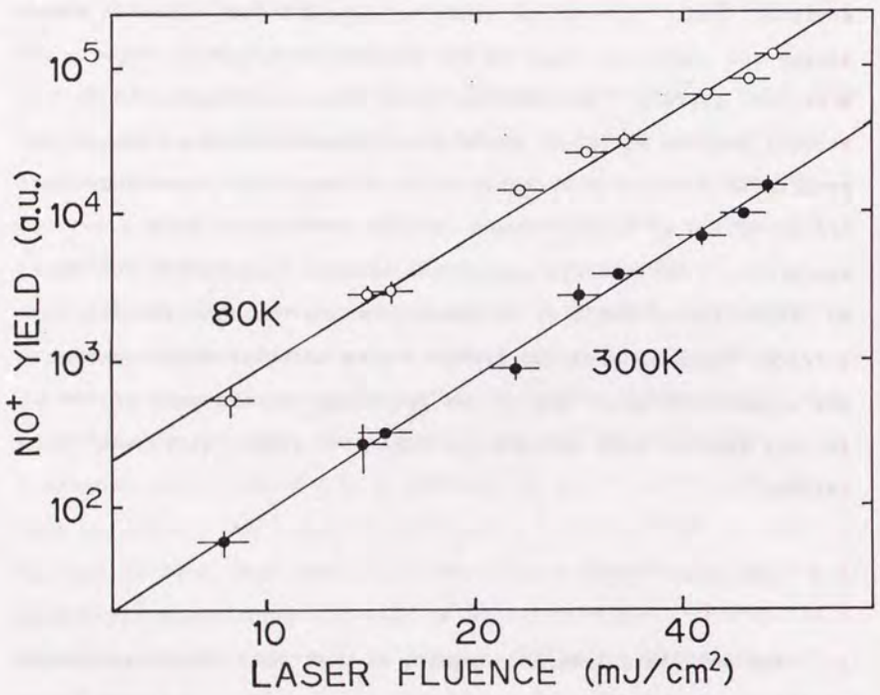

Fig. 3-6. Laser fluence dependence of the NO^+ yield for photo-ionization of NO adsorbed on a clean Pt(001)-(20x5) surface at 80 (open circle) and 300 K (closed circle). The abscissa is laser fluence on the surface. The solid lines indicate the regression lines fitted by the least-squares method. The gradients of the regression lines for 80 and 300 K are 2.92 and 3.04, respectively.

laser fluence range from 9 to 54 mJ/cm^2 at both 80 and 300 K. The NO^+ yield for NO adsorbed at 80 K was about one order of magnitude larger than that at 300 K.

Figure 3-7 shows TOF spectra which reflect the translational energy distributions of NO^+ ions generated on the NO-saturated Pt(001) surface at 80 K. As stated in Section 3.2, a grounded short drift tube and a discriminator were used for these measurments. The length of the field-free region between the Pt surface and the rear mesh of the drift tube was 57.2 mm. Every spectrum was averaged over 1024 laser shots. The intense peak for the incident photons at 0 μs was omitted in the figure. The peak position and the FWHM of the TOF spectra were independent of laser fluence. The temperature of a Maxwell distribution, the peak position of which was fitted to that of the TOF spectra, was 3200 K. The FWHM of the observed spectrum was a little smaller than that of the Maxwell distribution. The translational energy distributions of the NO^+ ions can be easily transferred from the data in the TOF spectra using the appropriate Jacobian. The translational energy distribution was found to be peaked at about 0.25 eV. The translational energy distributions of NO^+ ions generated on the NO-saturated Pt(001) surface at 300 K were not measured because of the small signal.

I also carried out preliminary measurements of decay curves of the NO^+ yield for the NO-saturated Pt(001) surface at 80 and 300 K irradiated by a sequence of laser shots. The results are shown in fig. 3-8. The Pt(001) surface was initially exposed to NO to the saturation coverage and the residual NO gas was quickly

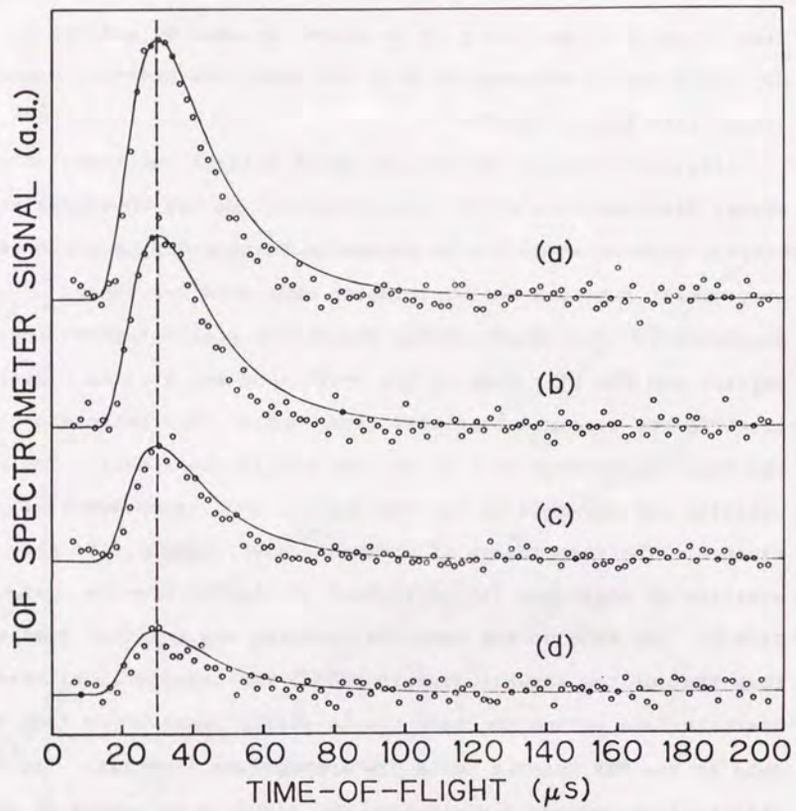

Fig. 3-7. TOF spectra reflecting the translational energy distribution of NO^+ ions from an NO-saturated Pt(001) surface at 80 K for laser fluence of (a) 54±4, (b) 44±4, (c) 34±2, and (d) 21±2 mJ/cm^2. The dashed line indicates the peak position. The solid lines represent Maxwell distributions of the form $f(v) = Av^3 \exp(-mv^2/2k_B T)$, where A is a fitting parameter, v the velocity of the molecules, m the mass, k_B the Boltzmann constant, and T the translational temperature of 3200 K. The transformation of coordinate system from v to TOF was performed using the appropriate Jacobian.

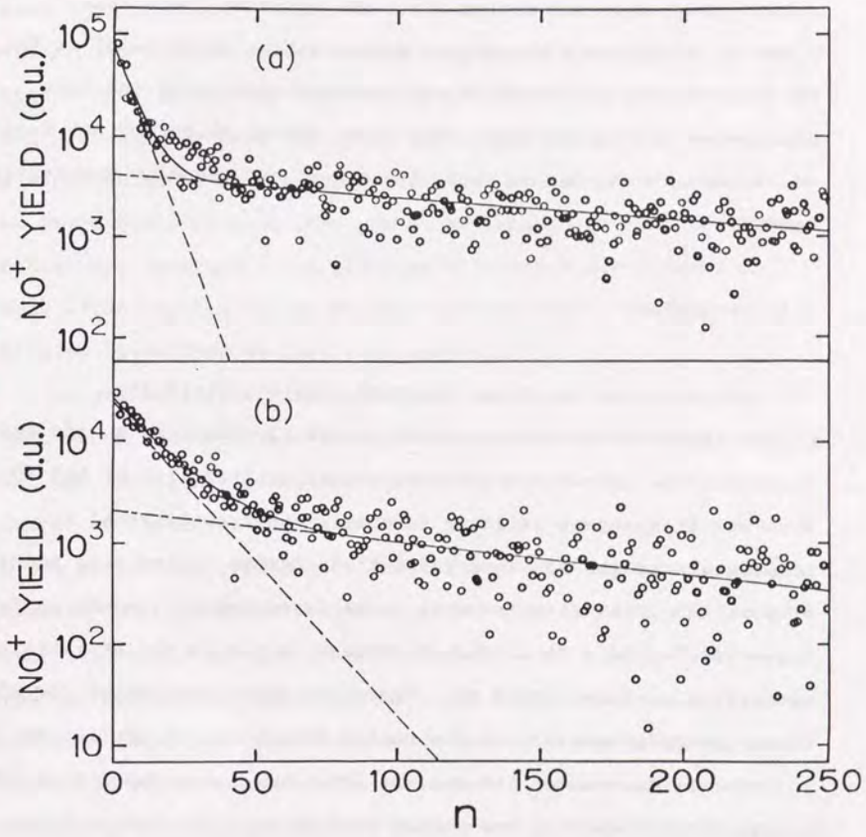

Fig. 3-8. Semilogarithmic plots of the NO^+ yield against the n'th laser shot without further NO exposure. (a) At 80 K. Laser fluence on the surface is 52±4 mJ/cm^2. (b) At 300 K. Laser fluence on the surface is 51±4 mJ/cm^2. The both decay curves are fitted by a curve (solid line) composed of the fast (dashed line) and the slow exponential decays (dot-dash line).

pumped out. The NO pressure was less than 4×10^{-10} Torr during the measurements. Since the laser repetition rate was 3 Hz, the amount of NO exposure during 250 laser shots was less than 0.033 L. To improve the signal-noise raitio, every point of the decay curves at 80 and 300 K was averaged over three and four measurements, respectively. The decay curves at 80 and 300 K can be fitted by a curve composed of the fast and the slow exponential decays.

3.4 Discussion

As stated in the former section, the NO^+ yield was proportional to the third power of laser fluence over a wide laser fluence range. The translational energy distribution of the NO^+ ions was independent of laser fluence. The translational temperature of the NO^+ ions (3200 K) is beyond the melting point of platinum (2047 K). The most probable mechanism accounting for these results is a three-photon process involving photostimulated desorption of chemisorbed NO. There are three candidates for the three-photon process: (1) One-photon desorption of neutral NO followed by two-photon ionization. (2) Two-photon desorption of excited NO followed by one-photon ionization. (3) Three-photon desorption of NO^+. The first model is most probable, because the desorption cross section for neutral molecules is usually a few orders of magnitude larger than that for excited neutrals or ions [1, 16-19]. As mentioned in Section 3.2, neutral NO is efficiently ionized by a two-photon process for 193 nm. Since the spectra

in fig. 3-7 show that the maximum velocity of a desorbed NO is 3000 m/s, a desorbed NO travels 33 μm at most during the 11-ns laser shot duration. Since the diameter of the laser beam on the surface was ~300 μm, every desorbed NO has a opportunity to be subsequently ionized by the same laser shot. The second model is less probable, because the cross section of two-photon desorption is expected to be much smaller than that of one-photon desorption. The third model is much less probable, because no NO^+ desorption channel was observed in an electron-stimulated ion desorption study of NO chemisorbed on Pt(001) for the incident electron energies below 2000 eV [20] (see Section 2.1).

As stated in the former section, the decay curves of the NO^+ yield at 80 and 300 K can be fitted by a curve composed of the fast and the slow exponential decays. The fast exponential decay clearly reflects the decrease of an NO species on the surface due to the photostimulated desorption. The double exponential decay suggests that there are at least two NO species with a different desorption cross section at both 80 and 300 K. Some of the previous electron-stimulated desorption studies have also reported that the desorption cross section is strongly dependent on the adsorption state of adsorbates [1, 17, 18]. Assuming that the photostimulated desorption is a one-photon process, the desorption cross section for a specific NO state σ_d (cm^2) is given by

$$\sigma_d = -G/\Phi, \qquad (3\text{-}1)$$

where G is the gradient of the exponential decay of the NO^+ yield in the semilogarithmic plots (see fig. 3-8), and Φ the photon flux density per one laser shot (photons/cm^2). The fast and the slow

decays at 80 K, and the fast and the slow decays at 300 K give desorption cross sections of 3.5×10^{-18}, 1.0×10^{-19}, 1.4×10^{-18}, and 1.6×10^{-19} cm^2, respectively. These values contain a little uncertainty due to arbitrariness of the fitting curve and the incomplete uniformity of the incident laser beam. The reduction of electric field in the vicinity of a metal surface is not considered in the calculation. The relatively large values of the desorption cross section support that one-photon desorption of neutral NO followed by the two-photon ionization is the dominant process.

There are two probable mechanisms for the photostimulated desorption. One is an MGR-type mechanism (see Section 2.3 and fig. 1-6) in which the desorption is induced by the valence-electron excitation in the chemisorbed NO. This mechanism is most probable, because the values of the desorption cross section estimated in the present study were comparable with those estimated for electron-stimulated desorption of neutral molecules induced by valence-electron excitations in chemisorbed molecules [1, 16-18]. The incident photon energy of 6.41 eV is expected to be large enough to excite the valence-electron of the chemisorbed NO, because the threshold energy for electron-stimulated desorption was reported to be ~6 eV for NO chemisorbed on Pt(111) [21] (see Section 1.4). In the other probable mechanism, the initial step is the one-electron excitation from the conduction band of the metal to a state above the Fermi level. Then, the excited electron tunnels into an unoccupied state of chemisorbed NO. The motion of NO along the potential surface of the

intermediate negative ion state followed by deexcitaion leads to the desorption of the neutral molecule. This mechanism was found to be responsible for the laser stimulated desorption of NO chemisorbed on Pt(111) for 1064, 532, and 355 nm (1.2, 2.3, and 3.5 eV, respectively) (see Section 1.4) [2]. The desorption yield per photon was reported to be $\sim5\times10^{-8}$ for 355 nm, corresponding to a desorption cross section lower than 1×10^{-21} cm^2. This value is, however, three or four orders of magnitude smaller than those estimated in the present study. Therefore, this second mechanism is not likely to be the dominant process in the present case.

Laser-induced thermal desorption (LITD) of neutral NO followed by the two-photon ionization in the vicinity of the surface is another probable mechanism for the NO^+ formation. This model is, however, excluded by the present results. Several groups have investigated the laser fluence dependence of the LITD yield for molecules chemisorbed on metal surfaces, and reported the following results: (1) There is an apparent threshold of laser fluence necessary to induce LITD [22-25]. (2) When the laser beam distribution is Gaussian, the LITD yield increases approximately linearly above the threshold laser fluence, and reaches a saturation value [22-25]. (3) When the laser beam distribution is uniform, the LITD yield increases exponentially above the threshold and quickly reaches a saturation value [22, 23]. (4) At the saturation region, most of the adsorbates in the laser irradiation area are desorbed with one laser shot [22-25]. (5) Even at medium laser fluence, the yield for the second laser shot is about one order of magnitude smaller than

that for the first laser shot [24]. The present experimental results are thoroughly in contrast to those of the LITD studies. Figure 3-9 shows the laser fluence dependence of the NO desorption yield, which was calculated from the data shown in fig. 3-6 assuming two-photon ionization. The NO desorption yield is linearly proportional to the laser fluence over a wide range from 0 to 54 mJ/cm^2. There is no apparent threshold laser fluence for the NO desorption. Furthermore, even at laser fluence of 52 mJ/cm^2, the NO$^+$ yield for a sequence of laser shots showed relatively gradual decay (see fig. 3-8).

The translational energy distribution of molecules desorbed from metal surfaces has been also measured in several LITD studies [24, 26-29]. The common results in those studies are as follows: (1) The translational energy distribution follows a Maxwell distribution when the effect of collisions among the desorbed molecules is negligible. (2) The translational temperature (T_d) increases as the maximum surface temperature (T_s) increases. (3) T_d is equal to or smaller than T_s. The present results are again much different from the above results in the LITD studies. The translational energy distribution is independent of laser fluence, and consequently independent of the maximum surface temperature. The temperature of a Maxwell distribution, the peak position of which is fitted to that of the present translational energy distribution, is 3200 K (see fig. 3-7). The temperature is one order of magnitude higher than the calculated maximum surface temperature of 350 K. On the basis of the above discussion, I conclude that the photochemical desorption process dominate over

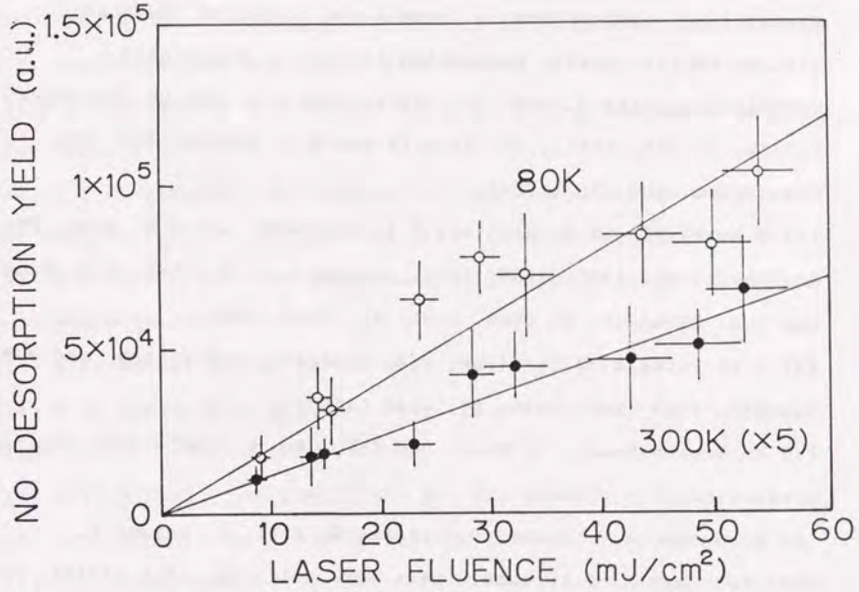

Fig. 3-9. Laser fluence dependence of the NO desorption yield at 80 (open circle) and 300 K (closed circle), which was calculated from the data shown in fig. 3-6 assuming two-photon ionization. The NO desorption yield at 300 K is expanded by a factor of five. The solid lines indicate the curves of the form y = Ax fitted by the least-squares method, where y is the NO desorption yield, A a parameter, and x laser fluence.

the LITD process under the present experimental conditions.

References

[1] Desorption Induced by Electronic Transitions, DIET-1, eds. N.H. Tolk, M.M. Traum, J.C. Tully, and T.E. Madey (Springer-Verlag, Berlin, 1983); Desorption Induced by Electronic Transitions, DIET-2, eds. W. Brenig and D. Menzel (Springer-Verlag, Berlin, 1985); Desorption Induced by Electronic Transitions, DIET-3, eds. R.H. Stulen and M.L. Knotek (Springer-Verlag, Berlin, 1987); Ph. Avouris and R.E. Walkup, Ann. Rev. Phys. Chem. 40, 173 (1989).

[2] S.A. Buntin, L.J. Richter, R.R. Cavanagh, and D.S. King, Phys. Rev. Lett. 61, 1321 (1988); S.A. Buntin, L.J. Richter, D.S. King, and R.R. Cavanagh, J. Chem. Phys. 91, 6429 (1989).

[3] J.A. Prybyla, T.F. Heinz, J.A. Misewich, M.M.T. Loy, and J.H. Glownia, Phys. Rev. Lett. 64, 1537 (1990).

[4] R. Schwartzwald, A. Mödl, and T.J. Chuang, Surf. Sci., in press.

[5] F. Budde, A.V. Hamza, P.M. Ferm, G. Ertl, D. Weide, P. Andresen, and H.-J. Freund, Phys. Rev. Lett. 60, 1518 (1988); P.M. Ferm, F. Budde, A.V. Hamza, S. Jakubith, G. Ertl, D. Weide, P. Andresen, and H.J. Freund, Surf. Sci. 218, 467 (1989).

[6] X. Guo, J. Yoshinobu, and J.T. Yates, Jr., J. Chem. Phys. 92, 4320 (1990).

[7] M.A. Van Hove, R.J. Koestner, P.C. Stair, J.P. Bibérian, L.L. Kesmodel, I. Bartoš, and G.A. Somorjai, Surf. Sci. 103, 189 (1981).

[8] J.F. Ready, Effects of High-Power Laser Radiation (Academic Press, New York, 1971).

[9] Handbook of Optical Constants of Solids, ed. E.D. Palik (Academic Press, Orlando, 1985).

[10] Thermophysical Properties of Matter, Vol. 1, eds. Y.S. Touloukian, R.W. Powell, C.Y. Ho, and P.G. Klemens (IFI/Plenum, New York, 1970); Thermophysical Properties of Matter, Vol. 4, eds. Y.S. Touloukian and E.H. Buyco (IFI/Plenum, New York, 1970).

[11]J.R. Woodworth, T.A. Green, and C.A. Frost, J. Appl. Phys. 57, 1648 (1985).

[12] P.F.A. Alkemade, S. Deckers, F.H.P.M. Habraken, and W.F. van der Weg, Surf. Sci. 189/190, 161 (1987), and references therein.

[13] G.N. Derry and P.N. Ross, Surf. Sci. 140, 165 (1984), and references therein.

[14] H.P. Bonzel and G. Pirug, Surf. Sci. 62, 45 (1977).

[15] R.J. Gorte, L.D. Schmidt, and J.L. Gland, Surf. Sci. 109, 367 (1981).

[16] A.R. Burns, Phys. Rev. Lett. 55, 525 (1985); A.R. Burns, J. Vac. Sci. Technol. A 4, 1499 (1986).

[17] T.E. Maday and J.T. Yates, Jr., J. Vac. Sci. Technol. 8, 525 (1971), and references therein.

[18] M. Nishijima and F.M. Propst, Phys. Rev. B 2, 2368 (1970).

[19] I.G. Newsham and D.R. Sandstrom, J. Vac. Sci. Technol. 10, 39 (1973).

[20] U. Schwalke, H. Niehus, and G. Comsa, Surf. Sci. 137, 23 (1984).

[21] A.R. Burns, E.B. Stechel, and D.R. Jennison, Phys. Rev. Lett. 58, 250 (1987); A.R. Burns, D.R. Jennison, and E.B. Stechel, J. Vac. Sci. Technol. A 5, 671 (1987); A.R. Burns, E.B. Stechel, and D.R. Jennison, J. Vac. Sci. Technol. A 6, 895 (1988).

[22] R.B. Hall and A.M. DeSantolo, Surf. Sci. 137, 421 (1984).

[23] J.L. Brand and S.M. George, Surf. Sci. 167, 341 (1986).

[24] G. Wedler and H. Ruhmann, Surf. Sci. 121, 464 (1982).

[25] E.G. Seebauer, A.C.F. Kong, and L.D. Schmidt, Surf. Sci. 176, 134 (1986).

[26] D. Burgess, Jr., R. Viswanathan, I. Hussla, P.C. Stair, and E. Weitz, J. Chem. Phys. 79, 5200 (1983); D.R. Burgess, Jr.,I. Hussla, P.C. Stair, R. Viswanathan, and E. Weitz, Rev. Sci. Instrum. 55, 1771 (1984).

[27] J.P. Cowin, D.J. Auerbach, C. Becker, and L. Wharton, Surf. Sci. 78, 545 (1978).

[28] I. Hussla, H. Coufal, F. Trager, and T.J. Chuang, Can. J. Phys. 64, 1070 (1986).

[29] D. Burgess, Jr., D.A. Mantell, R.R. Cavanagh, and D.S. King, J. Chem. Phys. 85, 3123 (1986); D. Burgess, Jr., R.R. Cavanagh, and D.S. King, J. Chem. Phys. 88, 6556 (1988).

CHAPTER 4

Ultraviolet-Laser Stimulated Desorption of NO Chemisorbed on Pt(001) Studied Using (2+2) Resonance-Enhanced Multiphoton Ionization

Photostimulated desorption of NO chemisorbed on Pt(001) at 80 K is studied using an ArF excimer laser (λ = 193 nm, 6.41 eV) and a (2+2) resonance-enhanced multiphoton ionization ((2+2)REMPI) technique. The rotational temperature of desorbed NO in the v" = 0 level of the ground electronic state ($X^2\Pi_{1/2}$) is found to be ~300 K. The temperature of the Maxwell distribution, the peak position of which is fitted to that of the observed translational energy distribution of desorbed NO in the $X^2\Pi_{1/2}$ (v"=0,J"=23/2) state, is 530 K. These results support that desorption of NO chemisorbed on Pt(001) is induced by valence-electron excitation.

4.1 Introduction

In the former chapter, I have stated photostimulated desorption of NO chemisorbed on a Pt(001) surface at 80 and 300 K using a pump laser (λ = 193 nm, 6.41 eV) and a positive ion detection system. This study presented the first evidences of ultraviolet-laser stimulated desorption induced by valence-electron excitation of molecules chemisorbed on metal. To clarify the detailed mechanism of photostimulated desorption, I have constructed an apparatus to detect neutral NO molecules desorbed from metal using a (2+2) resonance-enhanced multiphoton ionization ((2+2)REMPI) technique. The rotational temperature of desorbed NO in the v" = 0 level of the ground electronic state ($X^2\Pi_{1/2}$) was found to be ~300 K. The temperature of the Maxwell distribution, the peak position of which was fitted to that of the translational energy distribution of desorbed NO in the $X^2\Pi_{1/2}$ (v"=0,J"=23/2) state, is 530 K. These results support that desorption of NO chemisorbed on Pt(001) is induced by valence electron excitation.

4.2 Experiment

The apparatus used was improved as compared with that describedin Section 3.2. Surface cleaning, characterization, and photostimulated desorption measurements in the present chapter were carried out in one UHV chamber (base pressure < 1×10^{-10} Torr) equipped with LEED/AES optics. The details of the sample preparation are same as those described in Section 2.2. Figure 4-1 shows

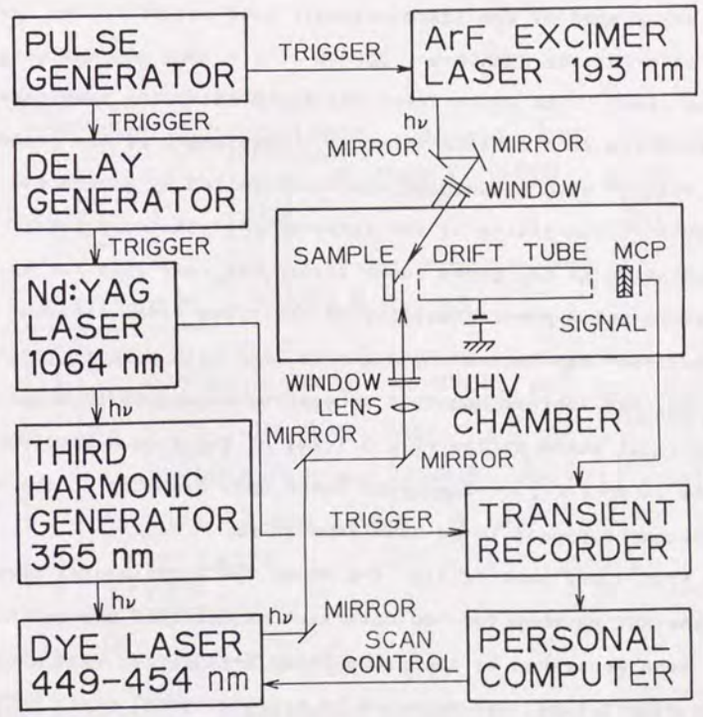

Fig. 4-1. Experimental arrangement for the state-selective study of ultraviolet-laser stimulated desorption using (2+2)REMPI.

the experimental arrangement for the state-selective study of ultraviolet-laser stimulated desorption using (2+2)REMPI. An ArF excimer laser was used as a pump laser. The pump laser irradiated the Pt(001) surface at 25° from the surface normal via a quartz window. The typical pump laser spot diameter on the surface was 3 mm. The typical laser shot repetition rate was 10 Hz. A tunable pulsed Coumarin 460 dye laser (Spectra-Physics Quanta-Ray PDL-2, λ = 449~454 nm, line width = 0.2 cm^{-1}, pulse duration = 6 ns) pumped by the third harmonic (355 nm) of Nd:YAG laser (Spectra-Physics Quanta-Ray DCR-11-3, λ = 1064 nm) was used as a probe laser. The probe laser was fired after the pump laser irradiation at a certain interval. Wavelength of the probe laser was scanned with a stepping motor controlled by a personal computer. The jitter of the interval from the pump laser irradiation to the probe laser firing was less than ±20 ns. The pulse-to-pulse power stability of the probe laser was ±8%. The probe laser was focused by a quartz lens with a focal length of 250 mm, and ionized desorbed neutral NO molecules in a specific rotational state of the v" = 0 level of the ground electronic state ($X^2\Pi_{1/2,3/2}$). The probe laser spot diameter at the focal point was supposed to be some tens of μm.

The upper part of fig. 4-2 shows the experimental arrangement in the UHV chamber for the detection of desorbed neutral NO. The NO^+ ions generated by the probe laser irradiation were accelerated to a flight tube, and detected by a microchannel plate (MCP) assembly. The NO^+ signals were amplified, and stored as a time-of-flight (TOF) spectrum. The lower part of fig. 4-2 shows a TOF

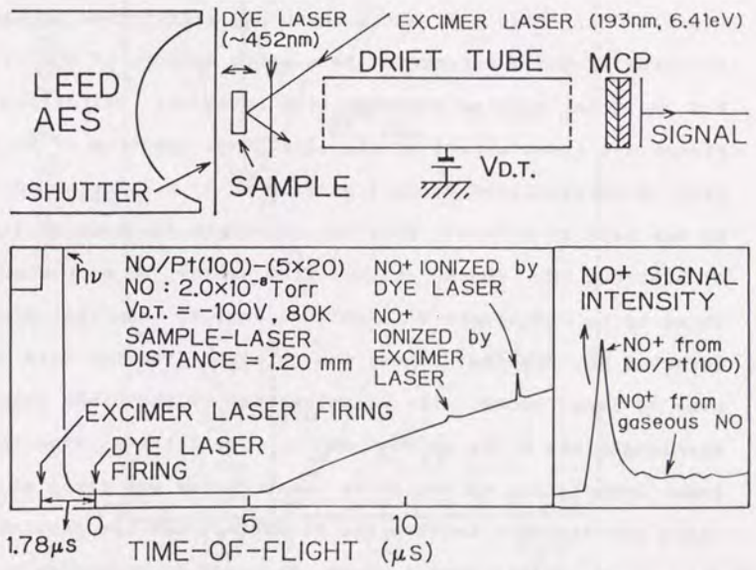

Fig. 4-2. Upper part: Experimental arrangement in the UHV chamber for the detection of desorbed neutral NO. Lower part: Time-of-flight (TOF) spectrum for the NO^+ signals from NO desorbed from Pt(001).

spectrum. Since the electric potential at the focal point of probe laser beam is different from that in the vicinity of the Pt surface, the signal for the NO^+ ions generated by the probe laser irradiation appears at a different position in a TOF spectrum from that for the NO^+ ions generated by the pump laser irradiation in the vicinity of the surface. Therefore, the peaks of the two NO^+ signals are easily distinguished. I have measured the NO^+ signal as a function of the probe laser wavelength. When the two-photon energy of the probe laser is equal to the transition energy of

$$A^2\Sigma(v'=0,J') \leftarrow X^2\Pi_{1/2,3/2}(v''=0,J''),$$

the ionization cross section of NO is resonantly enhanced ((2+2)REMPI) (fig. 4-3) and a sharp NO^+ signal peak appears in the spectrum (v and J represent the quantum numbers of the vibration and the total angular momentum (the rotation), respectively [1].) Figure 4-4 shows a part of the (2+2)REMPI spectrum of NO desorbed from an NO-saturated Pt(001) surface at 80 K. The ambient gaseous NO was kept at 2.0×10^{-8} Torr to compensate the loss of the amount of adsorbed NO. The NO^+ signal from ambient NO molecules was found to be two orders of magnitude smaller than that from desorbed NO. The NO^+ signal was obtained from the data averaged over 32 laser shots. The scanning step of the probe laser wavelength was 0.004 nm (0.2 cm^{-1}). The interval from the pump laser irradiation to the probe laser firing was fixed at 1.78 μs. Since the distance between the Pt surface and the focused probe laser beam was fixed at 1.20 mm, desorbed NO molecules with a velocity of 670 m/s were detected in the measurement.

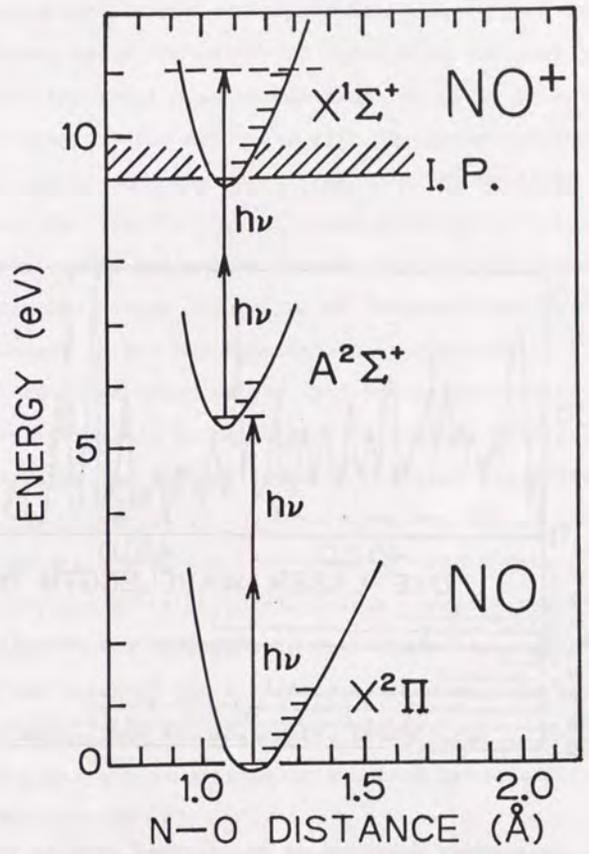

Fig. 4-3. Potential curves for NO free molecule in the $X^2\Pi$ and $A^2\Sigma$ states. The (2+2)REMPI process is shown with arrows.

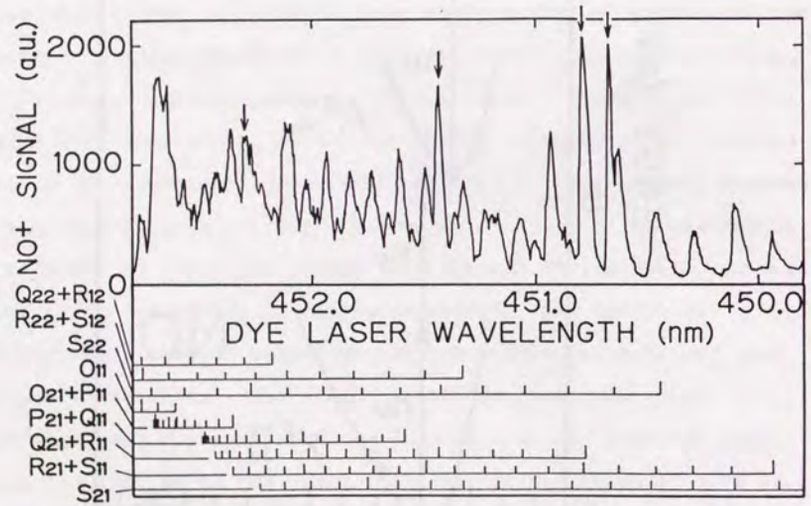

Fig. 4-4. (2+2)REMPI spectrum of NO desorbed from an NO-saturated Pt(001) surface at 80 K. Arrows indicate the exceptionally enhanced NO^+ signals because of a (2+1+1)REMPI process.

4.3 Results

O, P, Q, R, and S branches ($\Delta J = J'-J'' = -2, -1, 0, +1$, and +2, respectively) are observable in a (2+2)REMPI spectrum. The ground state ($X^2\Pi$) is split by the spin-orbit interaction into two sets of rotational levels corresponding to the $X^2\Pi_{1/2}$ and the $X^2\Pi_{3/2}$ states, where the subscript represents the z-principal axis component of the total angular momentum (Ω) [1]. On the other hand, each level of the $A^2\Sigma$ state with the given quantum number of the total angular momentum apart from spin (K) consists of two components, i.e. the $A^2\Sigma(v',K',J')$ and $A^2\Sigma(v',K',J'+1)$ levels [1]. However, the energy difference between the two components is smaller than the energy resolution of the probe laser. Therefore, twelve branches in all are expected to be resolved in a (2+2)REMPI spectrum. The lower part of fig. 4-4 shows the transition energies for $J'' \leq 39/2$ calculated using a table of expressions for energy levels of the $A^2\Sigma$ and $X^2\Pi_{1/2,3/2}$ states [2]. The first number of the subscript in the branch representation indicates the level of the $A^2\Sigma$ state, i.e. the numbers 1 and 2 denote the $A^2\Sigma(v',K',J')$ and $A^2\Sigma(v',K',J'+1)$ levels, respectively. The second number of the subscript in the branch representation indicates the level of the $X^2\Pi$ state, i.e. the numbers 1 and 2 denote the $X^2\Pi_{1/2}$ and $X^2\Pi_{3/2}$ levels, respectively. Some of the NO^+ signal peaks are exceptionally enhanced because of a (2+1+1)REMPI process [3].

To estimate the rotational temperature of desorbed NO qualitatively, I compared the $R_{21}+S_{11}$ branch of the (2+2)REMPI

spectrum of NO desorbed from Pt(001) at 80 K with that of gaseous NO at 300 K (fig. 4-5). The intensity of the NO^+ signal of the low rotational levels for the gaseous NO is enhanced, owing to the NO molecules scattered from the Pt(001) surface at 80 K which was placed close to the ionization region. The intensity ratio of the NO^+ signal of the higher to the lower levels in the high rotational energy region ($\sim 21/2 < J'' < \sim 37/2$) for desorbed NO is comparable with that for the gaseous NO at 300 K. This result suggests that the rotational temperature of desorbed NO is ~300 K. I have estimated the Pt surface temperature rise using an equation for laser-induced surface heating derived by Ready [4], and found that the temperature rise is 6 K (see Section 3.3). Since the initial surface temperature is 80 K, this result indicates that NO is desorbed by a photochemical process.

I have also preliminarily measured the NO^+ signal as a function of the interval from the pump laser irradiation to the probe laser firing, which corresponds to the time-of-flight (TOF) of neutral NO from desorption to ionization. Since the distance between the Pt(001) surface and the focused probe laser beam was fixed at 1.20 mm during the measurement, the TOF spectrum reflects the translational energy distribution of desorbed NO. Figure 4-6 shows one of the TOF spectra for the $X^2\Pi_{1/2}(v''=0, J''=23/2)$ state (S_{21} branch). The Pt(001) surface was initially exposed to NO to the saturation coverage at 80 K, and the residual NO gas was pumped out. The reduction effect in the amount of adsorbed NO induced by photostimulated desorption is not corrected. The effect, however, is not serious, because the shape of the TOF

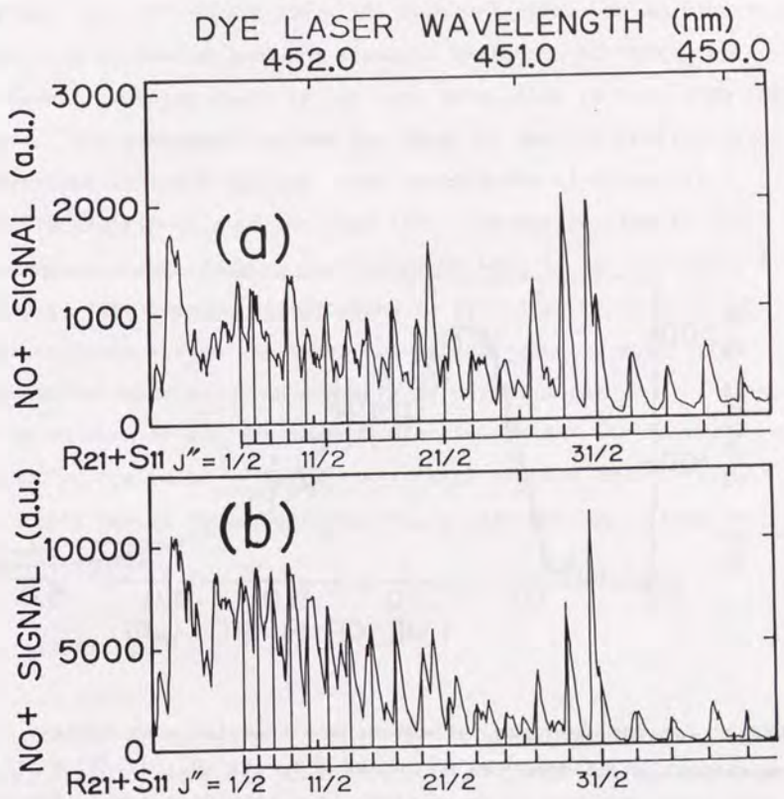

Fig. 4-5. (2+2)REMPI spectrum of (a) NO desorbed from an NO-saturated Pt(001) surface at 80 K (pump laser fluence on the surface is 1.2±0.1 mJ/cm^2) and (b) gaseous NO with the pressure of 5.0×10^{-7} Torr at 300 K. The effect of the probe laser fluence change during wavelength scanning is not corrected in both cases.

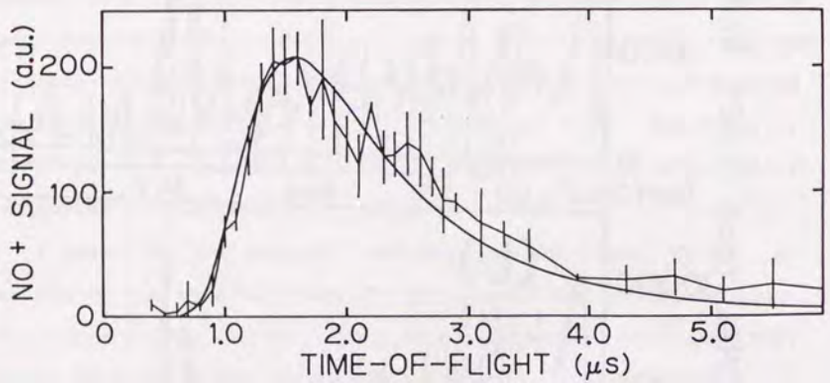

Fig. 4-6. TOF spectrum reflecting the translational energy distribution of desorbed NO in the $X^2\Pi_{1/2}$ (v"=0,J"=23/2) state. Pump laser fluence on the surface is 0.38±0.04 mJ/cm^2. The curved solid line represents the Maxwell distribution of the form $f(v) = Av^3 \exp(-mv^2/2k_B T)$, where A is a fitting parameter, v the velocity of the molecules, m the mass, k_B the Boltzmann constant, and T the translational temperature of 530 K. The transformation of coordinate system from v was performed using an appropriate Jacobian ($dv/dz \propto 1/t \propto v$, where z is the distance between the Pt(001) surface and the focused probe laser beam, and t the TOF).

spectrum was not significantly changed when the spectrum was reversely scanned. The NO$^+$ signal was obtained from the data averaged over 16 laser shots. The vertical error bar in the figure was estimated from the standard deviation of three data. The signal-to-noise ratio is not good especially in the large TOF region. The peak position and the shape of the TOF spectra were independent of laser fluence. The temperature of a Maxwell velocity distribution of the form $f(v) = Av^3 \exp(-mv^2/2k_B T)$ [5], the peak position of which was fitted to that of the TOF spectra, is 530 K. The Maxwell distribution is peaked at ~0.05 eV, when the coordinate system was transformed from velocity v to translational energy E using an appropriate Jacobian ($dv/dE \propto 1/v$). The calculated Pt surface temperature rise is 2 K for laser fluence of 0.4 mJ/cm^2. Since the initial surface temperature is 80 K, this result also shows that NO is desorbed by a photochemical process.

4.4 Discussion

As is stated in the former section, the translational energy distribution of desorbed NO in the $X^2\Pi_{1/2}$ (v"=0,J"=23/2) state was fitted by the Maxwell distribution with a translational temperature of 530 K. This result differs from the result in Chapter 3, in which I detected NO$^+$ ions generated by a three-photon process under the pump laser irradiation. As is stated in Section 3.3, the translational energy distribution of NO$^+$ ions was fitted by the Maxwell distribution with a translational

temperature of 3200 K. There are a few probable origins responsible for the discrepancy. The two-photon ionization of neutral NO at 193 nm may be preferential to vibrationally excited NO (v" > 0) [6], which has a different translational energy distribution from that for NO in the v" = 0 level. Or, the NO$^+$ ions might have been accelerated by a stray electronic field in the previous study. Further experiments are required to find the true origin.

The mechanism of the observed photostimulated desorption will be discussed in Section 6.4 after every results obtained in the present study are discribed.

References

[1] G. Herzberg, Molecular Spectra and Molecular Structure I, 2nd ed. (Van Nostrand Reinhold, New York, 1950).

[2] W.G. Mallard, J.H. Miller, and K.C. Smyth, J. Chem. Phys. 76, 3483 (1982).

[3] T.C. Steimle and H.-T. Liou, Chem. Phys. Lett. 100, 300 (1983).

[4] J.F. Ready, Effects of High-Power Laser Radiation (Academic Press, New York, 1971).

[5] G. Comsa and R. David, Surf. Sci. Rep. 5, 145 (1985).

[6] A.M. Wodtke, L. Huwel, H. Schluter, G. Meijer, P. Andersen, and H. Voges, Opt. Lett. 13, 910 (1988).

CHAPTER 5

Ultraviolet-Laser Stimulated Desorption of NO Chemisorbed on Pt(001) Studied Using (1+1) Resonance-Enhanced Multiphoton Ionization I

Photostimulated desorption of NO chemisorbed on Pt(001) at 80 K is studied using an s-polarized ArF excimer laser (λ =193 nm, 6.41 eV) and a (1+1) resonance-enhanced multiphoton ionization ((1+1)REMPI) technique. The internal energies up to 1000 cm^{-1} for desorbed NO in the $X^2\Pi_{1/2}$ (v"=0) and $X^2\Pi_{3/2}$ (v"=0) states are found to be represented by nearly-Boltzmann distributions with rotational temperatures of 303 and 283 K, respectively. In the higher energy region (>1000 cm^{-1}), however, the internal energies deviate from the Boltzmann distribution to a higher rotational temperature. The results are compared in detail with those of the other state-selective studies of electron-stimulated and photostimulated desorption studies.

5.1 Introduction

In the former chapter, I have stated a study of photo-stimulated desorption of NO chemisorbed on Pt(001) at 80 K using a pump laser (λ = 193 nm, 6.41 eV) and a (2+2) resonance-enhanced multiphoton ionization ((2+2)REMPI) technique. However, the detailed informations on the internal-energy distributions for desorbed NO were not obtained, because the (2+2)REMPI method does not provide quantitative internal energy distributions. To overcome the problem, I have improved the apparatus, and detected desorbed neutral NO using a (1+1)REMPI technique. (1+1)REMPI, as well as laser-induced fluorescence (LIF), is a state-selective detection technique, which has proved to be a powerful tool in elucidation of desorption mechanisms [1] (see Sections 1.3 and 1.4). The internal energy distributions were quantitatively measured for NO in the $X^2\Pi_{1/2}$ (v"=0) and $X^2\Pi_{3/2}$ (v"=0) states desorbed from an NO-saturated Pt(001) surface at 80 K irradiated by an s-polarized ArF excimer laser. For the internal energies less than 1000 cm^{-1}, the distributions are found to be represented by nearly-Boltzmann distributions for both the spin-orbit states. The population for low rotational quantum numbers in the $X^2\Pi_{3/2}$ state, however, was found to be slightly enhanced than that in the $X^2\Pi_{1/2}$ state. The rotational temperature in the low-energy region was 303 and 283 K for the $X^2\Pi_{1/2}$ and $X^2\Pi_{3/2}$ states, respectively. Furthermore, in high internal energy region, the internal energies deviate from the Boltzmann distribution to a higher rotational temperature. The present results were compared in detail with

those reported in the other state-selective studies of electron-stimulated and photostimulated desorption.

5.2 Experiment

Figure 5-1 shows the improved experimental arrangement for the state-selective study of ultraviolet-laser stimulated desorption using (1+1)REMPI. An ArF excimer laser was linearly polarized using a quartz plate placed at Brewster's angle. The polarized laser (typical polarization > 95%) was used as the pump laser. The direction of the polarization can be changed with a $\lambda/2$ wavelength plate. The typical pump laser spot diameter on the Pt(001) surface was 3 mm. A tunable pulsed Coumarin 460 dye laser was frequency-doubled in a β-barium borate (BBO) crystal to generate a tunable s-polarized probe laser (λ = 225~227 nm) for the (1+1)REMPI detection. The probe laser path was adjusted during the wavelength scan, so that the position of the ionization region did not change. The probe laser was gently focused by a quartz cylindrical lens with a focal length of 500 mm, and ionized desorbed NO molecules state-selectively. The probe laser spot size at the ionization region was 1x3 mm^2. Both the pump laser and the probe laser power were monitored, and adjusted to a constant value during a sequence of measurements. The NO^+ ions generated by the probe laser irradiation were accelerated to the flight tube, and detected by an MCP assembly. An ion deflector was mounted between the flight tube and the MCP, so that the pump laser photons could not impinge on MCP. Figure 5-2 shows the

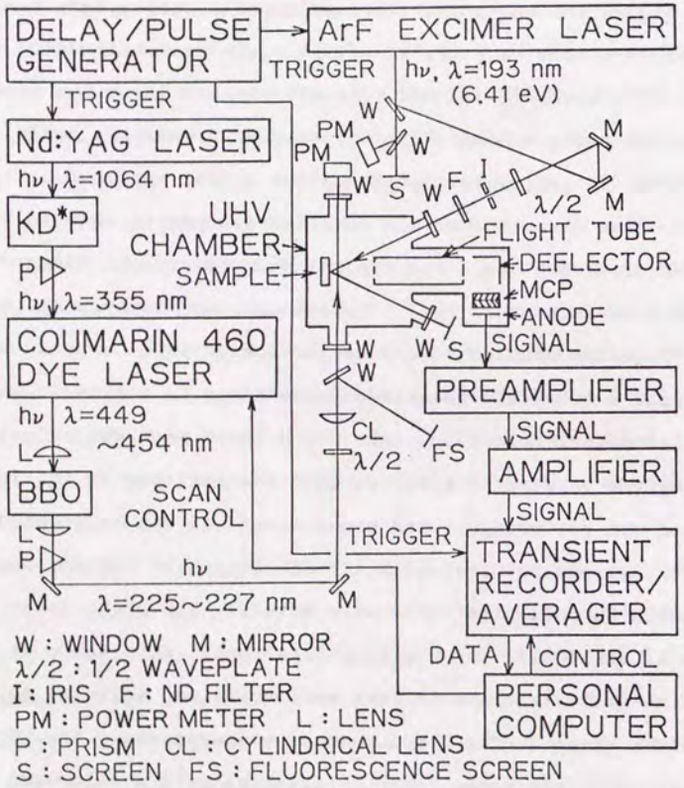

Fig. 5-1. Schematical drawing of the improved experimental arrangement for the state-selective study of ultraviolet-laser stimulated desorption using (1+1)REMPI.

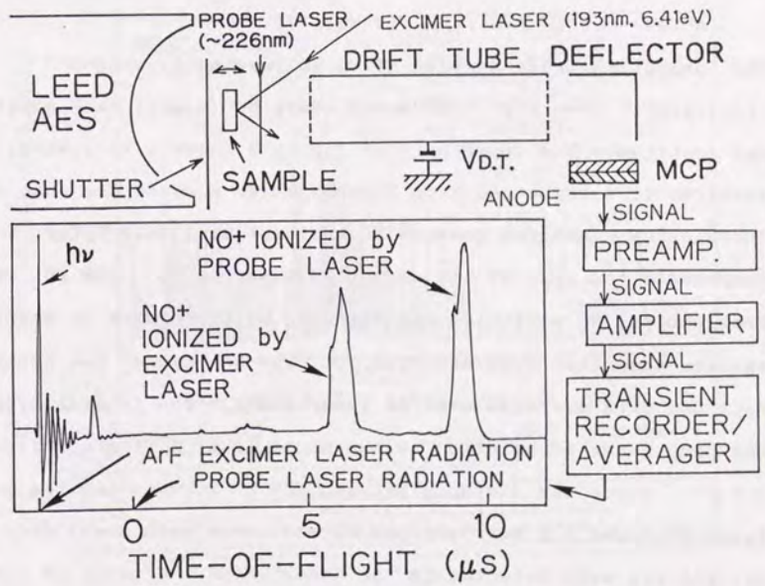

Fig. 5-2. Upper part: Experimental arrangement in the UHV chamber for the detection of desorbed neutral NO. Lower part: TOF spectrum for the NO^+ signals from NO desorbed from Pt(001).

experimental arrangement in the UHV chamber for the detection of desorbed neutral NO, and the Time-of-flight (TOF) spectrum for the $NO^{\cdot}$ signals from NO desorbed from Pt(001). The other details of the apparatus and the experimental conditions are same as those described in Section 4.2.

5.3 Results

I have measured the $NO^{\cdot}$ signal as a function of the probe laser wavelength. When the one-photon energy of the probe laser is equal to the transition energy of

$$A^2\Sigma(v'=0,J') \leftarrow X^2\Pi_{1/2,3/2}(v''=0,J''),$$

the ionization cross section of NO is resonantly enhanced ((1+1)REMPI) (see fig. 4-3) and a sharp $NO^{\cdot}$ signal peak appears in the spectrum. The upper part of fig. 5-3 shows a (1+1)REMPI spectrum of desorbed NO from Pt(001) at 80 K under the pump laser irradiation. Ambient gaseous NO was kept at 2.0×10^{-8} Torr to compensate the loss of the amount of adsorbed NO. The $NO^{\cdot}$ signal from ambient NO molecules was found to be two orders of magnitude smaller than that from desorbed NO. The $NO^{\cdot}$ signal was obtained from the data averaged over 32 laser shots. The interval from the pump laser irradiation to the probe laser firing was fixed at 3.0 μs. Since the distance between the Pt surface and the probe laser beam was 2.2 mm, desorbed NO molecules with a velocity of 570~900 m/s were detected in the measurement. Fluence of the pump laser and the probe laser were 2.2 and 0.87 mJ/cm^2, respectively. The lower part of fig. 5-3 shows the transition energies for

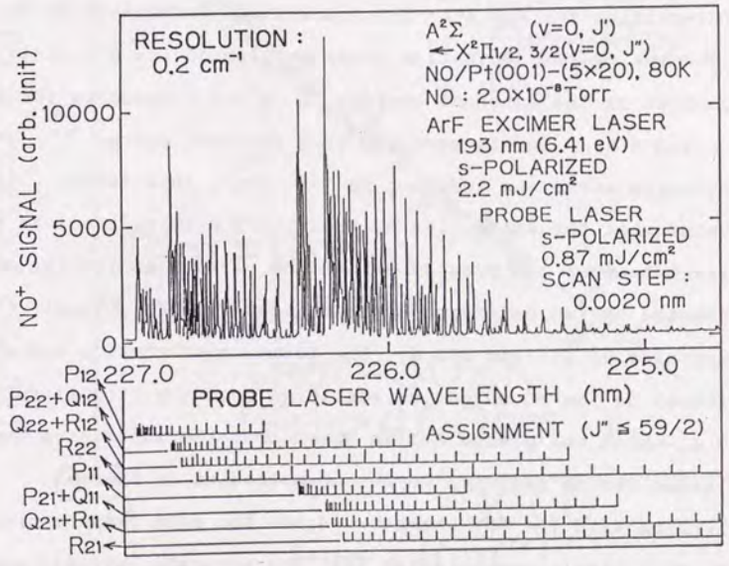

Fig. 5-3. (1+1)REMPI spectrum of NO molecules in the $X^2\Pi_{1/2}(v''=0)$ and $X^2\Pi_{3/2}(v''=0)$ states desorbed from Pt(001) at 80 K under the s-polarized pump laser irradiation.

J" ≤ 59/2 calculated using a table of expressions for energy levels of the $A^2\Sigma$ and $X^2\Pi_{1/2,3/2}$ states [2]. R, Q, and P branches correspond to the transition sets with $\Delta J = J'-J"$ = +1, 0, and -1, respectively (see Section 4.3).

To ascertain that the present experimental arrangement gives the accurate internal energy distribution, a (1+1)REMPI spectrum for the gaseous NO molecules was measured under the ambient NO pressure of 5.0×10^{-7} Torr. The other conditions are the same as those in the above photostimulated desorption measurement except for no pump laser irradiation. The population in a particular internal energy was calculated from the (1+1)REMPI spectrum using the intensities for the $A^2\Sigma \leftarrow X^2\Pi$ transitions formulated by Earls [3], and taking the ionization cross section of the $A^2\Sigma$ state as independent of the internal energy. R, Q and P branches for the $X^2\Pi_{1/2}$ and $X^2\Pi_{3/2}$ levels gave the same internal energy distribution curve, as is shown in fig. 5-4. This result indicates that the saturation of the $A^2\Sigma \leftarrow X^2\Pi$ transitions is not significant under the present conditions. The distribution can be represented by two Boltzmann distributions with rotational temperatures of 115 and 302 K. The former distribution was attributed to the NO molecules scattered from the Pt(001) surface at 80 K, which was placed 2.2 mm apart from the ionization region. The latter can be assigned to the NO molecules in thermal equilibrium with the UHV chamber. Since the room temperature was 299 K, this result demonstrates that the accurate internal energy distributions can be obtained in the present procedure.

Figure 5-5 shows the internal energy distributions for

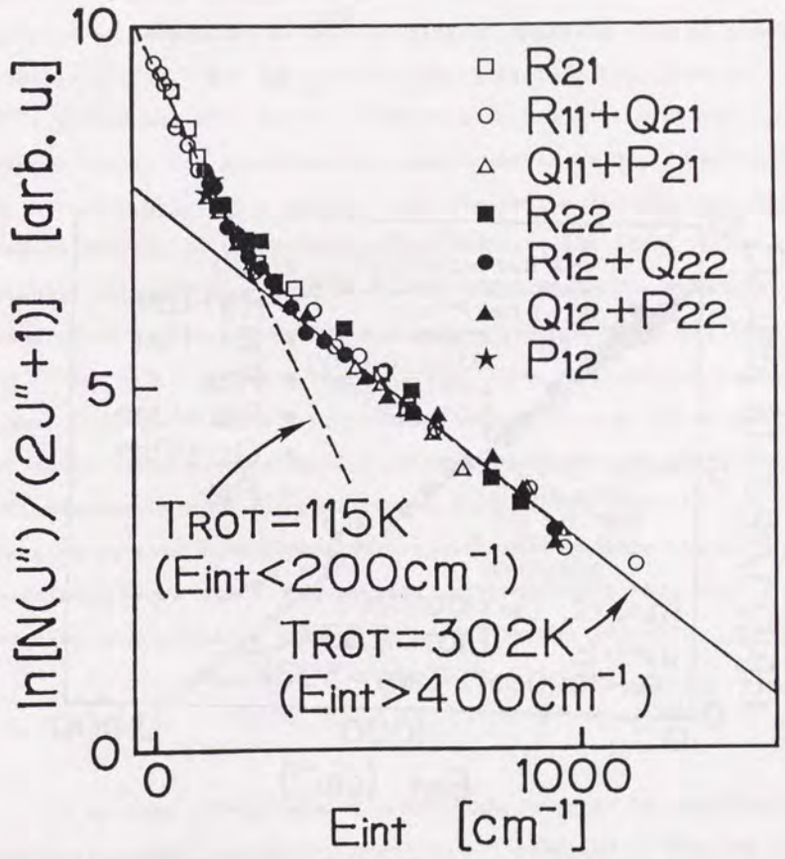

Fig. 5-4. Internal energy distributions for gaseous NO molecules in the $X^2\Pi_{1/2}$ (v"=0) and $X^2\Pi_{3/2}$ (v"=0) states.

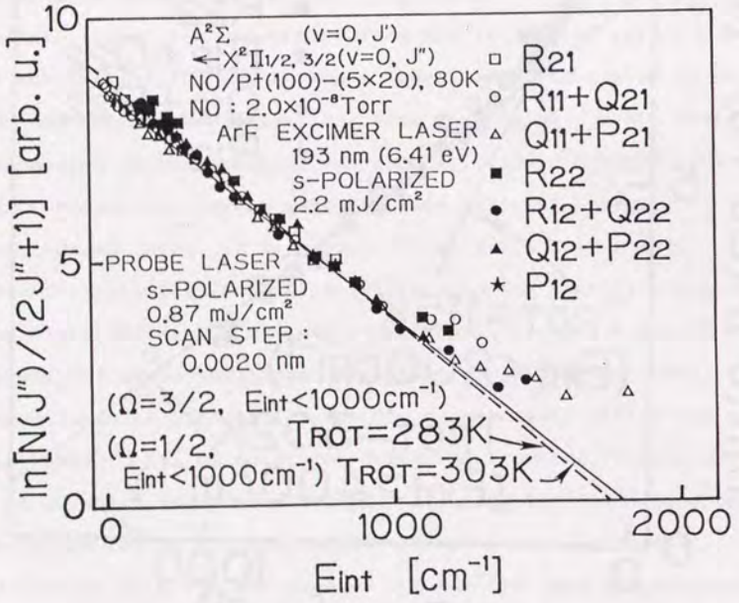

Fig. 5-5. Internal energy distributions for NO molecules in the $X^2\Pi_{1/2}$ (v"=0) and $X^2\Pi_{3/2}$ (v"=0) states desorbed from Pt(001) at 80 K under the s-polarized pump laser irradiation.

desorbed NO molecules calculated from the (1+1)REMPI spectrum in fig. 5-3. The data were corrected by subtracting the (1+1)REMPI signal from the ambient NO molecules. R, Q, and P branches gave the same internal energy distribution curves. This result indicates that 2π electron in the desorbed NO occupies the orbital parallel or perpendicular to the plane of rotation with an equal probability [4]. For the internal energies less than 1000 cm^{-1} ($J'' \leq 23+1/2$ and $J'' \leq 21+1/2$ in the $X^2\Pi_{1/2}$ and $X^2\Pi_{3/2}$ states, respectively), the distributions were found to be nearly Boltzmann for both the spin-orbit states. The population for low rotational quantum numbers in the $X^2\Pi_{3/2}$ state, however, was found to be slightly enhanced than that in the $X^2\Pi_{1/2}$ state. The rotational temperature in the low-energy region was 303 and 283 K for the $X^2\Pi_{1/2}$ and $X^2\Pi_{3/2}$ states, respectively. These values are much higher than the maximum surface temperature of 86 K, which was estimated using an equation for laser-induced surface heating [5]. Furthermore, in high internal energy region, the internal energies deviate from the Boltzmann distribution to a higher rotational temperature. These results demonstrate that the observed desorption is induced by a non-thermal process.

5.4 Discussion

In an electron-stimulated desorption study of NO chemisorbed on Pt(111) using (1+1)REMPI, Burns et al. proposed a detailed model in which NO is desorbed via a long-lived relatively-free-rotor excited state created by the $2\pi_a \leftarrow 5\sigma$ excitation of

chemisorbed NO [6] (see Section 1.4). The internal energy distributions of the desorbed NO reported by Burns et al. are in good agreement with the present results in the following aspects (fig. 5-6(a) and (b)): (1) The internal energies are characterized by a nearly-Boltzmann distribution in the low-energy region. (2) The internal energies deviate from the Boltzmann distribution to the higher rotational temperature in the high-energy region. Furthermore, the translational energy distribution of desorbed NO measured in the present study using (2+2)REMPI (see Chapter 4) is also in good agreement with those reported by Burns et al. (see fig. 5-7). However, there are also several differences between the two studies: (1) The rotational temperature observed in the electron-stimulated desorption study (543 K) is higher than those found in the present study (283 and 303 K). (2) The 2π electron in the desorbed NO was found to have a tendency to occupy the orbital perpendicular to the plane of rotation (antisymmetric Λ doublets) in the electron-stimulated desorption study, while such a preference was not measurable in the present study.

The above common characteristics in the translational and internal energy distributions of desorbed NO were also reported by Prybyla et al. in a photostimulated desorption study of NO chemisorbed on Pd(111) using (1+1)REMPI and 200-fs laser pulse of 2.0-eV photon energy [7] (see fig. 5-6(a) and (c), and Section 1.4). The laser fluence dependence of the desorption yield was found to be represented by a power-law relation with an exponent of n = 3.3. The $X^2\Pi(v"=1)/X^2\Pi(v"=0)$ population ratio is ~0.3 corresponding to a vibrational temperature of 2200 K. They

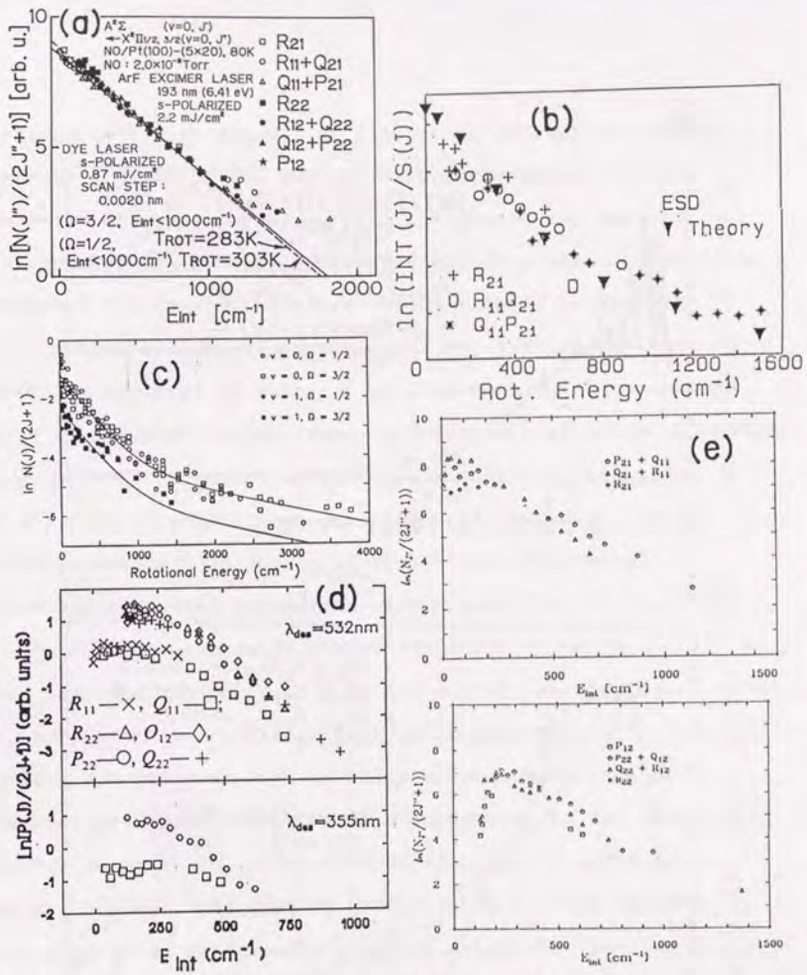

Fig. 5-6. Comparison of the internal energy distributions of desorbed neutral NO molecules measured in the present study with those measured in the other state-selective studies of electron-stimulated and photostimulated desorption of adsorbed NO. (a) The present study. Pt(001)-NO, $h\nu$ = 6.41eV. (b) Pt(111)-NO, incident electron energy = 325eV (from ref. [6]). (c) Pd(111)-NO, $h\nu$ = 2.0 eV (200 fs) (from ref. [7]). (d) Pt(111)-NO, $h\nu$ = 2.3 and 3.5eV (from ref. [8]). (e) Ni(001)-NiO-NO, $h\nu$ = 6.4eV (from ref. [9]). (See Section 1.4.)

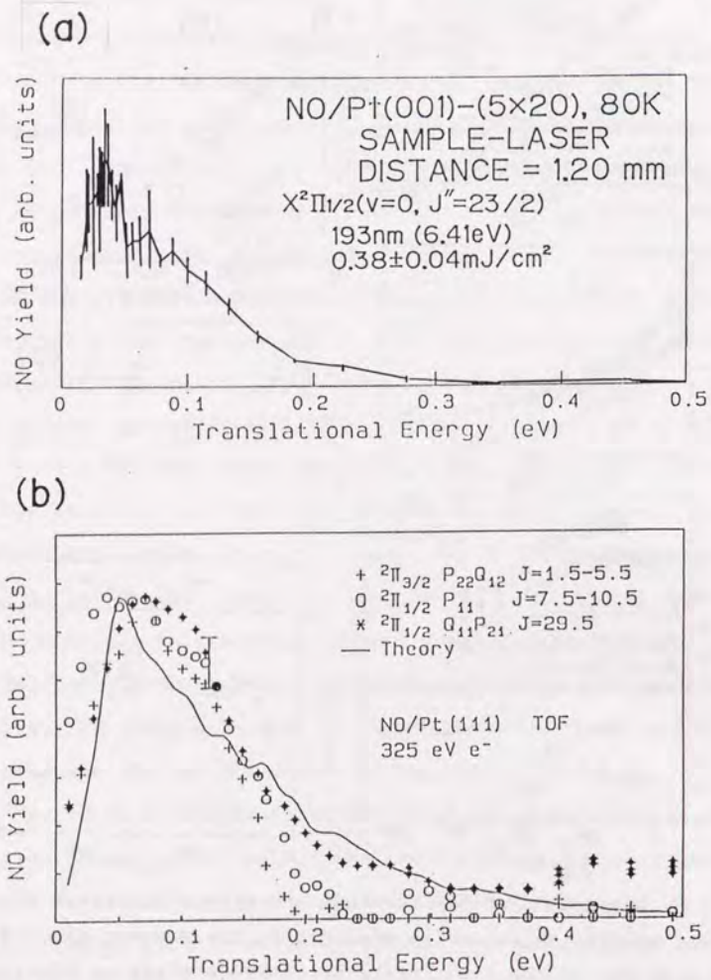

Fig. 5-7. Comparison of (a) the translational energy distribution of desorbed NO in the $X^2\Pi_{1/2}(v"=0, J"=23/2)$ state measured in the present study using (2+2)REMPI (see Chapter 4 and fig. 4-6) with (b) those reported in an electron-stimulated desorption study of NO chemisorbed on Pt(111) at 80 K by Burns et al. (from ref. [6]).

concluded that high density of electronic excitation in the substrate induced by the 200-fs laser pulse leads to novel desorption channels involving both the ground and excited electronic states of the chemisorbed NO. The short-pulse laser stimulated desorption, however, may be induced by the same photochemical process responsible for the electron-stimulated desorption reported by Burns et al., because the three photon energy of the short-pulse laser is comparable with the threshold energy obseved in the electron-stimulated desorption study (~6 eV). Burns et al. have also reported that desorbed NO molecules show a high degree of vibrational excitation ($X^2\Pi(v"=1)/X^2\Pi(v"=0)$ population ratio is ~0.58) [6].

In a laser-stimulated desorption study of NO on Pt(111) at 1064, 532, and 355 nm (1.2, 2.3, and 3.5 eV, respectively) using LIF, Buntin et al. concluded that NO is desorbed via a temporal negative ion state created by electron tunneling from photo-generated hot carriers in the metal substrate to the unoccupied state of chemisorbed NO [8] (see Section 1.4). The present results, however, are greatly different from those reported in their study such as markedly inverted spin-orbit population, non-Boltzmann rotational energy distributions (see fig. 5-6(a) and (d)), translational energy distributions peaked at high energy, and low desorption cross sections ($<10^{-21}$ cm^2). The present results are also different from those in a photostimulated desorption study of NO on non-metallic Ni-NiO, where pronounced spin-orbit selectivity in low rotational levels (see fig. 5-6(a) and (e)) and translational energy distributions peaked at high

energy were observed (see Section 1.4) [9].

References

[1] D.S. King and R.R. Cavanagh, in: Advances in Chemical Physics Vol. 75, ed. K.P. Lawley (John Wiley & Sons, New York, 1989) p.45.

[2] W.G. Mallard, J.H. Miller, and K.C. Smyth, J. Chem. Phys. 76, 3483 (1982).

[3] L.T. Earls, Phys. Rev. 48, 423 (1935).

[4] M.H. Alexander and P.J. Dagdigian, J. Chem Phys. 80, 4325 (1984).

[5] J.F. Ready, Effects of High-Power Laser Radiation (Academic Press, New York, 1971).

[6] A.R. Burns, E.B. Stechel, and D.R. Jennison, Phys. Rev. Lett. 58, 250 (1987); A.R. Burns, E.B. Stechel, and D.R. Jennison, J. Vac. Sci. Technol. A 5, 671 (1987); A.R. Burns, E.B. Stechel, and D.R. Jennison, J. Vac. Sci. Technol. A 6, 895 (1988).

[7] J.A. Prybyla, T.F. Heinz, J.A. Misewich, M.M.T. Loy, and J.H. Glownia, Phys. Rev. Lett. 64, 1537 (1990).

[8] S.A. Buntin, L.J. Richter, R.R. Cavanagh, and D.S. King, Phys. Rev. Lett. 61, 1321 (1988); S.A. Buntin, L.J. Richter, D.S. King, and R.R. Cavanagh, J. Chem. Phys. 91, 6429 (1989).

[9] F. Budde, A.V. Hamza, P.M. Ferm, G. Ertl, D. Weide, P. Andresen, and H.-J. Freund, Phys. Rev. Lett. 60, 1518 (1988); P.M. Ferm, F. Budde, A.V. Hamza, S. Jakubith, G. Ertl, D. Weide, P. Andresen, and H.J. Freund, Surf. Sci. 218, 467 (1989).

CHAPTER 6

Ultraviolet-Laser Stimulated Desorption of NO Chemisorbed on Pt(001) Studied Using (1+1) Resonance-Enhanced Multiphoton Ionization II

Photostimulated desorption of NO chemisorbed on Pt(001) at 80 K is studied using (1+1)REMPI. An s- and a p-polarized ArF excimer laser are used as the pump laser. The desorption yield rapidly increases when the amount of NO exposure exceeds ~1.8 L. This result suggests that the majority of the observed photo-stimulated desorption is derived from NO chemisorbed on the on-top sites in the reconstructed Pt-(20x5) area probably with a straight configuration. The NO desorption yield is proportional to pump laser fluence for both the polarizations. The translational and internal energy distributions of desorbed NO are independent of the polarization of the pump laser. On the basis of these results, the mechanism of photostimulated desorption is discussed. The perspectives of the present work are described.

6.1 Introduction

In the present chapter, I report an advanced study of photostimulated desorption of NO chemisorbed on Pt(001) at 80 K using (1+1)REMPI. An s- and a p-polarized ArF excimer laser are used as the pump laser. The desorption yield was found to increase abruptly when the amount of NO exposure exceeds ~1.8 L. This result suggests that the majority of the observed photostimulated desorption is derived from NO chemisorbed on the on-top sites in the reconstructed Pt-(20x5) area probably with a straight configuration. The NO desorption yield was found to be proportional to pump laser fluence for both the polarizations. This result indicates that NO is desorbed by a one-photon process. The translational and internal energy distributions of desorbed NO were, however, found to be independent of the polarization of the pump laser within the errors. These results suggest that both the s- and the p-polarized laser irradiations create the same excited state, from which photostimulated desorption proceeds.

6.2 Experiment

The apparatus used is improved compared with that described in Section 5.2 as follows: (1) An ArF excimer laser is linearly polarized efficiently using a polarizer (Showa Kouki). (2) The polarized laser irradiates the Pt(001) surface at 81° from the surface normal. (3) The second harmonic of a high-resolution tunable Coumarin 460 dye laser (Spectra-Physics Quanta-Ray PDL-3,

line width = 0.07 cm^{-1}) is used as the probe laser. The typical pump laser spot area on the surface is 0.16 mm^2. The other details of the apparatus and the experimental procedure are same as those described in Section 5.2.

6.3 Results

Figure 6-1 shows the decays of the NO desorption yield against a sequence of the p-polarized pump laser irradiation. Before every measurement, the Pt(001)-(20x5) clean surface was exposed to NO at 80 K, and the residual NO gas was quickly pumped out. The probe laser wavelength is fixed at the band edge of the $P_{21}+Q_{11}$ branch, i.e., NO in the $X^2\Pi_{1/2}$ (v"=0,J"=1/2~9/2) states are probed. The probe laser spot size at the ionization region is ~1x1 mm^2. The interval from the pump laser irradiation to the probe laser firing is fixed at 2.5 μs. Since the distance between the Pt(001) surface and the probe laser is 2.0 mm, desorbed NO molecules with a velocity of 600~1000 m/s were detected in the measurement. Fluences of the pump laser and the probe laser are ~1.0 and ~3.2 mJ/cm^2, respectively. The initial fast decay from the first to the ~500th laser shot is probably derived from NO chemisorbed on defect sites (steps or kinks), because the desorption amount was much smaller than the total desorption amount after NO exposure of 6.0 L. The NO desorption yield increases rapidly when the amount of NO exposure exceeds ~1.8 L.

The desorption yields of NO in the $X^2\Pi_{1/2}$ (v"=0,J"=11/2) state are shown in fig. 6-2 as a function of pump laser fluence. The

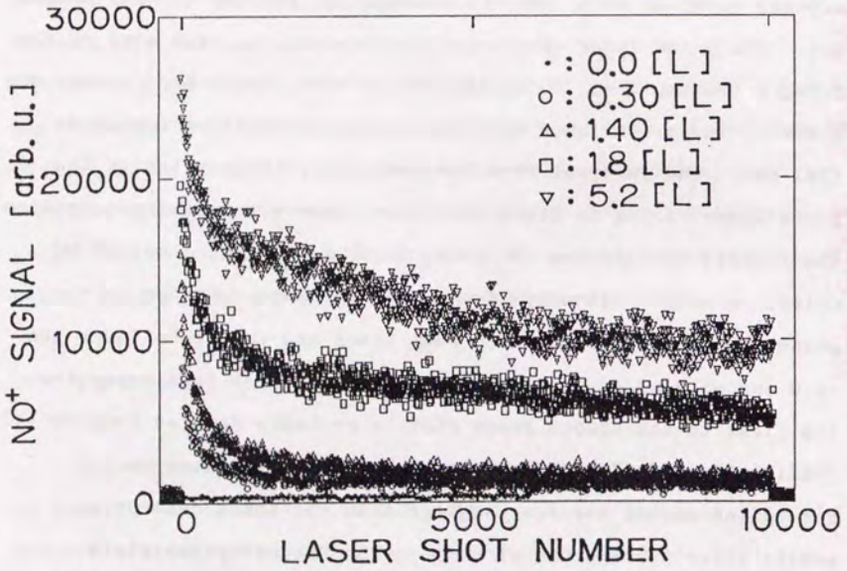

Fig. 6-1. Decay curves of the NO desorption yield against a sequence of the p-polarized pump laser irradiation.

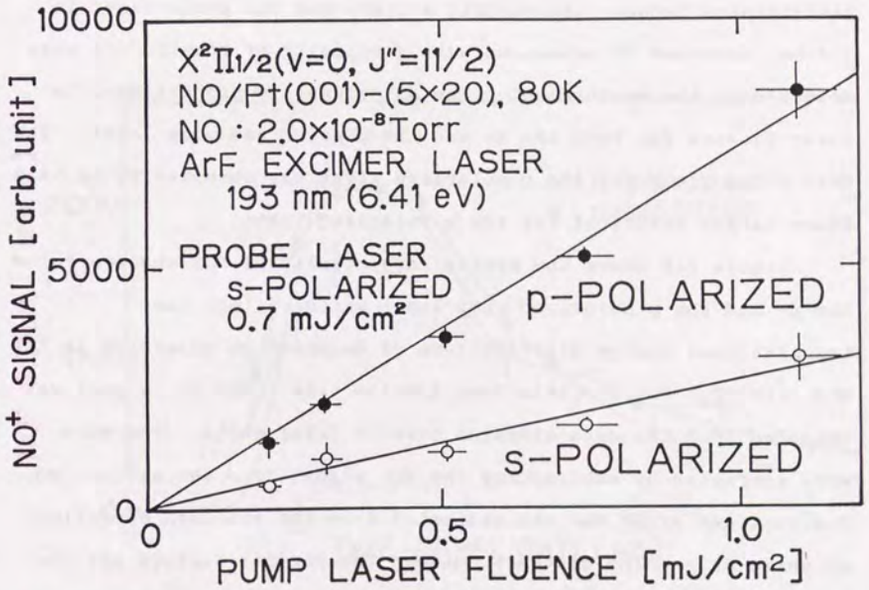

Fig. 6-2. Laser fluence dependence of the yield of NO in the $X^2\Pi_{1/2}$(v"=0,J"=11/2) state desorbed from Pt(001) at 80 K under the s- and the p-polarized pump laser irradiations. The abscissa is laser fluence on the surface. The reduction of electric field in the vicinity of the surface is not considered. The solid straight line is the regression line fitted by the least-squares method.

ambient gaseous NO is kept at 2.0×10^{-8} Torr during the measurements to compensate the loss of the amount of adsorbed NO. The NO^+ signal was obtained from the TOF spectrum averaged over 32 laser shots. The data were corrected by subtracting the NO^+ signal from the ambient NO. The vertical error bar is estimated from the standard deviation of three data. The probe laser spot size at the ionization region is $\sim 1 \times 3$ mm^2. The interval from the pump laser irradiation to the probe laser firing is 3.3 μs. Since the distance between the Pt(001) surface and the probe laser is 1.7 mm, desorbed NO molecules with a velocity of 360~660 m/s were detected in the measurement. The NO^+ signal is proportional to laser fluence for both the s- and the p-polarized pump laser. The desorption yield for the p-polarized light was observed to be ~2.9 times larger than that for the s-polarized light.

Figure 6-3 shows the preliminary results of TOF spectra for the s- and the p-polarized pump laser which reflect the translational energy distributions of desorbed NO molecules in the $X^2\Pi_{1/2}$ (v"=0,J"=11/2) state (see Section 4.3). The NO^+ signal was obtained from the data averaged over 16 laser shots. The data were corrected by subtracting the NO^+ signal from the ambient NO. The vertical error bar was estimated from the standard deviation of three data. The distance between the Pt(001) surface and the focused probe laser was 1.8 mm. The peak position and the shape of the TOF spectra are independent of the polarization of the pump laser within the errors. The temperature of a Maxwell velocity distribution, the peak position of which was fitted to that of the TOF spectra, is 400 K. The temperature of the fitted Maxwell

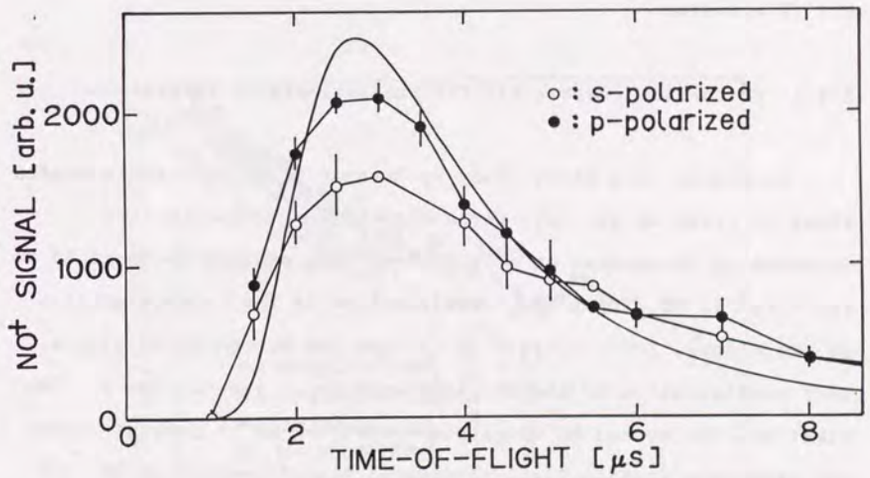

Fig. 6-3. TOF spectra reflecting the translational energy distributions of NO in the $X^2\Pi_{1/2}$ (v"=0,J"=11/2) state desorbed from Pt(001) at 80 K under the s- and the p-polarized pump laser irradiations. The curved solid line represents the Maxwell distribution of the form $f(v) = Av^3 \exp(-mv^2/2k_B T)$, where T is the translational temperature of 400 K (see Section 4.3 and fig. 4-6).

distribution is lower than that for desorbed NO in the $X^2\Pi_{1/2}$ (v"=0,J"=23/2) state (530 K, see Section 4.3 and fig. 4-6). These results suggest that the translational energy of desorbed NO increases as the rotational quantum number increases.

Figure 6-4 shows the preliminary data of the internal energy distributions of desorbed NO molecules for the s- and p-polarized pump laser. The data were not corrected for the NO· signal from the ambient NO. The internal energy distributions are independent of the polarization of the pump laser within the errors.

6.4 Discussion

6.4.1 NO species responsible for photostimulated desorption

According to a RAIRS study by Gardner et al. [1] and a HREELS study by Pirug et al. [2], three chemisorbed NO species are supposed to be present on a Pt(001) surface exposed to NO at 80 K. The first is NO with a bent configuration in the reconstructed Pt-(20x5) area (ν_{N-O} = ~1680 cm^{-1}), and the second is NO with a bent configuration in the Pt-(1x1) area (ν_{N-O} = ~1630 cm^{-1}). The first and the second NO species are reported to be present before and after the (20x5)→(1x1) structural transformation of the top-most Pt layer at 90 K, respectively [1] (see Section 1.2 and fig. 1-4). In the present study the (20x5)→(1x1) transformation occurs in the NO exposure range of 0.8-1.0 L, as is stated in Section 2.3.4. The third species is NO in the Pt-(20x5) area probably with a straight configuration (ν_{N-O} = ~1790 cm^{-1}), which

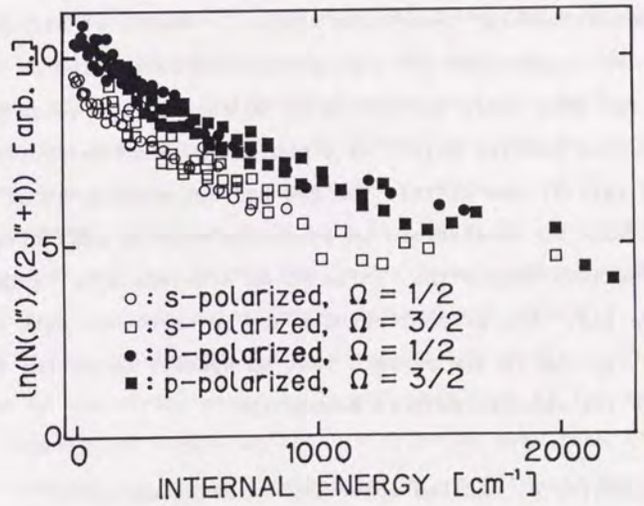

Fig. 6-4. Internal energy distributions for NO molecules in the $X^2\Pi_{1/2}$ (v"=0) and $X^2\Pi_{3/2}$ (v"=0) states desorbed from Pt(001) at 80 K under the s- and the p-polarized pump laser irradiations.

is reported to be present after NO exposure of 5 L at 140 K [2] (see Section 1.2 and fig. 1-3). On the other hand, NO desorption yield is found to increase rapidly when the amount of NO exposure exceeds ~1.8 L in the present study (see fig. 6-1). This result suggests that the third NO species is most sensitive for photostimulated desorption, while both the first and the second NO species with a bent configuration exhibit similar small sensitivity. Therefore, the majority of the observed photo-stimulated desorption from an NO-saturated Pt(001) sruface at 80 K is probably derived from the third NO species on the Pt-(20x5) area probably with a straight configuration.

The adsorption state selectivity is also reported in the other photostimulated desorption studies. Buntin et al. assigned the species responsible for photostimulated desorption of NO on Pt(111) for 1064, 532, and 355 nm to NO chemisorbed on an on-top site [3] (see Section 1.4). In a photostimulated desorption study of NO on Ag(111) and Cu(111) for 250-680 nm, Franchy et al. reported that NO chemisorbed on an on-top site is sensitive for photostimulated desorption, while NO on a bridge site is not sensitive [4]. The present results are in agreement with these previous reports in the respect that NO species on on-top sites is sensitive for photostimulated desorption.

6.4.2 Lifetime of excited molecules on metal surfaces

Before discussing the mechanism of the observed photo-stimulated desorption, I briefly review the related studies.

First, I introduce several theoretical and experimental studies on the lifetimes and the potential energy curves of excited states for molecules adsorbed on metal surfaces in this section. These issues are extremely important for understanding the mechanism of desorption induced by electronic excitations [5]. Then, I survey the mechanisms proposed by the other groups in photo- or electron-stimulated desorption studies of NO chemisorbed on metal surfaces in Section 6.4.3.

The most rapid deexcitation process on metal is the resonant electron tunneling. The characteristic time (τ) of the resonant tunneling is given by $\tau = h/2\pi\Gamma$, where Γ is the width of the resonance. Nordlander and Tully have carried out calculations of the shifts and lifetimes of the excited states for a hydrogen atom and alkali atoms interacting with jellium surfaces, using density functional potentials, non-local exchange and correlation energies, and the complex scaling theory [6]. For an excited hydrogen at a typical metal-adsorbate distance of ~3 Å from a model Al surface (jellium with $r_s = 2$), the resonance widths are calculated to be ~0.3 eV for the $2s+2p_z$ state, and ~3 eV for the $2s-2p_z$ state (corresponding to the lifetimes of $\sim 2\times10^{-15}$ and $\sim 2\times10^{-16}$ s, respectively), as is shown in fig. 6-5(a). The lifetime of the $2s+2p_z$ state is longer than that of the $2s-2p_z$ state, because the $2s+2p_z$ orbital is oriented away from the surface whereas the $2s-2p_z$ orbital is oriented toward the surface. The resonant widths can also be estimated in the linewidth measurements. In an electron spectroscopic study using synchrotron radiation, Schönhense et al. reported that the

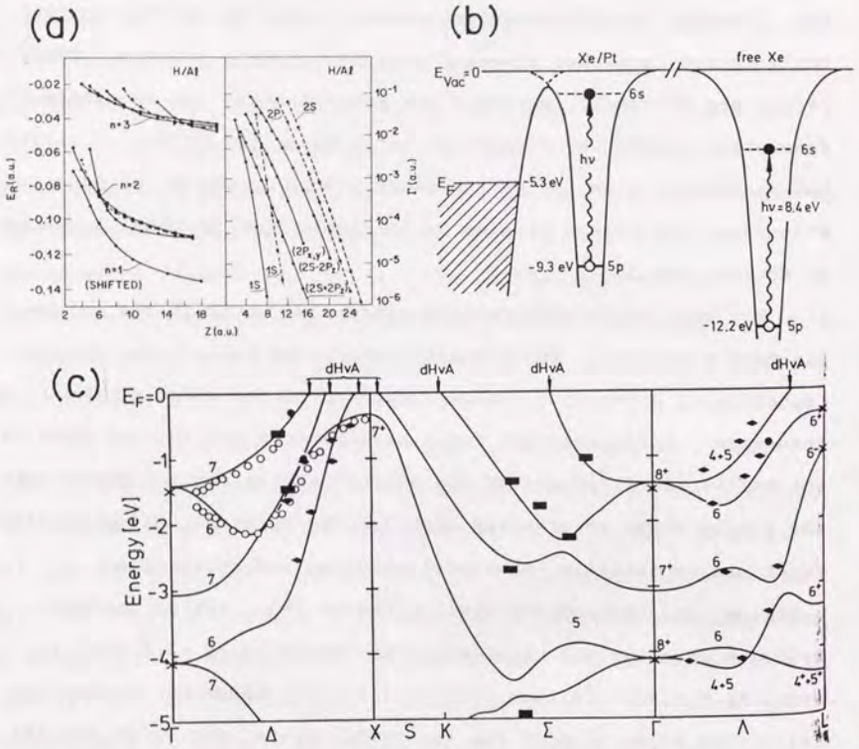

Fig. 6-5. (a) Calculated energy level shifts (left) and resonance widths (right) in atomic units (a.u., 1 a.u. = 27.2 eV and 1 a.u. = 0.529 Å)) for the lowest hydrogen states on Al. Dashed lines in the right-hand figure are the results from an earlier calculation. (From ref. [6].) (b) Schematic drawing of effective one-electron potential curves for Xe on Pt(111), and free Xe. (From ref. [7].) (c) Calculated (solid lines) and experimental (symbols) valence band structure of Pt. (From ref. [8].)

linewidth of the 6s←5p transition for Xe on Pt(111) to be <0.08 eV [7]. The 5p level of the physisorbed Xe is located ~4 eV below the Fermi level (fig. 6-5(b)), whereas the valence band of Pt locates in the region of 0~5 eV below the Fermi level [8] (fig. 6-5(c)). Therefore, this result indicates that the characterstic time of the resonant tunneling from the Pt valence band to the 5p hole of Xe^{*} is at least longer than $\sim 9\times10^{-15}$ s.

The time taken for desorption (t) is estimated to be $\sim10^{-14}$ s [5]. Since the probability of desorption depends on the exponential of the decay rate of the intermediate excited state, the above calculated and observed characteristic time of the resonant tunneling for molecules chemisorbed on metal ($10^{-14}\sim10^{-15}$ s) suggest that desorption may proceed with substantial probability for certain systems even when the intermediate excited state can decay by the resonant electron tunneling.

Avouris et al. carried out self-consistent calculations of the potential energy curves for ions interacting with a model Al surface on the basis of a local density functional theory, which fully accounts for screening by the electrons within the metal valence band [9]. The calculated potential energy curves for the $F^{-}(2s^2\,2p^6)$, $F(2s^2\,2p^5)$, $F^{*}(2s^1\,2p^6)$, and $F^{*}(2s^2\,2p^4)$ states are shown in fig. 6-6(a). The ground state for an adsorbed fluorine atom is found to be the F^{-} state, which is bounded by a potential curve described by the balance between image-like attraction and short range electron-electron repulsion. The neutral $F(2s^2\,2p^5)$ and $F^{*}(2s^1\,2p^6)$ states are found to be repulsive, because the image attraction has been removed. The potential energy curve for F^{*},

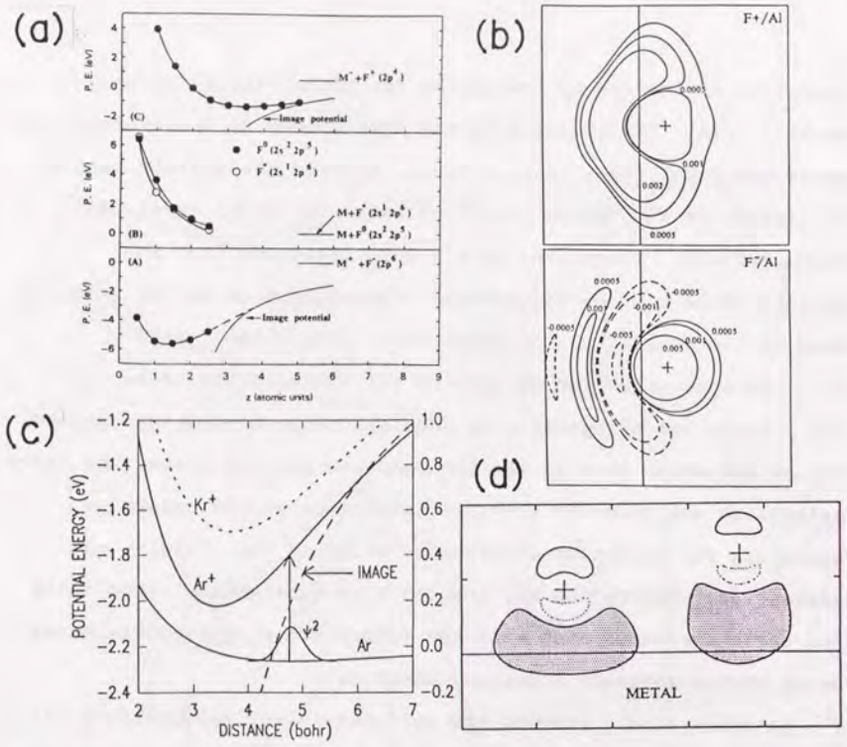

Fig. 6-6. (a) Calculated potential energy curves of F on Al for (A) $F^-(2s^2 2p^6)$, (B) $F(2s^2 2p^5)$ and $F^+(2s^1 2p^6)$, and (C) $F^+(2s^2 2p^4)$. (From ref. [5].) (b) Charge-difference contours of F on Al ($\Delta\rho = \rho(Al\text{-}F)-\rho(F)-\rho(Al)$) for Al-$F^+$ (upper) and for Al-F^- (lower). Solid and dotted lines indicate increased and decreased density in atomic units ($a.u.^{-3}$, 1 a.u. = 0.529 Å), respectively. (From ref. [5].) (c) Calculated potential energy curves for Ar^+ and Kr^+ on metal. (From ref. [10].) (d) Charge-difference contours of Ar^+ on metal (M) ($\Delta\rho = \rho(M\text{-}Ar)-\rho(Ar)-\rho(M)$) at M-Ar distances of 4.25 a.u. (left) and 6.5 a.u. (right). Solid and dotted lines indicate density contours of 0.001 and -0.001 $a.u.^{-3}$, respectively. Image-like density (shaded area) is pushed toward the metal as Ar^+ approaches the surface. (From ref. [10].)

however, was found to be much less attractive as compared with that for F^-. The difference between the negative and positive ionic states was attributed to the different character of the screening. For the negative ionic state, the screening is image-like, and the electronic configuration is nominally $F^-(2s^2 2p^6)$. For the positive ionic state, in contrast, the low-lying fluorine 3s and 3p levels are pulled down in energy by the presence of the 2p hole. These broadened 3s and 3p levels now extend partly below the Fermi level, and are thus partially occupied by electrons from the metal surface. The charge-difference plots illustrating this behavior are shown in fig. 6-6(b). The image-like attraction between F^+ and metal is reduced, because the net charge in F^+ is decreased. The short range electron-electron repulsion between F^+ and metal is increased, because the electron density in both the surface region of the metal and the large radius 3s and 3p orbitals of F^+ is increased. Therefore, the potential energy curve for $F^+(2s^2 2p^4)$ state is weakly bonding with the potential minimum located at a great distance from the surface.

The same group have also carried out density-functional calculations for Ar^+ ions interacting with metal surfaces [10]. For intermediate distances from the surface, the attractive force was found to be considerably smaller than that predicted by the classical image potential (fig. 6-6(c)) because of the charge-transfer screening (fig. 6-6(d)). The calculated potential energy curves indicate that the ionization of Ar adsorbed on metal leads to the desorption of neutral Ar atoms by the Antoniewiz mechanism, i.e., the Ar^+ ion starts its motion toward the surface and decays

into the ground electronic state, then the neutral Ar atom is repelled by the repulsive region of the potential energy curve and desorbed from surface (see Section 1.3 and fig. 1-6(b)). The calculations based on the Antoniewiz-type model reproduced the translational energy distributions of the neutral Ar atoms desorbed from a Ru(001) surface observed in an electron-stimulated desorption study by Steinacker and Feulner [11].

6.4.3 Review of proposed mechanisms for stimulated desorption

In a photostimulated desorption study of NO on Pt(111) at 120 K for 1907, 1064, 532, and 355 nm ($h\nu$ = 0.65, 1.2, 2.3, and 3.5 eV, respectively) using laser-induced-fluorescence, Buntin et al. reported the following results (see Section 1.4) [3]: (1) NO is not desorbed when $h\nu < D \simeq 1$ eV, where D is the NO desorption energy. (2) The desorption yield is proportional to laser fluence. The desorption cross sections are 7×10^{-24}, 1×10^{-22}, and 2.5×10^{-22} for 1064, 532, and 355 nm, respectively. (3) The translational energy distribution is independent of laser fluence. (Non-Maxwell distributions, ~800 K for 1064 nm, and ~1200 K for 532 and 355 nm, if Maxwell distributions are assumed.) (4) The $X^2\Pi(v"=1)/X^2\Pi(v"=0)$ population ratios for 355, 532, and 1064 nm are 0.04, 0.04, and <0.004, respectively. (NO in thermal equibilium at 840 K gives a v"=1/v"=0 ratio of 0.04.) (5) The internal energy exhibits non-Boltzmann distributions with markedly inverted spin-orbit population (see Fig. 5-6). (6) The desorption flux exhibits a forward-peaked distribution of $\sim\cos^{11}\theta$. (7) The

desorption yields for s- and p-polarized light at the incidence angles of 0° and 70° are propotional to the calculated absorption coefficient of the Pt substrate rather than the magnitude of the electric field normal or parallel to the surface. On the basis of these results, Buntin et al. proposed a mechanism as follows. The initial step is the electronic excitations in the Pt substrate. Then, inelastic electron scattering from the photogenerated hot electrons in the substrate into the unoccupied $2\pi_a$ orbital of chemisorbed NO creates the temporal negative ionic state (fig. 6-7(a)). The NO^- ion starts its motion toward the surface owing to the image potential of the metal surface. After the succeeding deexcitation into the ground electronic state, NO is repelled by the repulsive potential energy curve and is desorbed from the surface, if the lifetime of the negative ionic state is long enough (Antoniewicz model, see Section 1.3) (fig. 6-7(b)). Gazuk et al. have carried out dynamical calculations using a one-dimensional wavepacket propagation method, where the Pt-NO distance is considered [12, 13]. The potential energy curve for the temporal negative ionic state is modeled on the basis of the classical image potential argument. They estimated the lifetime of the temporal negative ionic state as $\sim10^{-15}$ s from the observed vibrational energy distributions. The calculations showed that the above Antoniewicz-type mechanism leads to the considerable desorption even for such a short-lived intermediate excited state. Using the same theoretical method, Gazuk et al. also showed that the Antoniewicz-type mechanism can explain the results of an electron-stimulated desorption study of atomic oxygen chemisorbed

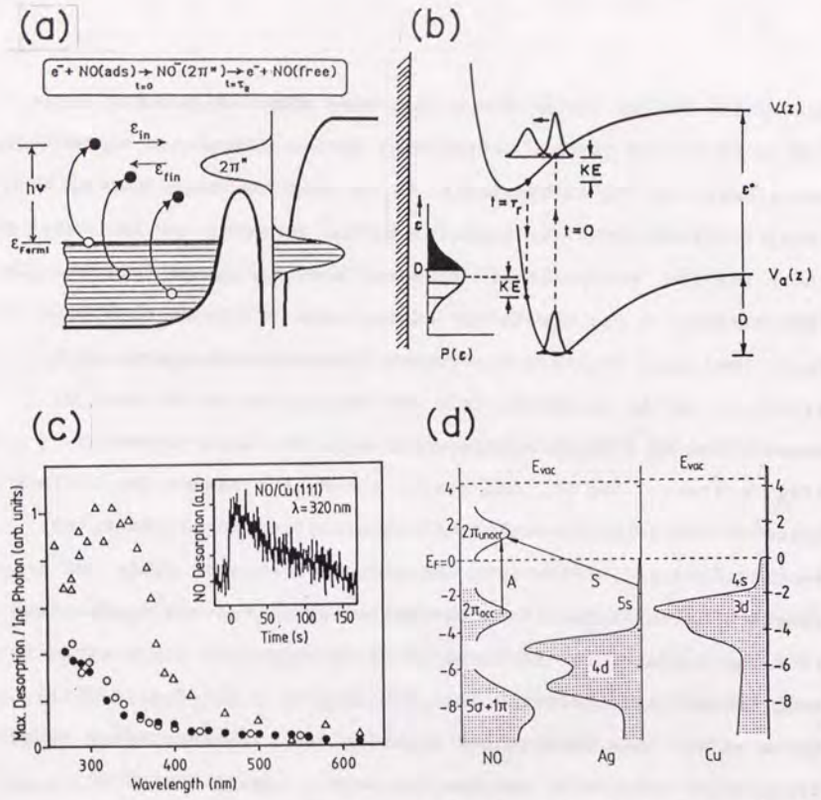

Fig. 6-7. (a) Energy level diagram for the hot electron scattering through the $2\pi_a$ resonance of chemisorbed NO. (From ref. [12].) (b) Potential energy curves for chemisorbed and negative ionic NO on metal illustrating the Antoniewicz model for desorption. (From ref. [12].) (c) Wavelength dependences of the desorption yield of NO from Ag(111) (○), Cu(111) (●), and Si(111)-(7x7) (△). Inset shows a decay of the desorption yield of NO from Cu(111). (From ref. [4].) (d) Schematic drawing of the band structures for Ag and Cu, and the occupied and unoccupied levels of chemisorbed NO. Two probable initial processes responsible for photostimulated desorption, i.e., the $2\pi_a \leftarrow 2\pi_b$ transition in adsorbed NO (A) and the hot electron scattering from the substrate into the $2\pi_a$ level of NO (S) are illustrated. (From ref. [4].)

on Pd(111) [12, 14, 15] carried out by Hoffman et al. [15].

In a photostimulated desorption study of NO on Ag(111) and Cu(111) at 85 K for 250-680 nm ($h\nu$ = 5.0-1.8 eV) using HREELS and TPDS, Franchy et al. reported the following results [4]: (1) There are two NO species for Ag(111) and Cu(111). One is chemisorbed on an on-top site, while the other is on bridge site. Only the NO species on an on-top site is sensitive for photo-stimulated desorption. (2) The wavelength dependence of the desorption yield is found to be simmilar for Ag(111) and Cu(111) (fig. 6-7(c)), although the valence band structure is greatly different between the two metals (fig. 6-7(d)). The desorption cross sections for 320 nm are 3.1×10^{-18} cm^2 for Ag(111), and 2.2×10^{-18} cm^2 for Cu(111). On the basis of these results, Franchy et al. suggested that the valence-electron transition from the $2\pi_b$ orbital to the $2\pi_a$ orbital in the chemisorbed NO molecules is responsible for photostimulated desorption of NO on both Ag(111) and Cu(111) for photon energies ≥ 3.4 eV (see fig. 6-7(d)).

In an electron-stimulated desorption study of NO on Pt(111) at 80 K using (1+1)REMPI, Burns et al. observed a dominant low-energy desorption channel [16] (see Section 1.4). The desorption channel exhibited the following characteristics: (1) The desorption threshold energy is ~6 eV. The desorption yield exhibited an enhancement at ~12 eV with total width of ~6 eV (fig. 6-8(a)). (2) The translational energy distribution is peaked at ~0.05 eV for the excitation energy of 325 eV (corresponding to ~580 K, if a Maxwell distribution is assumed) (fig. 6-8(b)). (4) The $X^2\Pi(v''=0):X^2\Pi(v''=1):X^2\Pi(v''=2):X^2\Pi(v''=3)$ population ratios

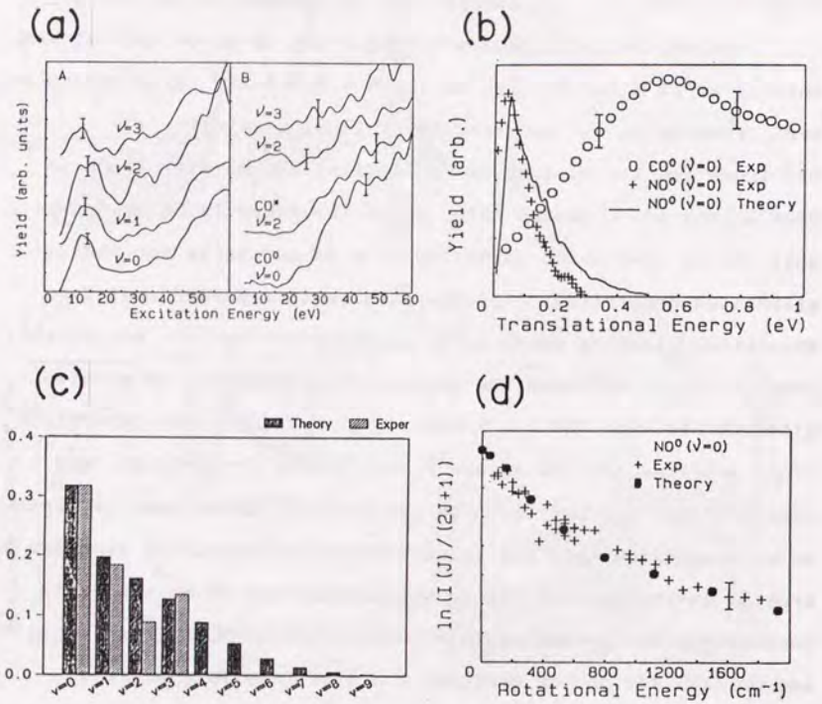

Fig. 6-8. (a) Excitation energy dependences of the desorption yield of NO and CO from Pt(111). (b) Theoretical and experimental translational energy distribution of NO in the $X^2\Pi(v''=0)$ state desorbed from Pt(111). (c) Theoretical and experimental vibrational energy distribution of NO in the $X^2\Pi(v''=0)$ state desorbed from Pt(111). (d) Boltzmann plot of the theoretical and experimental rotational energy distribution of NO in the $X^2\Pi(v''=0)$ state desorbed from Pt(111). (From ref. [16].)

for the excitation energy of 325 eV are 1.00, 0.58, 0.26, and 0.43, respectively (fig. 6-8(c)). (3) The two spin orbit states (the $X^2\Pi_{1/2}$ and $X^2\Pi_{3/2}$ states) for the excitation energy of 325 eV exhibited similar rotational energy distributions characterized by nearly-Boltzmann distributions with rotational temperatures of 543, 581, 642, and 481 K (±5%) for the v"=0, 1, 2, and 3 levels, respectively (fig. 6-8(d)). On the basis of these results, they proposed a mechanism that the valence-electron transition from the 5σ orbital to the $2\pi_a$ orbital in the chemisorbed NO is responsible for electron-stimulated desorption. The $2\pi_a \leftarrow 5\sigma$ transition is expected to be resonantly induce by the excitation energy of 12 eV. The $2\pi_a \leftarrow 5\sigma$ transition creates an almost neutral excited state with a screened 5σ hole. The 5σ hole locating below the Pt valence band is expected to have a relatively long lifetime, because the resonant electron tunneling from the Pt substrate is blocked (see Section 6.4.2). They also carried out a calculation based on a single-atom approximation, and found that the 5σ hole has a relatively long lifetime of 10^{-13}~10^{-14} s. The calculation showed also that the 1π hole decays ~20 times faster than the 5σ hole. They speculated that the potential energy curve for the intermediate excited state with a screened 5σ hole is simmilar to that for an O_2 molecule on Pt(111). Since O_2 is known to be weakly adsorbed on Pt(111) by ~0.3 eV with a configuration parallel to the surface, they concluded that the succeeding deexcitation creates a rotated NO molecule in the ground electronic state in a repulsive potential curve, from which desorption proceeds. They carried out dynamical calculations using a two-

dimensional wavepacket propagation method, where the Pt-NO distance and the Pt-NO polar angle are considered. The potential energy curve for the intermediate state is modeled on the basis of the assumption that NO with a screened 5σ hole resembles O_2 on Pt(111). The calculations reproduced the experimentally observed translational and rotational energy distributions as is shown in figs. 6-8(b) and (d). The experimentally observed vibrational energy distribution is also reproduced in the dynamical calculations where the N-O distance is assumed to be enlonged by 0.13 atomic units (0.069 Å) as is shown in fig. 6-8(c).

6.4.4 Initial electronic excitations responsible for photostimulated desorption

As is stated in Section 6.3, the NO desorption yield is proportional to pump laser fluence for both the polarizations (see fig. 6-2). This result indicates that NO desorption is induced by a one-photon process for both the polarizations. As is stated in the former section, there are two probable mechanisms for the initial one-photon process. The first is the direct valence-electron excitation in the chemisorbed NO. The second is the electronic excitations in the Pt substrate followed by electron scattering from the photogenerated hot electrons in metal into the unoccupied orbital of the chemisorbed NO. The first mechanism is more probable, because the probability of the electron scattering in the second model is expected to be too small to account for the relatively large desorption cross sections (σ_d) of 10^{-19}~10^{-18} cm^2

estimated in the present study (see Section 3.4). As is stated in the former section, photostimulated desorption of NO on Ag(111) and Cu(111) for 320 nm with large cross sections (σ_d = 3.1×10^{-18} and 2.2×10^{-18} cm^2 for Ag(111) and Cu(111), respectively) is suggested to be induced by the direct valence-electron excitation of the chemisorbed NO [4], while photostimulated desorption of NO on Pt(111) for 1064, 532, and 355 nm with small cross sections (σ_d = 7×10^{-24}, 1×10^{-22}, and 2.5×10^{-22} cm^2, respectively) is concluded to be induced by the valence-band excitations in the Pt substrate [3].

Table 6-1 shows the substrate absorption coefficient (1-R) and the surface mean square electric field components ($\langle E^2_x \rangle$, $\langle E^2_y \rangle$, and $\langle E^2_z \rangle$) for 193 nm at the incidence angle (θ) of 81° calculated on the basis of classical electromagnetic theory [17] using optical constants of Pt [18]. The z-direction is defined as the surface normal, and the x-z plane is taken to be the plane of incidence. As is stated in Section 6.3, the observed desorption yield ratio for the p-polarized pump laser to the s-polarized pump laser is ~2.9. If direct valence-electron excitations in the chemisorbed NO are responsible for the observed photostimulated desorption, this result indicates that both the normal and parallel electric fields ($\langle E^2_x \rangle+\langle E^2_y \rangle$ and $\langle E^2_z \rangle$, respectively) contribute to photostimulated desorption with 1:3 weighting ratio. The desorption mechanism initiated by electronic excitations in the Pt substrate, however, is not excluded by the present data, because the substrate absorption ratio for the p-polarized light to the s-polarized light is calculated to be 3.22 (see Table 6-1).

Table 6-1. Substrate absorption coefficients and surface mean square electric field components for 193 nm at the incidence angles of 25° and 81°, and their ratios between the two angles.

	s-polarized			p-polarized		
	1-R	$\langle E^2_y \rangle$	$\langle E^2_z \rangle$	1-R	$\langle E^2_x \rangle$	$\langle E^2_z \rangle$
θ = 81°	0.185	0.025	≃0	0.596	0.005	0.203
θ = 25°	0.714	0.503	≃0	0.787	0.527	0.115
(θ = 25°)/(θ = 81°)	3.86	20.0		1.32	105	0.57

The valence-electron excitations allowed by the Fermi's golden rule and the consideration based on symmetry are shown in fig. 6-9 for NO chemisorbed with a straight configuration irradiated by the s- and the p-polarized laser with photon energy of 6.41 eV. The $2\pi_a \leftarrow 5\sigma$ and $6\sigma \leftarrow 2\pi_b$ excitations, and the $2\pi_a \leftarrow 2\pi_b$ and $2\pi_a \leftarrow 1\pi$ excitations are supposed to be allowed for the s- and the p-polarization, respectively. The translational and internal energy distributions of the desorbed NO are, however, independent of the polarization of the pump laser (see figs. 6-3 and 6-4). These results suggest that both the s- and the p-polarized laser irradiation create the same excited state, from which photo-stimulated desorption proceeds. Further investigations are required to determine the initial electronic excitation process responsible for photostimulated desorption.

6.4.5 Probable mechanisms of photostimulated desorption

On the basis of the discussion in the above sections, I discuss several probable mechanisms for the observed photo-stimulated desorption in this section. The first is the model proposed by Burns et al, i.e., NO is desorbed via an almost neutral excited state with a screened 5σ hole created by the $2\pi_a \leftarrow 5\sigma$ transition in the chemisorbed NO (see Section 6.4.3). This mechanism is the most favorable candidate, because the $2\pi_a \leftarrow 5\sigma$ transition is accessible for an s-polarized laser with photon energy of 6.41 eV (see fig. 6-9), and because this mechanism can account for the relatively large desorption cross

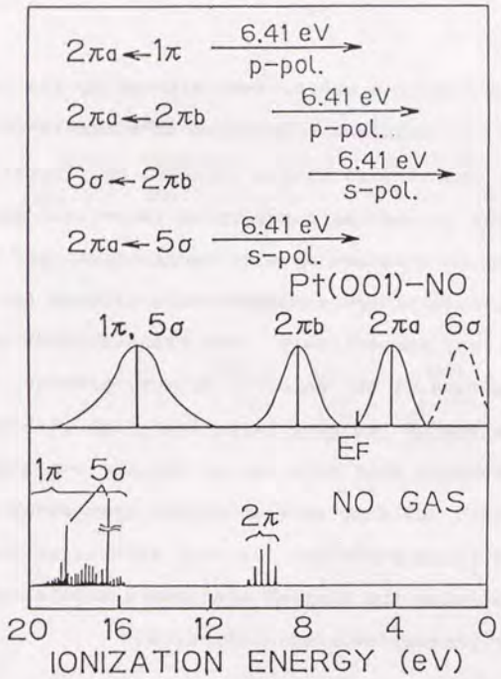

Fig. 6-9. Allowed valence-electron excitations for NO chemisorbed with the straight configuration irradiated by the s- and the p-polarized laser with photon energy of 6.41 eV. The position of the occupied orbitals (4σ, $1\pi+5\sigma$, and $2\pi_b$) is estimated from a UPS study of NO chemisorbed on Pt(001) at 300 K by Bonzel and Pirug [19] (see Section 1.2 and fig. 1-2). The position of the $2\pi_a$ orbital is estimated from a study of NO chemisorbed on Pt(111) using inverse photoemission spectroscopy (IPS) by Dose [20]. The $2\pi_b$ and the $2\pi_a$ orbital are created by the hybridization of the half-filled 2π orbital of NO and the d orbital of Pt, where the subscripts represent the bonding character between the chemisorbed NO and the metal. The positions, however, contains uncertainty of 2~3 eV because UPS and IPS probes positive and negative ionic states instead of a neutral state, respectively. The 6σ orbital which corresponds to the $A^2\Sigma$ state of a NO free molecule (see fig. 4-3) has not yet been measured for chemisorbed NO.

sections of 10^{-18}~10^{-19} cm^2. Furthermore, the observed and calculated translational and internal energy distributions reported in the electron-stimulated desorption study by Burns et al. [16] are in excellent agreement with the present results (see Section 5.4, fig. 5-6, and fig. 5-7). One objection to this mechanism is that the $2\pi_a \leftarrow 5\sigma$ transition is not allowed for p-polarized light, if NO is chemisorbed with a straight configuration (see Section 6.4.4). The $2\pi_a \leftarrow 5\sigma$ transition, however, can be induced by p-polarized light, when NO is chemisorbed in a slightly bent configuration. Although Pirug et al. suggested that the NO species responsible for photostimulated desorption is probably in a straight configuration on the basis of the N-O stretching frequency (see Sections 1.2 and 6.4.1), NO may be chemisorbed in a slightly bent configuration, because the N-O stretching frequency can not predict the configuration of the chemisorbed NO exactly.

Another probable mechanism is an MGR-type model that NO is desorbed via an almost neutral excited state with a screened 1π hole created by the $2\pi_a \leftarrow 1\pi$ transition in the chemisorbed NO (see fig. 6-9). The 1π hole is also expected to decay mainly by the intramolecular Auger process, because it is located below the Pt valence band (see Section 6.4.2). However, this mechanism is less probable as compared with the first one, because the calculations by Jennison et al. showed that the lifetime of the 1π hole is much shorter than that of the 5σ hole [16] (see Section 6.4.3).

The third probable mechanism is an MGR-type model that NO is desorbed via a intermediate excited state with a screened $2\pi_b$ hole created by the $2\pi_a \leftarrow 2\pi_b$ or $6\sigma \leftarrow 2\pi_b$ transitions followed by the

resonant tunneling of the excited electron into the Pt conduction band. The potential energy curve for the intermediate excited state is expected to be repulsive, because the $2\pi_b$ orbital has a bonding character between Pt and NO. This mechanism, however, is much less probable, because the lifetime of the $2\pi_b$ hole is expected to be extremely short ($\sim 10^{-15}$ s) owing to the resonant tunneling into the Pt valence band (see Section 6.4.2).

The fourth mechanism is an Antoniewicz-type model that NO is desorbed via a temporal negative ionic state created by the $2\pi_a \leftarrow 2\pi_b$, $2\pi_a \leftarrow 1\pi$, or $2\pi_a \leftarrow 5\sigma$ transitions followed by the resonant electron tunneling from the Pt valence band into the hole of NO. This mechanism is simmilar to the model proposed in a photo-stimulated desorption study by Buntin et al. [3], in which the temporal negative ionic state is created by the resonant electron scattering from the photogenerated hot electrons in the Pt substrate into the unoccupied $2\pi_a$ orbital of the chemisorbed NO. Although the excited $2\pi_a$ electron can decay by the resonant tunneling into the Pt conduction band, the lifetime of the $2\pi_a$ electron is expected to be longer than that of the $2\pi_b$ hole, because the $2\pi_a$ orbital is oriented away from the surface whereas the $2\pi_b$ obital is oriented toward the surface (see Section 6.4.2). Indeed, Franchy et al. also suggested that the $2\pi_a \leftarrow 2\pi_b$ transition is responsible for photostimulated desorption of NO adsorbed on Ag(111) and Cu(111) for photon energies $\geq$ 3.4 eV [4] (see Section 6.4.3). This mechanism as well as the model proposed by Buntin et al., however, is not likely to be the dominant desorption channel in the present case, because the translational and internal energy

distributions, and the desorption cross sections reported by Buntin et al. are greatly different from those observed in the present study (see Sections 3.4 and 5.4, and fig. 5-6).

6.5 Perspectives

As is stated in the former sections, further investigations are required to elucidate the mechanism of photostimulated desorption of NO chemisorbed on Pt(001). The most effective approach to determine the initial electronic excitation responsible for photostimulated desorption is to measure the desorption yield as a function of the incidence angle, the polarization, and the wavelength of the pump laser. I am now making the preparations for the desorption yield measurements for s- and p-polarized pump lasers of 193, 248, and 353 nm (6.4, 5.0, and 3.5 eV, respectively) at the incidence angles of 25° and 81°. Since the substrate absorption coefficient and the surface mean square electric field components are known to depend on the polarization and the angle of incidence of the pump laser (see table 6-1), these experiments are expected to determine whether the excitation of the metal substrate or the direct excitation of the chemisorbed NO is responsible for photostimulated desorption. The desorption yield for s-polarized light at the incidence angle of 25°, for example, is expected to be enhanced by a factor of ~20 as compared with that for s-polarized light at the incidence angle of 81°, if the direct excitaion of NO induced by the surface electric field parallel to the surface is responsible for photo-

stimulated desorption (see table 6-1). Furthermore, measurements as a function of the photon energy of the pump laser are also expected to offer valuable information, because the $2\pi_a \leftarrow 5\sigma$, $6\sigma \leftarrow 2\pi_b$, and $2\pi_a \leftarrow 1\pi$ transitions in the chemisorbed NO are not accessible for the pump laser with photon energies of 5.0 and 3.5 eV.

The comprehensive measurements of translational, vibrational, and internal energy distributions, and the rotational alignment of desorbed NO is expected to bring about new information on the potential energy surface and the lifetime of the intermediate excited state responsible for photostimulated desorption as is shown in fig. 6-10. The translational and internal energy distributions of NO in the $X^2\Pi_{1/2,3/2}$ (v"=1) states can be measured by a (1+1)REMPI technique using a probe laser of 222~224 nm. The rotational alignment of desorbed NO can be estimated by the probe laser polarization dependence of the (1+1)REMPI signal [21]. These investigations can be also realized by further modification of the present apparatus.

References

[1] P. Gardner, M. Tüshaus, R. Martin, and A.M. Bradshaw, Vacuum 41, 304 (1990).

[2] G. Pirug, H.P. Bonzel, H. Hopster, and H. Ibach, J. Chem. Phys. 71, 593 (1979).

[3] S.A. Buntin, L.J. Richter, R.R. Cavanagh, and D.S. King, Phys. Rev. Lett. 61, 1321 (1988); S.A. Buntin, L.J. Richter, D.S. King,

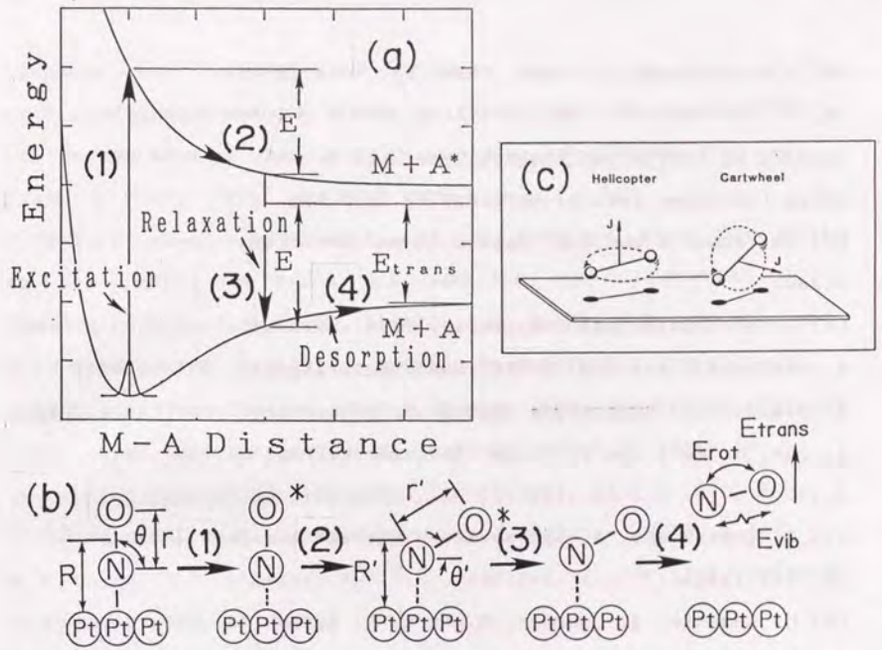

Fig. 6-10 (a) MGR-type model for desorption induced by valence-electron excitation in NO chemisorbed on Pt(001) (See Section 1.3 and fig. 1-6). M and A represent Pt(001) and NO, respectively. The desorption process is composed of the four elementary processes, i.e. (1) excitation, (2) motion along the potential surface of the excited state, (3) deexcitation, and (4) motion along the potential surface of the ground state. (b) Schematical drawings of the configuration of NO before and after each process in the model. R and r represent the Pt(001)-NO and the N-O distance, respectively. θ represents the polar angle between the N-O axis and the surface plane. The displacements in R and r are expected to be mainly reflected into the translational and vibrational energy distributions of desorbed NO, respectively. On the other hand, the displacement in θ is expected to be mainly reflected into the rotational energy distributions and rotational alignment of desorbed NO. (c) Rotational alignment relative to the surface plane. (From ref. [21].)

and R.R. Cavanagh, J. Chem. Phys. 91, 6429 (1989).

[4] R. Franchy, S.K. So, Z.C. Ying, and W. Ho in: Desorption Induced by Electronic Transitions, DIET-4, eds. G. Betz and P. Varga (Springer-Verlag, Berlin, 1990), p.85.

[5] Ph. Avouris and R.E. Walkup, Annu. Rev. Phys. Chem. 40, 173 (1989).

[6] P. Nordlander and J.C. Tully, Phys. Rev. Lett. 61, 990 (1988); P. Nordlander and J.C. Tully, Surf. Sci. 211/212, 207 (1989); P. Nordlander in: Desorption Induced by Electronic Transitions, DIET-4, eds. G. Betz and P. Varga (Springer-Verlag, Berlin, 1990), p.12.

[7] G. Schönhense, A. Eyers, and U. Heinzmann, Phys. Rev. Lett. 56, 512 (1986).

[8] G. Leschik, R. Courths, H. Wern, S. Hüfner, H. Eckardt, and J. Noffke, Solid State Commun. 52, 221 (1984).

[9] Ph. Avouris, R. Kawai, N.D. Lang, and D.M. Newns, Phys. Rev. Lett. 59, 2215 (1987); Ph. Avouris, R. Kawai, N.D. Lang, and D.M. Newns, J. Chem. Phys. 89, 2388 (1988).

[10] R.E. Walkup, Ph. Avouris, N.D. Lang, and R. Kawai, Phys. Rev. Lett. 63, 1972 (1989); R.E. Walkup, Ph. Avouris, and N.D. Lang, in: Desorption Induced by Electronic Transitions, DIET-4, eds. G. Betz and P. Varga (Springer-Verlag, Berlin, 1990), p.24.

[11] E. Steinacker and P. Feulner, Phys. Rev. B 40, 11348 (1989).

[12] J.W. Gadzuk in: Desorption Induced by Electronic Transitions, DIET-4, eds. G. Betz and P. Varga (Springer-Verlag, Berlin, 1990), p.2.

[13] J.W. Gadzuk, L.J. Richter, S.A. Buntin, D.S. King, and R.R.

Cavanagh, Surf. Sci. 235, 317 (1990).

[14] J.W. Gadzuk and C.W. Clark, J. Chem. Phys. 91, 3174 (1989).

[15] A. Hoffman, X. Guo, J.T. Yates, Jr., J.W. Gadzuk, and C.W. Clark, J. Chem. Phys. 90, 5793 (1989).

[16] A.R. Burns, E.B. Stechel, and D.R. Jennison, Phys. Rev. Lett. 58, 250 (1987); A.R. Burns, D.R. Jennison, and E.B. Stechel, J. Vac. Sci. Technol. A 5, 671 (1987); A.R. Burns, E.B. Stechel, and D.R. Jennison in: Desorption Induced by Electronic Transitions, DIET-3, eds. R.H. Stulen and M.L. Knotek (Springer-Verlag, Berlin, 1987), p.67; E.B. Stechel, D.R. Jennison, and A.R. Burns in: Desorption Induced by Electronic Transitions, DIET-3, eds. R.H. Stulen and M.L. Knotek (Springer-Verlag, Berlin, 1987), p.136; A.R. Burns, E.B. Stechel, and D.R. Jennison, J. Vac. Sci. Technol. A 6, 895 (1988).

[17] Expressions for the substrate absorption coefficients and surface electric field components based on classical electromagnetic theory are stated in a large literature. For example, see R.G. Greenler, Surf. Sci. 69, 647 (1977).

[18] Handbook of Optical Constants of Solids, ed. E.D. Palik (Academic Press, Orlando, 1985), p.340.

[19] H.P. Bonzel and G. Pirug, Surf. Sci. 62, 45 (1977).

[20] V. Dose, Surf. Sci. Rep. 5, 337 (1985).

[21] D.C. Jacob, K.W. Kolasinski, S.F. Shane, and R.N. Zare, J. Chem. Phys. 91, 3182 (1989).